MANIFESTATIONS OF CLASSICAL PHASE SPACE STRUCTURES IN QUANTUM MECHANICS

O. BOHIGAS[a], S. TOMSOVIC[a,b] and D. ULLMO[a]

[a]*Division de Physique Théorique, Institut de Physique Nucléaire, 91406 Orsay Cedex, France*
[b]*Department of Physics, FM-15, University of Washington, Seattle, WA 98195, USA*

NORTH-HOLLAND

PHYSICS REPORTS (Review Section of Physics Letters) 223, No. 2 (1993) 43–133.
North-Holland

PHYSICS REPORTS

Manifestations of classical phase space structures in quantum mechanics

O. Bohigas[a], S. Tomsovic[a,b] and D. Ullmo[a]

[a] *Division de Physique Théorique, Institut de Physique Nucléaire, 91406 Orsay Cedex, France*[1]
[b] *Department of Physics, FM-15, University of Washington, Seattle, WA 98195, USA*

Received July 1992; editor: I. Procaccia

Contents:

1. Introduction 45
2. The classical system 49
   2.1. General properties 50
   2.2. Surfaces of section 51
   2.3. Phase space volume 55
   2.4. Hamiltonian transport across barriers 56
3. The quantum system 61
   3.1. "Quantum phase space" 62
   3.2. Level densities 63
   3.3. The spectral calculations 66
4. Regular states 71
   4.1. EBK quantization 72
   4.2. Dynamical quasidegeneracies 78
   4.3. Separation of regular levels and quantum number assignments 79
   4.4. Resonances 86
   4.5. Chaos assisted tunneling 88
5. Chaotic spectrum 93
   5.1. Association of a quantum subspace to a classical region 93
   5.2. Relation between flux and matrix elements 97
   5.3. Random matrix modeling 102
   5.4. The spectral fluctuations 106
6. Localization of chaotic eigenstates 111
   6.1. A semiclassical mechanism of localization 112
   6.2. Semiclassical versus quantum localization 124
7. Summary and conclusions 126
Appendix A 130
References 130

Abstract:

Using two coupled quartic oscillators for illustration, the quantum mechanics of simple systems whose classical analogs have varying degrees of non-integrability is investigated. By taking advantage of discrete symmetries and dynamical quasidegeneracies it is shown that Percival's semiclassical classification scheme, i.e., eigenstates may be separated into a regular and an irregular group, basically works. This allows us to probe deeply into the workings of semiclassical quantization in mixed phase space systems. Some observations of intermediate status states are made. The standard modeling of quantum fluctuation properties exhibited by the irregular states and levels by random matrix ensembles is then put on a physical footing. Generalized ensembles are constructed incorporating such classical information as fluxes crossing partial barriers and relative fractions of phase space volume occupied by interesting subregions. The ensembles apply equally well to both spectral and eigenstate properties. They typically show non-universal, but nevertheless characteristic level fluctuations. In addition, they predict "semiclassical localization" of eigenfunctions and "quantum suppression of chaos" which are quantitatively borne out in the quantum systems.

[1] Unité de Recherche des Universités Paris 11 et Paris 6 Associée au CNRS.

1. Introduction

Semiclassical mechanics has a long, illustrious history of providing deep physical insight into a variety of quantum mechanical problems encompassing most fields of physics. Being a wave mechanics based firmly on classical dynamics, it focuses all the attention on a quantum system's classical analog. Just observing a few classical trajectories suffices to begin to develop an intuition for many quantum behaviors. Though often relied upon in this way, semiclassical mechanics is much more than a qualitative picture [1–4]. As an approximation, it can be surprisingly precise even in circumstances where the underlying classical dynamics is extremely intricate [5]. In spite of this possible accuracy, some longstanding, often fundamental, problems still exist in the theory, which can be traced to the nature of the classical dynamics. Those problems upon which we shall concentrate arise in the presence of non-integrable dynamics. Our aim here is to address systems far from integrability. They display widespread chaos in which regions dominated by quasiperiodic motion are embedded. We shall refer to them as mixed systems, which reflects that they are partly chaotic and partly regular. Their intimate coexistence of regularity and chaos gives rise to special difficulties even from a purely classical point of view and will lead to the introduction of important time scales in the quantum–classical correspondence. Many of the resulting manifestations of those time scales will be relevant to fully chaotic systems as well.

Our interest in mixed systems is driven by their being in some sense generic. Choose a multi-degree of freedom Hamiltonian at "random" and one expects to find such a system. It is simple to conjure up examples of physical systems that would belong to this class. Of special interest is the hydrogen atom in a strong magnetic field [6], for which a great deal of experimental data already exists [7]. Other examples are provided by models of nuclear motion in simple molecules (for a review, see ref. [8]) and perhaps mesoscopic devices could be constructed with a wide range of dynamical features (see, for instance, ref. [9]).

The presence of a significant amount of chaotic motion lends itself to various methods of study. One could take a microscopic viewpoint and attempt to derive detailed quantum properties from the detailed classical dynamics. This is the philosophy behind much of the periodic orbit theory as initiated and embodied in Gutzwiller's papers [10], whereby the density of quantum eigenvalues is related to a sum over these orbits. This quite active field has recently seen some very beautiful progress in the investigation of purely chaotic systems [11]—mixed phase space systems have yet to be addressed in this way. A largely complementary avenue on which we shall concentrate here is motivated by the classical dynamics itself. Indeed, most of the present-day theoretical analyses of chaotic classical systems are concerned with a probabilistic description of the motion rather than with the computation of the detailed dynamics. This is exemplified by: (i) the stages describing the hierarchy of chaotic systems {ergodicity, mixing, K and B properties}, (ii) the study of transport, and (iii) the study of correlation decays. By adopting this probabilistic viewpoint, we shall explore new quantum features, such as "semiclassical localization" of wave functions, that are not as naturally evident in the microscopic viewpoint and whose interpretation will thus be greatly simplified [12, 13].

In fact, a remarkable property of universality has been established in the last few years for the spectral fluctuations of quantum systems with classically chaotic analogs [14, 15]. More precisely, it has been shown that the level fluctuations only depend on general space–time symmetry con-

siderations, and are the same as those of the random matrix ensembles of Wigner and Dyson [16–18]. Examples belonging to different universality classes have been found [19]. Important and natural extensions concerning the quasienergy spectra of time-dependent systems (spectra of the time evolution operator of periodically driven systems), and chaotic scattering, have also been made [20, 12]. In addition to the strong numerical evidence, there is also the beginning of a theory of this universality and of its regime of validity given by Berry [21]. It is based on the microscopic correspondence of the spectrum to periodic orbits and these orbits' tendency to explore phase space uniformly (uniformity principle) [22].

In contrast, integrable (regular) systems do not display the same spectral fluctuation behavior as chaotic systems. Roughly speaking, a universality class also exists for these systems, it being the Poisson class [23]. Poissonian fluctuations are characterized by a complete absence of level correlations, whereas random matrix spectra are typically very rigid with strong level correlations and so the two are easily distinguished. Therefore by studying level fluctuations of a quantum system we learn about the dynamics of the classical analog or vice versa. In our view, if it were not for this contrast they provide, the fluctuations of integrable systems would be of very little intrinsic interest.

The situation concerning fluctuations in mixed systems, which is the generic case, is more complicated and less clear. By varying a parameter in the Hamiltonian which induces a transition from the regular to the chaotic regime, several authors have investigated the transition properties of classical systems with few degrees of freedom (see ref. [24] and references therein). The corresponding quantum mechanical problem has also been studied and one observes a transition from the Poissonian spectral fluctuations characteristic of the regular regime to the random matrix spectral fluctuations characteristic of the chaotic regime [25]. Some general ideas based on semiclassical considerations have been put forward by Berry and Robnik, who proposed that the spectral statistics of mixed systems should be understood as resulting from an uncorrelated superposition of spectra from different universality classes, each spectrum being associated with a different chaotic or regular region in classical phase space [26]; this is sometimes referred to as the Berry–Robnik surmise. Recent investigations have shown that this certainly constitutes part of the story. However, the numerical "experiments" to date have often resulted in fluctuations inconsistent with this simple superposition prediction. Perhaps the most significant results are those of Zimmermann et al. [27], who show real deviations with long high quality spectral sequences. It has remained an open question, which we shall answer in this paper, why or in what way the superposition hypothesis is inadequate in these cases.

Needless to say, the richness of behaviors of the quantum system is not exhausted by spectral properties. An enormous body of information is encoded in the eigenfunctions, which being multidimensional are technically more difficult to study than the spectrum. As well as for spectral fluctuations, statistical descriptions have been put forward, starting from the most extreme case, for which the wave functions should behave as random functions, and which should apply for a chaotic structureless system [28, 29]. However, departures from this extreme case have been exhibited since the pioneering work of Mc Donald and Kaufman [30], and Heller has shown that semiclassical structures, dubbed "scarring" of eigenfunctions by periodic orbits [31], exist beyond the statistical realm. One way to develop insight into the properties of the wave functions and the dynamics, and to investigate departures from uniformity, consists in following the long time evolution of initially localized wave packets [32]. Time scales, traps, localization and other phenomena may then become apparent. In this connection, one should also mention that interesting localization phenomena have been exhibited when studying time dependent open systems such as the kicked rotor [33–36] (see also Chirikov in ref. [4], and ref. [12]). It is likely that there exist connections

amongst such different localization phenomena which would be of interest yet continue to remain unidentified.

In addressing these problems, it will be indispensible to illustrate some of the features with a concrete example. The system of two coupled quartic oscillators, previously studied by several authors [25, 27, 37], has been chosen for its simplicity and great variety of dynamical features, rather than for its relevance to a particular physical application. The hope is that it reflects generically phenomena occurring in physical systems with underlying mixed classical dynamics or important time scales. Rather than incorporate the regular classical structure of phase space only in a statistical way when going to quantum mechanics, we will execute a more ambitious task, namely the one of identifying explicitly in a quantum spectrum all the states which correspond to the regular part of classical phase space, i.e. the states which result from quantizing invariant tori. For example, the semiclassical quantization of Einstein–Brillouin–Keller (EBK) [38], i.e. the corrected version of the Bohr–Sommerfeld rule, may be applied (which we shall do in a detailed way) to the regular regions [39]. In this way, one really follows the program put forward by Percival almost twenty years ago [40]. Percival first described a semiclassical classification scheme which as a consequence leads to the discrete energy levels of a bound quantum system belonging to either a regular or an irregular class. So far, the attempts to systematically separate the regular and irregular states have been rather inconclusive because none of the criteria used, such as the behavior under a slowly changing perturbation, has been well suited. *) That this classification scheme holds and the separation can actually be performed will be illustrated as a part of our detailed investigation of the two coupled quartic oscillators system.

This will be made possible with the help of discrete symmetries. It happens that for a large range of the oscillators' coupling parameter all the invariant tori possess a distinct duplicate elsewhere in phase space. The duplicates can be located by application of at least one of the symmetry operators. The levels associated with quantizing tori appear therefore as quasidegenerate doublets (which we shall call "dynamical quasidegeneracies") belonging to different symmetry classes. These dynamical degeneracies allow one to "filter" the regular spectrum from the total one. These doublets will be split by the generalization (which has been dubbed "dynamical tunneling" by Davis and Heller [42]) of the well known tunneling in a one-dimensional symmetric double well potential (quasidegeneracies of parity doublets). In comparison with nearly integrable systems, the presence of the surrounding chaos noticeably modifies the behavior of the very small splittings. A new tunneling mechanism, which has been exhibited in ref. [43], takes place.

After separation, the regular and irregular spectra may be studied independently and they give rise to different kinds of physics. The regular levels afford a highly detailed examination into the working of EBK quantization in mixed systems. Our results show how well EBK works, how the structure interior to the regular regions gets resolved as E increases ($\hbar$ decreases), emphasizes the well known relationship linking resonances and tunneling between "accidental" degeneracies [44], and gives some indication of how the quantization works in the neighborhood of the regular–chaotic motion interface.

The chaotic levels here will only be statistically analyzed. One aim of the present paper is to give conclusive evidence that classical properties which have not been considered so far in this context have their counterpart in the quantum spectral fluctuations. Specifically, we investigate the role played by transport properties. If one has, for instance, two chaotic regions which communicate weakly (the rate of communication being characterized by the flux), this information can be translated in terms of random matrix theory. And, not surprisingly, the model of two (or

*) There is however an interesting new criterion recently proposed holding some promise, see ref. [41].

several) independent random matrix ensembles coupled by a random component, whose strength is determined by the classical flux, plays the crucial role. These ensembles are just as well adapted for answering questions about wave function behavior as spectral fluctuations. Constraints on the eigenfunction properties and thus on the long time propagation of initially localized states follow from the ensembles leading to a "semiclassical localization mechanism" and to "quantum suppression of classical chaos", respectively.

The material of the paper (partial results can be found in refs. [45, 43]) is organized as follows. In section 2 the classical properties of the coupled quartic oscillators are studied. Scaling and symmetry properties are examined as well as, through the study of Poincaré surfaces of section, how the transition from regular to irregular motion takes place when the coupling parameter is varied. The volume of chaotic and regular regions is evaluated. Special attention is then paid to transport and finite time properties, as for instance the presence of weakly connected chaotic regions. In this respect, the effect of breaking rational tori as sources of island chain barriers, is investigated.

In section 3, after discussing the general properties of the quantum spectrum and the semiclassical tools which allow the understanding of the smoothed level density, the quantum calculations are described. A semiclassical argument is used to select a method which is, in a sense to be explained later, well suited. For the most interesting values of the coupling parameter, we determine the first 20 000 to 30 000 levels. The precision of the eigenvalues is nearly always better than 10^{-5} (in units of the mean spacing), and is always $\leq 10^{-2}$. These very long and accurate spectra will serve effectively in limiting saturation effects in fluctuation statistics, in lowering the quantum corrections to the semiclassical theory developed and in providing excellent statistical significance.

In section 4 we review EBK quantization and perform the separation of the regular levels, of which there are typically several thousand. The quantum number assignments are then made without specific use of the classical actions, in order to generate independently a "quantum curve" giving the relationship between the classical actions of the tori contained on one energy surface. The comparison to the actual classical curve is quite instructive. The difficulties which arise in making the quantum number assignments with our method are discussed and the existence of intermediate status levels is noted. The complexities introduced by resonances are treated as well as how their structure gets resolved as $\hbar$ decreases. Finally a discussion is given on how the chaos assists the tunneling between states constructed on symmetric tori, and leads to larger and more erratic tunneling rates than what is observed for integrable systems.

Section 5 is devoted to the fluctuation properties of chaotic levels. Excepting the numerical comparisons, most of the results we derive here and in the final section are obtained without explicit reference to the quartic oscillators and should be applicable for a wide range of mixed or chaotic systems. The section begins by relating the classical transport, semiclassically, to constraints on the quantum Hamiltonian, which leads to a modeling of the chaotic level fluctuations in a form for which random matrix theory may be applied. This extends the Berry–Robnik surmise to include a quantum translation of the classical transport. The modeling contains no free parameters since all the quantities which enter it can be measured on the classical system. Finally, after the saturation effects are correctly disposed of, we apply this model to the quartic oscillators. For a sufficiently simple system (choice of coupling), we work everything out completely and the statistical fluctuations are correctly reproduced.

Section 6 extends the application of the previous section's statistical model to the behavior of wave functions. We describe how "semiclassical localization" of eigenstates can occur if the partial barriers are effectively limiting the transport. Its implications on the long time dynamics of wave packets is then treated. Some "non-classical" predictions are made, and verified quantitatively with

the quantum results. Finally, there are some brief speculations on the relationship existing between the "semiclassical localization mechanism" we have introduced and the more standard discussion of localization.

For easier reading, we make a final comment about the paper's organization. Since it is not intended as a review, the material of this paper largely contains either new results or applications of known tools which serve definite purposes. Sections 2 and 3 mainly fall in the latter category, with the exception of the numerical quantum spectral calculations. They introduce some of the basic concepts needed in the following sections. The reader less interested in the numerical techniques and who does not desire an acquaintance with the classical mixed system and transport properties, nor with the Wigner representation of operators, can proceed directly to section 4 and enter into the main subject.

2. The classical system

It would be good to have concrete examples of the phenomena which we wish to elucidate. Therefore a good part of our work will consist of studying numerically a model which should be considered as our "experiment". For this purpose we would like to select the simplest system which classically behaves in ways "representative" of the non-integrable conservative systems in which we are interested. This is well satisfied by the two-dimensional quartic oscillator governed by the Hamiltonian,

$$H(\lambda, b) = \frac{p_1^2 + p_2^2}{2m} + a(\lambda)(q_1^4/b + bq_2^4 + 2\lambda q_1^2 q_2^2)\,. \tag{2.1}$$

The factor $a(\lambda)(>0)$ has no effect on the trajectories since it can be eliminated by rescaling the time and, for convenience, it has been chosen such that the volume of phase space enclosed by an arbitrary energy surface E, is given by

$$\int \mathrm{d}\boldsymbol{p}\,\mathrm{d}\boldsymbol{q}\,\Theta(E - H) = (2\pi)^2 E^{3/2}, \tag{2.2}$$

where $\Theta(x)$ is the Heaviside step function [see eqs. (3.18), (3.21)]. The explicit expression for $a(\lambda)$ will be given in section 3. In eq. (2.1), $b > 0$ and $\lambda > -1$ insure that H is bounded from below. Here $b \neq 1$ is introduced to lower the system's symmetry and λ determines the desired coupling of the two modes (see refs. [25, 27]).

As we shall see in more detail ahead, this Hamiltonian is in fact quite suitable. First of all, by varying the parameter λ, the system can be changed continuously from an integrable case toward one regarded as "completely chaotic" in the sense that almost all trajectories explore the entire energy surface [37]*). In doing so the system goes through a wide variety of intermediate behaviors from which one can select depending on the interest. In the neighborhood of a regular case, the Kolmogorov–Arnol'd–Moser (KAM) and Poincaré–Birkhoff theorems [47] ensure that regular trajectories alternate densely with chaotic ones, which each explore only a tiny fraction of the energy surface. These systems are generally named quasi-integrable or "KAM systems". Further from integrability, systems become mixed. Regions where invariant tori and weakly chaotic motion

*) In fact very recently Dahlqvist and Russberg [46] have shown that even the pure $q_1^2 q_2^2$ potential contains some stable periodic orbits, giving rise to tiny regular islands which have not been detected by previous authors.

alternate densely, called KAM regions, may be thought of as being embedded in an overall chaotic background.

Secondly, the fact that the potential $V(\boldsymbol{q})$ is homogeneous implies scaling properties for H and the classical study is needed only on a single energy surface. This prevents the possibility of confusing deviations from the semiclassical limit with effects coming from the energy variation of the structure of phase space. Thirdly, the system has but two degrees of freedom, which is the minimum for a non-integrable time-independent Hamiltonian. Surfaces of section are two dimensional, which together with the scaling properties, greatly simplifies the classical numerical study. Finally, we remark that besides the uncoupled $(\lambda, b) = (0, b)$ or $(3,1)$ and radial $(1,1)$ integrable cases there are at least two non-trivial ones, $(3/2, 1/4)$ and $(3\sqrt{2}/4, 1/2\sqrt{2})$ [48]. Together with the essentially completely chaotic cases, one has a good "control" group on which to verify what is already known.

The only property of this system conceivably undesirable or in a sense non-generic arises from the fact that Arnol'd diffusion does not exist in systems having less than three degrees of freedom so that in two dimensions more than one isolated chaotic region may exist. However, diffusion-like processes still exist across weakly broken barriers (remnants of tori in phase space), which may have some similar effects on the quantum system as the diffusion of Arnol'd.

This being stated, we proceed with the description of the classical motion. We begin with some very general and basic comments and end this section with more specific ones concerning the phase space structure for a few selected cases.

2.1. General properties

As already stated, one of the most important characteristics of the system is its scaling properties. One can easily check that for any Hamiltonian of the form

$$H = \boldsymbol{p}^2/2m + V(\boldsymbol{q}), \tag{2.3}$$

if the potential V is such that

$$V(\alpha\boldsymbol{q}) = \alpha^{\mu} V(\boldsymbol{q}) \quad (\mu = 4 \text{ in our case}), \tag{2.4}$$

then to each solution

$$\boldsymbol{x}^0(t) = (\boldsymbol{p}^0(t), \boldsymbol{q}^0(t)) \quad \text{with } H(\boldsymbol{x}^0) = E^0 \tag{2.5}$$

of Hamilton's equations, we can associate at each energy E a solution given by

$$\boldsymbol{p}^E(t) = \left(E/E^0\right)^{1/2} \boldsymbol{p}^0(\gamma t), \qquad \boldsymbol{q}^E(t) = \left(E/E^0\right)^{1/\mu} \boldsymbol{q}^0(\gamma t), \tag{2.6}$$

$$\gamma = \left(E/E^0\right)^{[1/2-1/\mu]} \to \left(E/E^0\right)^{1/4}$$

(the arrow indicates the result for the quartic oscillator). In particular, this means that to a closed orbit with period T^0 there corresponds a closed orbit with period

$$T^E = (1/\gamma) T^0 \to \left(E/E^0\right)^{-1/4} T^0 \tag{2.7}$$

at the energy E. Moreover, each action integral

$$I^0 = \int_{C^0} \boldsymbol{p}^0 \cdot \mathrm{d}\boldsymbol{q}^0 \tag{2.8}$$

taken on a path C^0 just scales as

$$I^E = \int_{C^E} \boldsymbol{p} \cdot \mathrm{d}\boldsymbol{q} = \left(E/E^0\right)^{[1/2+1/\mu]} I^0 \to \left(E/E^0\right)^{3/4} I^0 \tag{2.9}$$

on the corresponding path C^E at energy E. For convenience then, in the rest of the paper E^0 will be set equal to one and the quantities so defined will be denoted by a superscript zero. It should also be noticed that in general the Hamiltonian is invariant under the group of transformations, reflections and time reversal, generated by

$$P_i : q_i \to -q_i,\ p_i \to -p_i \quad (i = 1,2), \qquad \mathrm{TR} : t \to -t. \tag{2.10}$$

This means that starting from a solution

$$\boldsymbol{x}(t) = (p_1(t), p_2(t), q_1(t), q_2(t)) \tag{2.11}$$

of Hamilton's equations, the corresponding motions

$$\begin{aligned} &(-p_1(t), p_2(t), -q_1(t), q_2(t)), \\ &(p_1(t), -p_2(t), q_1(t), -q_2(t)), \\ &(-p_1(-t), -p_2(-t), q_1(-t), q_2(-t)) \end{aligned} \tag{2.12}$$

as well as those constructed by a composition of such transformations are also solutions. Of course, the so generated solutions need not correspond to the same trajectory as the original one, although this may sometimes occur.

In some special cases, the system has a higher symmetry. For instance, when b is taken equal to one, the symmetry of the rectangle (i.e., P_1, P_2) is replaced by the symmetry of the square (i.e., P_1, P_2, P_{1+2}, where P_{1+2} is particle interchange or equivalently the reflection across the diagonal $q_1 + q_2$). In this particular case, by performing a $\pi/4$ rotation of the coordinate space, the Hamiltonian just becomes

$$H = \frac{p_1^2 + p_2^2}{2m} + a(\lambda)\,(1+\lambda)\left[q_1^4 + q_2^4 + 2\left(\frac{3-\lambda}{1+\lambda}\right) q_1^2 q_2^2\right] \tag{2.13}$$

[note: $a((3-\lambda)/(1+\lambda)) = a(\lambda)(1+\lambda)$], which means that the Hamiltonians corresponding to the parameters λ and $(3-\lambda)/(1+\lambda)$ are equivalent. The range of interest for $\lambda \in [-1, +\infty]$ can therefore be reduced to $[-1, +1]$. The case $\lambda = -1$ actually corresponds to $\lambda = +\infty$,

$$H = \frac{p_1^2 + p_2^2}{2m} + q_1^2 q_2^2, \tag{2.14}$$

which is essentially completely chaotic and is quite interesting, in part because the phase space is non-compact yet the spectrum is discrete [49].

2.2. *Surfaces of section*

As shall be implicit in sections 3 to 6, one can simplify the quantum, semiclassical and level statistic calculations with the symmetry of the rectangle, C_{2v}, rather than that of the square, C_{4v}. We have therefore chosen $b = \pi/4$, which is sufficiently far from unity to avoid being disturbed by

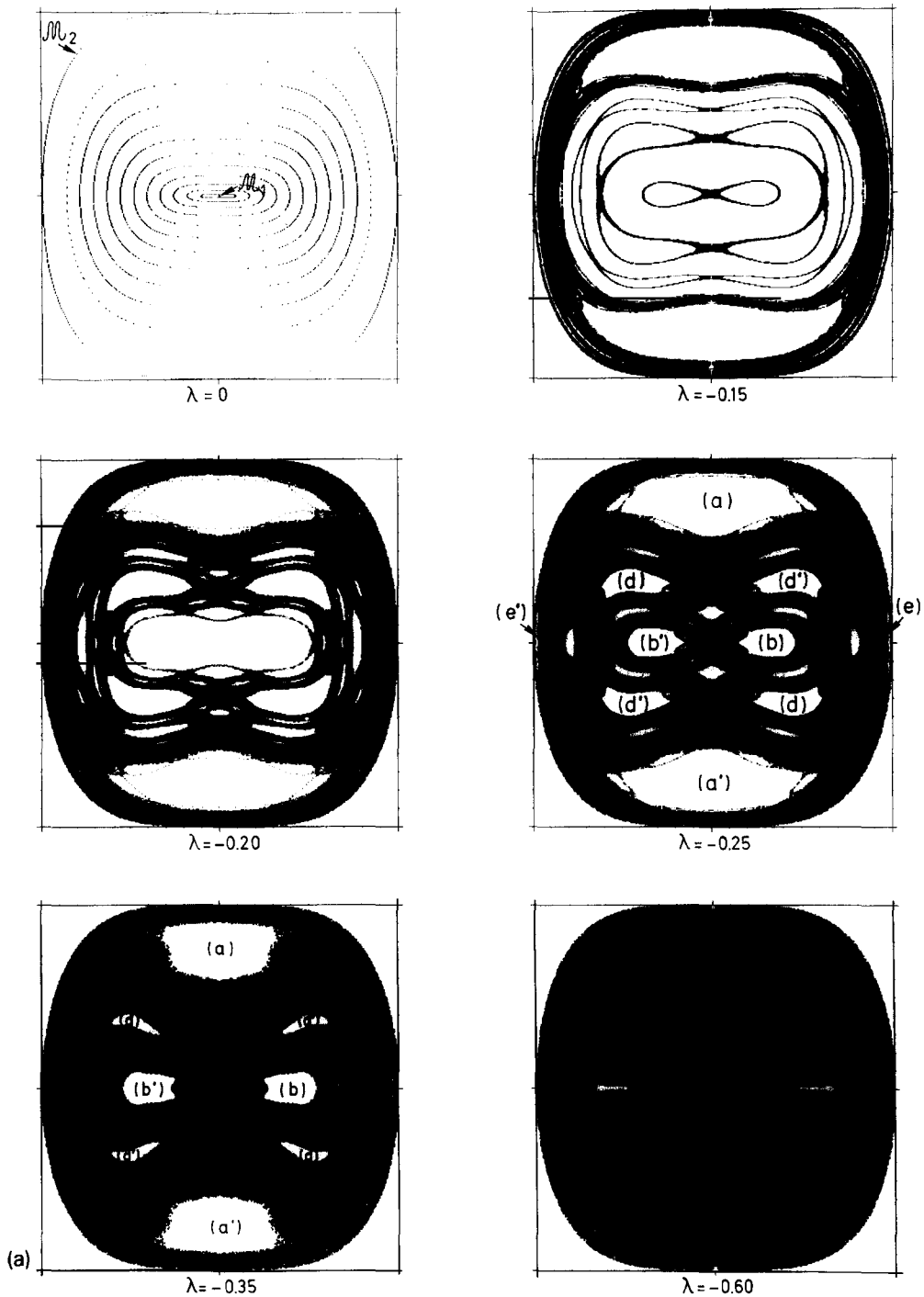

Fig. 1. Poincaré sections corresponding to the Hamiltonian given by eq. (2.1) for $b = \pi/4$ and ordered by decreasing values of λ (increasing coupling). For $\lambda = 0$, the location of the two one dimensional motions $\mathcal{M}_1$ and $\mathcal{M}_2$ shown in fig. 2 is indicated. (a) $q_1 = 0$ sections.

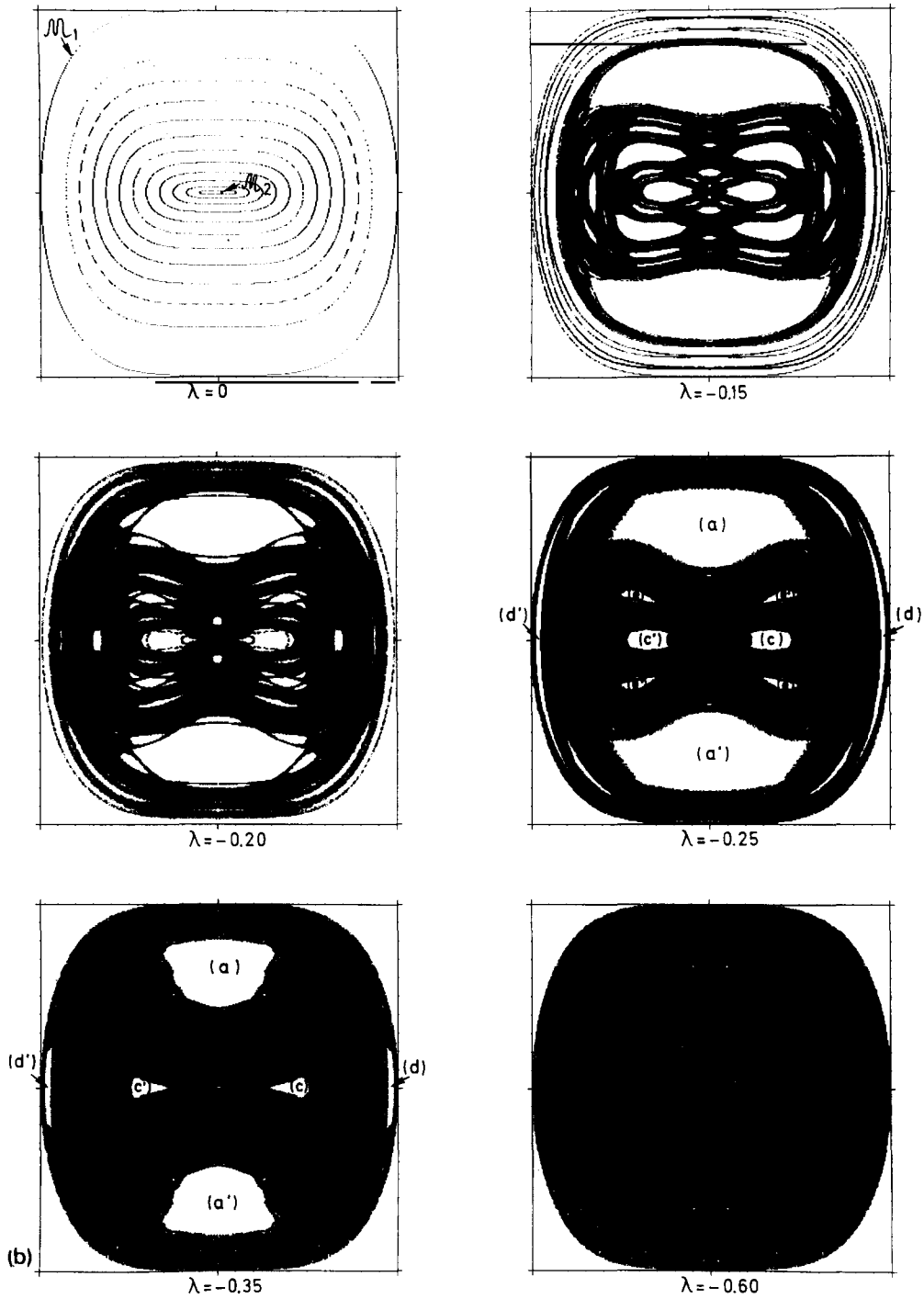

Fig. 1 (contd). (b) $q_2 = 0$ sections.

the nearness of the higher symmetry, and sufficiently close to it that the system is not effectively one dimensional.

For this value of b, although $H(\lambda, \pi/4)$ is not actually equivalent to $H((3-\lambda)/(1+\lambda), \pi/4)$, the neighborhood of the $b = 1$ case makes it reasonable not to expect any substantial differences between the ranges $\lambda \in [-1, +1]$ and $\lambda \in [+1, +\infty]$. Moreover, the case $(1, \pi/4)$ being not too far from rotational invariance, the range $\lambda \in [0, 1]$ just governs a competition between the order due to the absence of coupling and that due to the rotational symmetry. Thus, the degree of non-integrability reached in this range remains at a rather low level. We will therefore only consider the variation of λ from 0 to -1, which, as can be seen by analogy with the $b = 1$ case, will interpolate between integrability and (almost) completely chaotic behavior.

In order to organize information about the phase space structures, we shall rely heavily on surfaces of section. This, as usual, consists of numerically integrating the Hamilton equations with initial conditions taken from the relevant intersecting plane; for the quartic oscillators, it is convenient to consider two planes ($q_1 = 0$ and $q_2 = 0$) since there exist trajectories which do not intersect one of them but none which can avoid both. Then each time a trajectory crosses a plane, say $q_2 = 0$ (or $q_1 = 0$), with a positive momentum p_2 (or p_1) the intersection coordinates (q_1, p_1) or (q_2, p_2) are stored. Which means, in practice, that we blacken a pixel corresponding to this point's discretized position. For most of our computations, we use a 360 by 360 grid for the (q_i, p_i) projection, which is our surface of section; the only exceptions to this concern cases where we have used significantly larger grids to explore particular regions or to check precisions. When we take just one initial condition, we call the result after a large number of intersections a Poincaré section of the trajectory. This may define in the plane either a finite number of points, a closed curve, or a two-dimensional region depending on whether the initial point lies on a closed trajectory, on an invariant torus or in a chaotic region. With a proper sampling of Poincaré sections, the structure of the surface of section (i.e., the way it is filled with invariant tori and chaotic regions) can be drawn as carefully as one wishes. With our choice of planes we can also take advantage of the global symmetries of the system which require reflection symmetry with respect to the p_i and q_i axes. Had we chosen other $q_1 = \text{const.}$ or $q_2 = \text{const.}$ planes, the pictures would have had only the symmetry of reflection through the origin. These two surfaces of section then give a complete picture of the classical motion on the entire energy surface.

We may now apply this to understand how the chaos settles in as λ goes to -1; see fig. 1. For $\lambda = 0$, the motion is simply that of two uncoupled quartic oscillators. The appearance of the invariant tori in the surfaces of section are just concentric closed curves centered around the origin. The center of the map and the outer boundary correspond to the two one-dimensional motions $\mathcal{M}_1$ and $\mathcal{M}_2$ in configuration space shown in fig. 2.

As λ starts to decrease toward -1, the equipotential curves in configuration space undergo a concave deformation which raises a sort of hill on the q_1 and q_2 axes; we stress though that this does not create multiple wells and the energy surface remains simply connected. The trajectories $\mathcal{M}_1$ and $\mathcal{M}_2$ become hyperbolic closed orbits (here unstable and isolated), surrounded by a chaotic region which is increasing in size. At the same time, consistent with the KAM and Poincaré–Birkhoff theorems, the rational tori (i.e., the tori for which the winding number, the ratio of the frequencies along the two independent directions, is rational) are broken giving rise to island chains separated by hyperbolic fixed points. Other tori, sufficiently far from the rational ones, remain intact for a while albeit somewhat distorted. Amongst these islands, those which correspond to the trajectories oriented along the diagonal axes grow rapidly in size because of the focusing form of the equipotential corners (and because the rotation number of the original torus is equal to one) and appear as rather large regions of stability in comparison to the rest of the KAM regions.

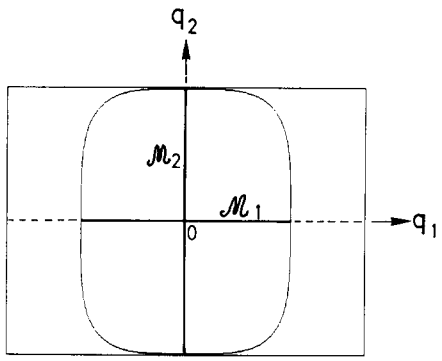

Fig. 2. Equipotential contour in configuration space and the two trajectories $\mathcal{M}_1$ and $\mathcal{M}_2$ along the q_1 and q_2 axes for $(\lambda, b) = (0, \pi/4)$.

When λ reaches a certain value λ^* (λ^* slightly below -0.20), the last irrational tori corresponding to the original structure are destroyed. The remaining tori can be considered as the remnants of the original KAM island structure. All of these tori have a lower symmetry than that of phase space. As a consequence, to each invariant torus there corresponds at least one duplicate which is symmetric by an element of the global symmetry group. This implies that, while the symmetric tori are clearly distinct and separated from the original one, their structure and classical motion are identical. This is a very important point to which we shall return in section 4.

As λ is further decreased from λ^* to -1.0, the proportion of phase space occupied by these regular regions diminishes continually, and reaches a value lower than 0.5% for $\lambda = -0.6$. For $\lambda = -0.7$, no remaining invariant tori can be located within our numerical accuracy. Although some tiny invariant tori may certainly remain, perhaps even until $\lambda = -1.0$, for all practical purposes systems possessing a value of λ in the range $[-1.0, -0.6]$ can be considered as completely chaotic.

2.3. Phase space volume

Let us now introduce some of the classical quantities which will be linked to the quantum properties. One of them is the Liouville measure (volume) of some chaotic or KAM region. Semiclassically, these volumes can be related to the quantum density of levels, and we shall therefore need to evaluate them numerically. However, due to the finite size of $\hbar$, the quantum system at finite energies will certainly not be sensitive to the finest details of phase space, such as very small islands or complicated structures at the boundary of KAM regions. Thus, any method of calculation introducing a coarse graining much smaller than the one due to $\hbar$ appears, for our purposes, as relevant (or more) as one whose aim would be to reach the exact "mathematical" volume. This allows us to use a very simple method that we shall describe now for the example of a chaotic region. The adaptation necessary for any other kind of region is immediate.

Let R^E be the region explored by a single chaotic trajectory belonging to the energy surface E.*) Its relative volume is given by the ratio:

$$f(R^E) = \frac{\int_{R^E} \mathrm{d}\boldsymbol{p}\, \mathrm{d}\boldsymbol{q}\, \delta(E - H)}{\int \mathrm{d}\boldsymbol{p}\, \mathrm{d}\boldsymbol{q}\, \delta(E - H)}. \tag{2.15}$$

*) More properly, R^E is the region covered by a coarse grained single chaotic trajectory.

The first step in calculating eq. (2.15) consists in obtaining a very dense Poincaré section of a trajectory starting in R^E for the two planes $(q_2 = 0)$ and $(q_1 = 0)$. We thus define two surfaces R_1 and R_2 in the spaces (q_1, p_1) and (q_2, p_2) which represent the intersection of R^E with $(q_2 = 0)$ and $(q_1 = 0)$. It should be clear that each region R^E can be scaled to a corresponding region $R^{E'}$ on any other energy surface E'. The fraction $f(R^E)$ is thus independent of the energy. Or, in other words, by separately integrating numerator and denominator over E in eq. (2.15) we find

$$f(R^E) = f(\mathcal{R}) = \frac{\int_{\mathcal{R}} \mathrm{d}\boldsymbol{p}\,\mathrm{d}\boldsymbol{q}\;\Theta(E - H)}{\int \mathrm{d}\boldsymbol{p}\,\mathrm{d}\boldsymbol{q}\;\Theta(E - H)}, \tag{2.16}$$

where $\mathcal{R}$ is the four-dimensional region of the phase space obtained as the union of the $R^{E'}$'s $(0 \leq E' < \infty)$.

We therefore simply apply the following Monte-Carlo method. We select a large number of points at random (with respect to the measure $\mathrm{d}\boldsymbol{p}\,\mathrm{d}\boldsymbol{q}$) lying interior to some suitable energy surface E. Whatever the actual energy of the points obtained, they belong to the region $\mathcal{R}$ if and only if their scaled analogs on $H(\boldsymbol{q},\boldsymbol{p}) = E$ belong to R^E. Thus, we start trajectories from these scaled points and let them evolve until they reach the $q_1 = 0$ or $q_2 = 0$ plane. If the intersecting point belongs to R_1 (or R_2), the original point is then considered to be in $\mathcal{R}$. $f(\mathcal{R})$ is simply the number of points counted divided by the total number. The statistical uncertainty due to the Monte-Carlo method is

$$\Delta f(\mathcal{R}) = \sqrt{f(\mathcal{R})\,[1 - f(\mathcal{R})]/N}, \tag{2.17}$$

where N is the number of initial conditions. Using a value of $N = 10\,000$ (which we do) always leads to $\Delta f(\mathcal{R}) < 0.5\%$.

Control over the boundaries and coarse graining is implied by the use of the Poincaré section on a grid (whose size can vary). For example, small islands and fractal boundary structures between chaotic and regular regions are not taken into account when their size is less than a few pixels (or we blacken/whiten them). When the volumes of separated chaotic regions are needed, and more generally of any region defined through its intersection with the Poincaré sections, this method applies with no essential modifications.*)

2.4. Hamiltonian transport across barriers

We may think of the phase space volumes just introduced as pertaining to an infinite time property of the system in the sense that to know the boundaries of a chaotic region perfectly well essentially requires following a trajectory for an infinite time. It turns out that information concerning the finite time evolution of the classical system, namely the transport properties, has a noticeable effect on the quantum spectral and eigenfunction properties. Our interest here lies in large scale structuring effects deep within the chaotic sea and not in what is happening just exterior to the KAM islands. The former is more relevant to the chaotic spectrum fluctuations whereas the latter concerns more the separation of regular and irregular levels.

To make clear what we call transport properties, one may consider the example of a system constructed with two very chaotic billiards connected by a narrow bottleneck region. For such a

*) Actually, an even simpler method, which does not introduce the Monte-Carlo sampling errors, can be used (see Delande in ref. [6]). It simply consists in counting pixels in a surface of section with the proper weighting (which, with the canonical transformation (2.25), is given by the time between two successive hits of the section). Note also that for most of the KAM islands, eq. (4.23) provides a very good approximation of its volume.

system, the Lyapunov exponent will be quite large, and two close trajectories will instantaneously diverge one from each other. However the motion cannot be considered as completely randomized since, for times not too long, one is almost certain that a trajectory started in one of the billiards will end in the same one. Thus some very strong local chaos may coexist with certain correlations on a larger scale.

For mixed systems, the remnants of invariant tori may produce an equivalent effect for the motion in phase space. As shown by MacKay et al., both cantori [50] (corresponding to irrational original tori) and stable and unstable manifolds of island chains [51] (for rational ones) may act as partial barriers. Here, despite the fact that irrational tori resist destruction longer than rational tori under the influence of a perturbation, we found that in some systems the main role in limiting the transport is played by certain stable and unstable manifolds. As they give rise to a simpler classical investigation and quantum interpretation, and are ultimately relevant to the study of chaotic states, we shall concentrate on them. The simplest example of interest is that of the $(\lambda, b) = (-0.35, \pi/4)$ case. We therefore give an exhaustive study for this case.

The rough structure of the phase space consists of one large chaotic region, which represents about 87% of the phase space volume, and eight main KAM regions [(a), (a'), (b), (b'), (c), (c'), (d), (d')], see fig. 1. When a closer look is taken at the large chaotic region, it reveals that it can be separated into a certain number of weakly connected parts in which trajectories seem to be trapped for a while. As mentioned above, this structure may be traced back to the breaking of certain original rational tori. Consider, for instance, the two islands which constitute (a) and (a'). They correspond to the rational torus with winding number $\alpha = 1$ of the unperturbed system. We know therefore that they are associated with two hyperbolic (unstable) fixed points (here connected by time reversal) of order one, $\mathcal{H}_a$ and $\mathcal{H}_{a'}$, which both represent intersections with the $q_1 = 0$ plane of a hyperbolic closed orbit. Moreover, we know that from both of these closed orbits a stable and an unstable manifold can be generated.

We shall begin the description of how these manifolds may act as partial barriers, following refs. [52, 53], working in a Poincaré section. The interpretation for the continuous flow will be given afterwards. In a two-dimensional Poincaré section, any invariant closed curve forms a complete barrier. A closed curve which is mainly, but not completely, invariant, will in the same manner lead to a small but non-zero flux between the interior and exterior regions. Such a curve can be formed by patching together pieces of stable and unstable (invariant) manifolds.

Let us introduce the area preserving mapping $\mathcal{T}$ which to any point $X = (q_2, p_2)$ of the Poincaré section M_2 (i.e. $q_1 = 0$) associates $X' = \mathcal{T}(X)$, where X' is the next intersection with positive p_1 momentum of a trajectory starting in X, with the $q_1 = 0$ plane. We also denote by W_i^{u}, W_i^{s}, $(i = a, a')$ the curves which are the intersections of the unstable and stable manifolds of the ith periodic orbit with the $q_1 = 0$ plane. We recall that any point X_{s_i} of a curve W_i^{s} is such that

$$\lim_{(n\to\infty)} \mathcal{T}^n(X_{\mathrm{s}_i}) = \mathcal{H}_i \quad (i = a, a'), \tag{2.18}$$

whereas a point X_{u_i} of W_i^{u} satisfies

$$\lim_{(n\to\infty)} \mathcal{T}^{-n}(X_{\mathrm{u}_i}) = \mathcal{H}_i \quad (i = a, a'). \tag{2.19}$$

Moreover, the tangent in X_{s_i} to W_i^{s} corresponds to a direction where the map $\mathcal{T}$ is contracting and the tangent in X_{u_i} to W_i^{u} corresponds to a direction where the map $\mathcal{T}$ is stretching. It follows that, although a stable and an unstable manifold may cross, two stable or two unstable manifolds do not since a contraction or dilation in two independent directions contradicts the area preserving property of $\mathcal{T}$.

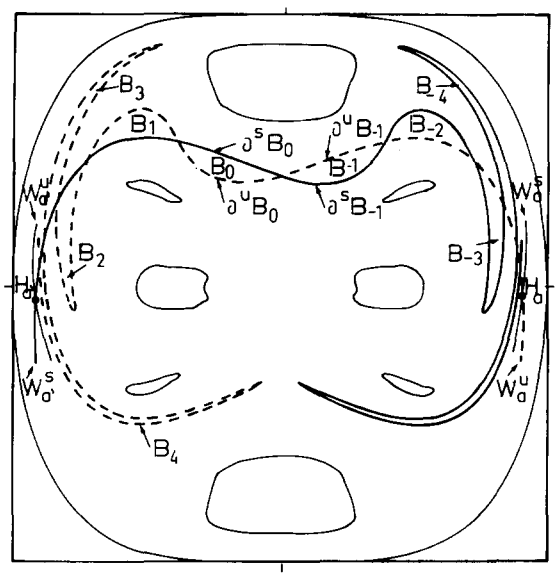

Fig. 3. Intersections of the stable and unstable manifolds W_i^s and W_i^u $(i = a, a')$ starting from the fixed hyperbolic points $H_a, H_{a'}$ and giving rise to a set of bounded regions B_n $(n = \ldots, -2, -1, 0, 1, 2, \ldots)$. H_a and $H_{a'}$ are associated to the islands (a) and (a') displayed in fig. 1. The case $(\lambda, b) = (-0.35, \pi/4)$ is illustrated on the M_2 Poincaré section $q_1 = 0$.

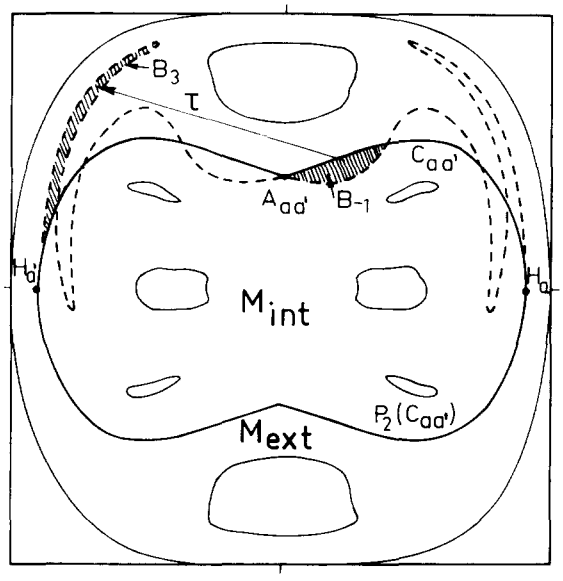

Fig. 4. Construction of a partial barrier illustrated on the $q_1 = 0$ Poincaré section M_2 for $(\lambda, b) = (-0.35, \pi/4)$. Starting from the two fixed hyperbolic points $H_a, H_{a'}$ one follows the stable and unstable manifolds to the primary homoclinic intersection point $A_{aa'}$ and its partner. The shaded flux loop maps in one iteration to the new loop as indicated. See text and fig. 3 for further explanation.

Consider now, for instance, the parts of W_a^u and $W_{a'}^s$ which approach and cross each other . They define a set of loops that we can number from $-\infty$ to $+\infty$, as shown in fig. 3. We thus obtain a set of regions $\ldots, B_{-n}, \ldots, B_0, \ldots, B_n, \ldots$ of M_2, with boundaries $\partial B_k = (\partial B_k^u) \cup (\partial B_k^s)$ (where ∂B_k^u is a portion of W_a^u and ∂B_k^s a portion of $W_{a'}^s$). As both W_a^u and $W_{a'}^s$ are globally invariant under $\mathcal{T}$, the image by $\mathcal{T}$ of any loop B_k must be some other loop $B_{k'}$ [with even $(k - k')$ since $\mathcal{T}$ is an orientation preserving mapping]. In our case,

$$\mathcal{T}(B_k) = B_{k+4}. \tag{2.20}$$

As $\mathcal{T}$ is area preserving, the area of the loop k,

$$I_k = \int_{\partial B_k} p_2 \, \mathrm{d}q_2 = \int_{\partial B_k} \boldsymbol{p} \cdot \mathrm{d}\boldsymbol{q} \tag{2.21}$$

(since $q_1 = 0 \Rightarrow p_1 \, \mathrm{d}q_1 = 0$), is the same for all the k and k' such that $k - k' = 4n$ $(n = \ldots, -1, 0, 1, \ldots)$. Moreover, it can be seen that, in fact, all the I_k are equal. First of all the figure is symmetric under the transformation $q_2 \to -q_2$, giving $I_0 = I_1$ and $I_{-1} = I_2$. Secondly, if we introduce the mapping $\mathcal{T}^*$ defined in the same way as $\mathcal{T}$, but without requiring that p_1 has positive momentum, $\mathcal{T} = (\mathcal{T}^*)^2$, it happens that (because of the time reversal invariance of the system), $\mathcal{T}^*(B_k)$ is symmetric to B_{k+2}. Thus $I_k = I$ for all k.

We can now use these two manifolds to define a continuous line $C_{aa'}$ joining $\mathcal{H}_a$ to $\mathcal{H}_{a'}$ whose construction can be easily understood by looking at fig. 4. Considering an arbitrary B_{k_0}, although

the areas of $B_{k_0+1}, B_{k_0+2}, \ldots$ are constant, the length of $\partial B^{\mathrm{u}}_{k_0+n}$ increases exponentially with n while that of $\partial B^{\mathrm{s}}_{k_0+n}$ exponentially decreases. In the same way, $\partial B^{\mathrm{u}}_{k_0-n}$ decreases with n while $\partial B^{\mathrm{s}}_{k_0-n}$ increases. We can therefore define $C_{aa'}$ as being equal, for all the k, to the shortest among $\partial B^{\mathrm{u}}_k$ and $\partial B^{\mathrm{s}}_k$. Thus, starting from $\mathcal{H}_a$, $C_{aa'}$ will follow W^{u}_a until some point $A_{aa'}$ of $W^{\mathrm{s}}_a \cap W^{\mathrm{u}}_{a'}$. Then $C_{aa'}$ switches to $W^{\mathrm{s}}_{a'}$, where it remains until $\mathcal{H}_{a'}$ is reached. $C_{aa'}$ and its symmetric $P_2(C_{aa'})$ [see eq. (2.10)] form a closed line which divides M_2 into an interior part M_{int} and an exterior part M_{ext}. A point X of M_{int} usually has its successive images $\mathcal{T}(X)$, $\mathcal{T}^2(X)$, and so on, in M_{int}. This lasts until, progressing from loop to loop, $\mathcal{T}^n(X)$ enters one of the loops B_{-1} or B_{-3}, which constitute the exit of the turnstile, or one of their twin brothers on the lower half of the Poincaré section, and is swept across the barrier. The same image applies to each point of M_{ext}. Thus, at each application of $\mathcal{T}$, there is but an area $4I$ of points of M_{int} which escape from it. The same area enters from M_{ext} (which must be the case, since the areas of M_{int} and M_{ext} must be conserved).

We have therefore obtained, in a simple well defined way, a closed curve of M_2 which allows only a limited flow through it by application of $\mathcal{T}$. As a limiting case, if we were considering a resonance in an integrable system, these two manifolds would simply form a separatrix (or equivalently loops of zero area), thus acting like a perfect barrier. At the opposite extreme such loops may have an area of the order of the areas $\mathcal{A}_{\mathrm{int}}$ or $\mathcal{A}_{\mathrm{ext}}$ of the regions it connects. When the area of points exchanged reaches the value $\mathcal{A}_{\mathrm{int}}\mathcal{A}_{\mathrm{ext}}/\ (\mathcal{A}_{\mathrm{int}} + \mathcal{A}_{\mathrm{ext}})$, the probability that a point P crosses the barrier is the same as if $\mathcal{T}(P)$ was chosen at random, making the barrier completely ineffective.

Since there is an infinity of hyperbolic fixed points in M_2, one has to decide "a priori" which are the ones giving rise to effective barriers. For systems, like the quartic oscillators, which can be obtained by perturbing a regular system, it is convenient to consider a resonant structure as a whole: the structure containing the KAM island and the stable and unstable manifolds. Such a structure may or may not survive when the coupling parameter is varied. For our purpose, only those resonances whose island is visible play a role in limiting the transport. We have performed this construction for each of the hyperbolic points which correspond to an island chain remaining from the original structure; note they belong to some of the shortest periodic orbits. It leads us to a separation of the chaotic region into eleven more or less connected regions. These regions are represented in fig. 5. Their area and the transport fluxes connecting them are given in table 1 as well as the relative volumes f_i of the associated regions in the energy surface $H = E$.

For the motion in phase space, a global image now follows. To begin with, we can associate a region on the energy surface to each one in the Poincaré section. The former is simply defined as the set of points on the energy surface such that the next intersection with the Poincaré section lies in the latter. This definition introduces a negligible arbitrariness (for the points intersecting the Poincaré section in a turnstile's loop) since the region defined on the energy surface slightly depends on the choice of the plane we use as a section. It should be possible to eliminate this arbitrariness by a more technical definition (for instance by requiring that the diameter of the turnstile's loop is minimum). But, since this arbitrariness concerns a region of negligible volume, we will simply forget about it.

Since the only way to go from one region to a neighboring one consists in crossing the turnstile's loops defined above, the flow in a unit of time between two regions is related to the flow across the turnstile's loops (which we generically denote by B) by

$$\Phi_B = \frac{1}{T} \int_{R_{[B\times T]}} \mathrm{d}\boldsymbol{p}\, \mathrm{d}\boldsymbol{q}\, \delta(E - H), \tag{2.22}$$

where $R_{[B\times T]}$ is the tube of trajectories which are going to cross the loop in less than the time T.

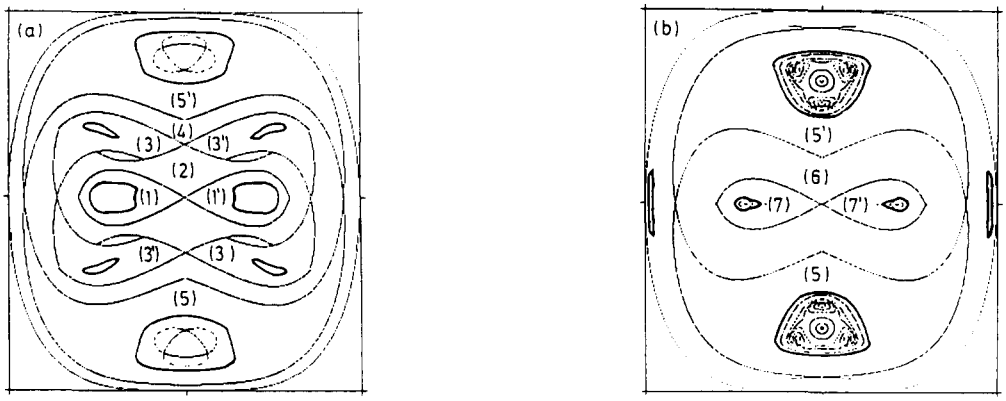

Fig. 5. Different regions in phase space separated by partial barriers for the case $(\lambda, b) = (-0.35, \pi/4)$; (a) $q_1 = 0$ Poincaré section, and (b) $q_2 = 0$ Poincaré section. The regular islands are also outlined. See text for further explanation.

If the concerned loop is, for instance, in the $q_1 = 0$ plane, the volume

$$V(R_{[B\times T]}) = \int_{R_{[B\times T]}} \mathrm{d}\boldsymbol{p}\,\mathrm{d}\boldsymbol{q}\;\delta(E-H) \tag{2.23}$$

can be calculated with the help of a simple canonical transformation. Namely, in the neighborhood of the loop and for sufficiently small times the action function

$$S(q_1, q_2, t, q_2^0) = \int_{\boldsymbol{q}^0=\binom{q_1^0=0}{q_2^0}}^{\boldsymbol{q}=\binom{q_1}{q_2}} \mathcal{L}(t')\,\mathrm{d}t' \tag{2.24}$$

Table 1
Relative volume f_i of chaotic phase space of the different regions shown in fig. 5 together with their area in the Poincaré section and their connecting flux. Area and fluxes are calculated for $E = 1$ and scale as $E^{3/4}$.

Region	Relative volume f_i	Area	Total flux	
1	0.03	0.3		
			1↔2	0.05
2	0.09	0.8		
			2↔3	0.07
3	0.13	1.2		
			3↔4	0.13
4	0.13	1.2		
			4↔5	0.21
5	0.36	2.6		
			5↔6	0.28
6	0.21	1.7		
			6↔7	0.12
7	0.05	0.4		

(where $\mathcal{L}$ is the Lagrangian function $\mathcal{L} = \boldsymbol{p}\cdot\boldsymbol{q} - H$) taken on a trajectory joining $\boldsymbol{q}^0$ to $\boldsymbol{q}$ in a time t, is perfectly defined and single valued. If we change coordinate variables to $\boldsymbol{Q} = (t, q_2^0)$, S can be used as the generating function of the transformation

$$(\boldsymbol{q},\boldsymbol{p}) \longrightarrow (\boldsymbol{Q},\boldsymbol{P}) \tag{2.25}$$

since $\partial S/\partial \boldsymbol{q} = \boldsymbol{p}$. The new momentum coordinates are then given by

$$P_1 = -\frac{\partial S}{\partial Q_1} = -\frac{\partial S}{\partial t} = -E\,, \qquad P_2 = -\frac{\partial S}{\partial Q_2} = -\frac{\partial S}{\partial q_2^0} = p_2^0\,. \tag{2.26}$$

Thus, $V(R_{[B\times T]})$ can be calculated as

$$V(R_{[B\times T]}) = T\cdot I\,, \tag{2.27}$$

where $I = \int_{\partial B}\boldsymbol{p}\cdot \mathrm{d}\boldsymbol{q}$, and $\Phi_B = I$. Once again, it is the size of the loops formed by the stable and unstable manifolds that regulates the transport between neighboring regions.

Let us finally note that, when transport takes place very slowly on a scale in which a region is being mixed, it is possible to think of the transport as a kind of Markovian process where every interior point has an equal probability of escaping, albeit small, at the next application of the map $\mathcal{T}$. This supposes of course that no important structures, such as cantori surrounding an island of stability, remains in the region considered. If there are none and the Markovian image is roughly valid, then there is an inverse relation predicted to hold between a suitably defined mean escape time and the relative volume escaping (flux/volume). This relation is confirmed to within 10% or so in the cases we checked, thus excluding the presence of significant barriers other than those we identified. When the effects of transport on the quantum system will be treated in section 5, it is this picture of the diffusion which we will have in mind.

3. The quantum system

We turn now to the quantum quartic oscillators. For quantum Hamiltonians whose potentials have the homogeneity property expressed in eq. (2.4), some special properties result. The eigenvectors and eigenvalues associated with

$$\hat{H} = \hat{\boldsymbol{p}}^2/2m + aV(\hat{\boldsymbol{q}}) \tag{3.1}$$

are simply related by

$$E_n^a = a^{2/(\mu+2)}E_n^0 \longrightarrow a^{1/3}E_n^0\,, \qquad \psi_n^a(\boldsymbol{q}) \propto \psi_n^0(a^{-1/(\mu+2)}\boldsymbol{q}) \longrightarrow \psi_n^0(a^{-1/6}\boldsymbol{q})\,, \tag{3.2}$$

where again the arrows indicate the results for the quartic oscillators and the superscript zero the value corresponding to $a = 1$. One also has (virial theorem)

$$\frac{2}{\mu+2}E_n = \langle\psi_n|\hat{V}|\psi_n\rangle\,. \tag{3.3}$$

Through arguments similar to those leading to eq. (3.2), it can be shown that here the energy eigenvalues are simply related to $\hbar$ eigenvalues of the Schrödinger equation that are found by fixing the energy and searching for solutions by varying $\hbar$; one has $\hbar_i = c_0 E_i^{-3/4}$ for the quartic oscillator,

where c_0 is a constant. This illustrates the equivalence between the $\hbar \to 0$ and $E \to \infty$ limit and we shall use whichever image is more convenient for a particular discussion.

As mentioned in the introduction we will be taking advantage of the discrete symmetries available to us. Excluding the isolated radial case $(\lambda, b) = (1, 1)$, we may select either the symmetry of the square $C_{4v}(b = 1)$, or of the rectangle, $C_{2v}(b \neq 1)$. C_{4v} has five representations, one of which is doubly degenerate. These exact degeneracies would complicate the separation of the regular and irregular levels performed in section 4. To a given energy, the non-degenerate representations each asymptotically contribute 1/8 of the number of states with the remaining half belonging to the doubly degenerate one. To quickly see this, consider the two component reflections and particle exchange. On the other hand, when $b \neq 1$ the symmetry group is C_{2v}. There are just four representations, non-degenerate, classifiable by component parity. Each of the parity sequences contributes 1/4 of the number of states to an energy E (we give a more exact result ahead) and later for the purposes of statistical measures they can be treated "democratically". We thus favor $b \neq 1$.

Our immediate goal is to calculate the spectrum as far and accurately as possible. Interestingly enough though, even this purely quantum "activity", matrix diagonalization, requires rudimentary semiclassical tools. So instead of just describing the quantum calculations made, we first review certain useful ideas that form the beginning of our comprehension of the spectrum. These are then applied to understanding the smoothed level density and finally the calculations.

3.1. "Quantum phase space"

We will find it useful, elsewhere in the paper as well as here, to have a direct intuitive link between classical and quantum systems. It would therefore be good to have the notion of a "quantum phase space". Some of the various possibilities along with their most important properties are reviewed in ref. [54], where these spaces are dubbed "mock phase spaces". For our purpose we can adopt the definition of Moyal [55]; he originally introduced it in order to incorporate the statistical interpretation of quantum mechanics more naturally into its foundations. The basic idea is that the most natural way to proceed is to consider the characteristic function of an eigenstate and its inverse Fourier transform. Then since we restrict ourselves to systems which are representable in either a $\boldsymbol{q}$ or a $\boldsymbol{p}$ representation (no spin for example), wave functions are associated with distributions in quantum phase space via the Wigner transform [56] and its inverse (given below). We shall not enter into the details here except to summarize the most interesting properties of which we shall make use.

First of all, the Wigner transform of an operator $\hat{A}$ and its inverse are given by

$$\begin{aligned} A(\boldsymbol{q},\boldsymbol{p}) \equiv [A]_{\mathrm{w}}(\boldsymbol{q},\boldsymbol{p}) &= \int \mathrm{d}\boldsymbol{x}\, \mathrm{e}^{-\mathrm{i}\boldsymbol{p}\cdot\boldsymbol{x}/\hbar} \langle \boldsymbol{q} + \tfrac{1}{2}\boldsymbol{x}|\hat{A}|\boldsymbol{q} - \tfrac{1}{2}\boldsymbol{x}\rangle , \\ \langle \boldsymbol{q}_1|\hat{A}|\boldsymbol{q}_2\rangle &= \frac{1}{(2\pi\hbar)^d} \int \mathrm{d}\boldsymbol{p}\, \mathrm{e}^{\mathrm{i}\boldsymbol{p}\cdot(\boldsymbol{q}_1-\boldsymbol{q}_2)/\hbar} A(\tfrac{1}{2}(\boldsymbol{q}_1 + \boldsymbol{q}_2), \boldsymbol{p}) , \end{aligned} \tag{3.4}$$

where d is the number of degrees of freedom. Note that this is consistent with the Weyl [57] prescription for constructing the corresponding quantum operator from a classical function in phase space; he arrived at this result by way of group considerations. In the case that $\hat{A}$ is a projector $\hat{\rho}_{kk} = |\psi_k\rangle\langle\psi_k|$, eq. (3.4) gives the Wigner transform and inverse of a wave function. Next we see that the trace just becomes an integral over the phase space volume element. For systems with d degrees of freedom,

$$\mathrm{Tr}(\hat{A}) = \frac{1}{(2\pi\hbar)^d} \int \mathrm{d}\boldsymbol{q}\, \mathrm{d}\boldsymbol{p}\ [A]_{\mathrm{w}}(\boldsymbol{q},\boldsymbol{p}) . \tag{3.5}$$

Also note that

$$\mathrm{Tr}(\hat{A}\hat{B}) = \frac{1}{(2\pi\hbar)^d}\int \mathrm{d}\boldsymbol{p}\,\mathrm{d}\boldsymbol{q}\;[A]_{\mathrm{w}}(\boldsymbol{q},\boldsymbol{p})[B]_{\mathrm{w}}(\boldsymbol{q},\boldsymbol{p})\,, \tag{3.6}$$

from which the cyclic invariance of the trace is clear. By combining traces and various combinations of operators of the form $\hat{\rho}_{lk} = |\psi_l\rangle\langle\psi_k|$, where the ψ_k form an orthonormal representation, we have the following orthogonality and completeness relations [note: $\rho^*_{lk}(\boldsymbol{q},\boldsymbol{p}) = \rho_{kl}(\boldsymbol{q},\boldsymbol{p})$],

$$\begin{aligned}
&\sum_l \rho_{ll}(\boldsymbol{q},\boldsymbol{p}) = 1\,,\\
&\frac{1}{(2\pi\hbar)^d}\int \mathrm{d}\boldsymbol{p}\,\mathrm{d}\boldsymbol{q}\;\rho_{lk}(\boldsymbol{q},\boldsymbol{p}) = \delta_{lk}\,,\\
&\frac{1}{(2\pi\hbar)^d}\int \mathrm{d}\boldsymbol{p}\,\mathrm{d}\boldsymbol{q}\;\rho_{lk}(\boldsymbol{q},\boldsymbol{p})\rho^*_{l'k'}(\boldsymbol{q},\boldsymbol{p}) = \delta_{ll'}\delta_{kk'}\,,\\
&\sum_{l,k}\rho_{lk}(\boldsymbol{q},\boldsymbol{p})\rho^*_{lk}(\boldsymbol{q}',\boldsymbol{p}') = (2\pi\hbar)^d\delta(\boldsymbol{q}-\boldsymbol{q}')\delta(\boldsymbol{p}-\boldsymbol{p}')\,.
\end{aligned} \tag{3.7}$$

This leads to the notion that the Wigner transform of any normalized wave function occupies a volume $(2\pi\hbar)^d$ in this phase space. Furthermore these volumes are non-overlapping for orthonormal wave functions in the sense that the third relation of eq. (3.7) holds with $k = l$ and $k' = l'$. In actual fact they may overlap; however, oscillations (negative densities) offset this to preserve eq. (3.7).

Finally we have the product rule,

$$[AB]_{\mathrm{w}}(\boldsymbol{q},\boldsymbol{p}) = [A]_{\mathrm{w}}(\boldsymbol{q}',\boldsymbol{p}')\mathrm{e}^{\mathrm{i}\hbar\overleftrightarrow{\Lambda}/2}[B]_{\mathrm{w}}(\boldsymbol{q}'',\boldsymbol{p}'')\big|_{\substack{\boldsymbol{q}'=\boldsymbol{q}''=\boldsymbol{q}\\ \boldsymbol{p}'=\boldsymbol{p}''=\boldsymbol{p}}}\,, \tag{3.8}$$

where $\overleftrightarrow{\Lambda}$ is the Moyal bracket,

$$\overleftrightarrow{\Lambda} = \overleftarrow{\nabla}_{\boldsymbol{q}'}\cdot\overrightarrow{\nabla}_{\boldsymbol{p}''} - \overrightarrow{\nabla}_{\boldsymbol{q}''}\cdot\overleftarrow{\nabla}_{\boldsymbol{p}'}\,. \tag{3.9}$$

To simplify notation, it is customary to insert Moyal brackets between the operators they act on and drop the primes. They play the role of the classical Poisson brackets. For the equation of motion for a density in phase space associated with a wave function this leads to

$$\partial\rho_{kk}(\boldsymbol{q},\boldsymbol{p})/\partial t = (2/\hbar)H(\boldsymbol{q},\boldsymbol{p})\sin(\hbar\overleftrightarrow{\Lambda}/2)\,\rho_{kk}(\boldsymbol{q},\boldsymbol{p})\,, \tag{3.10}$$

which, when higher order terms can be neglected, reduces to the form of the Liouville equation for densities in classical phase space, so that for times not too long, densities in this quantum phase space associated with a wave function transform in time exactly as their classical counterparts.

3.2. Level densities

These tools can be easily applied to study the mean level density $\bar{\rho}(E)$, which will be needed in section 5 to perform the unfolding necessary for the fluctuation studies [15]. Moreover the first term of the $\hbar$ expansion of $\bar{\rho}(E)$ will be used to define $a(\lambda)$ for reasons concerning the spectral calculations. Here we only consider the quantum spectrum on the roughest scale, that of the "locally smoothed" level density. By local smoothing we mean that we calculate an average level density,

$\bar{\rho}(E)$, as a function of the energy in intervals which are infinitesimal on the scale in which the average changes yet large enough that fluctuations disappear (only in the case that this is possible does it really make sense to discuss level fluctuations). A priori it is not clear such an averaging exists, yet in general it is found, for simple systems amenable to analytical $\bar{\rho}(E)$ calculations (it is necessary to avoid very narrow classically allowed regions, etc.), the first few terms of a formal expansion in powers of $\hbar$ works well right to the ground state. In fact a partial understanding of this problem comes by considering the trace formula over periodic orbits [10, 58] where the longest length fluctuations about $\bar{\rho}(E)$ are related to the shortest periodic orbit, so that, if one imagines smearing the energies such that each level acquires a width which spreads over several of these characteristic lengths, the fluctuations would disappear.

For simplicity, we present a standard approach, equivalent to using the time-dependent Green function, where successive terms in $\hbar$ follow recursively. Contrary to the Gutzwiller trace formula, this method selects by construction, though for reasons not fully understood, the average parts $\bar{\rho}(E)$ of the density operator (i.e., only the residue of the trace, $\mathrm{Tr}[\mathrm{e}^{-\beta\hat{H}}]$ located at the origin is kept).

We restrict ourselves to positive definite Hamiltonians whose potentials are differentiable. The first step is to consider the level density and its Laplace transform,

$$\begin{aligned} \rho(E) &= \mathrm{Tr}(\delta(E-\hat{H})) = \sum_i \delta(E-E_i)\,, \\ Z(\beta) &= \int_0^\infty \mathrm{e}^{-\beta E}\rho(E)\,\mathrm{d}E = \mathrm{Tr}(\mathrm{e}^{-\beta\hat{H}}) = \sum_i \mathrm{e}^{-\beta E_i} = \frac{1}{(2\pi\hbar)^d}\int \mathrm{d}\boldsymbol{q}\,\mathrm{d}\boldsymbol{p}\,[\mathrm{e}^{-\beta H}]_{\mathrm{w}}(\boldsymbol{q},\boldsymbol{p})\,, \end{aligned} \tag{3.11}$$

where the last form comes by simple application of eq. (3.5). For convenience we also introduce the integrated density (spectral staircase) $N(E)$, which counts the number of levels up to an energy E and is given by

$$N(E) = \mathrm{Tr}(\Theta(E-\hat{H})) = \sum_i \Theta(E-E_i)\,, \qquad \rho(E) = \mathrm{d}N(E)/\mathrm{d}E\,, \tag{3.12}$$

where Θ is the Heaviside step function. The real job now is to calculate the Wigner transform of $\exp(-\beta\hat{H})$. An equation is easily generated by taking a derivative with respect to β, applying the product rule in eq. (3.8) and recognizing that H commutes with any function of itself; we have

$$\begin{aligned} -\partial[\mathrm{e}^{-\beta H}]_{\mathrm{w}}(\boldsymbol{q},\boldsymbol{p})/\partial\beta &= [H]_{\mathrm{w}}(\boldsymbol{q},\boldsymbol{p})\cos(\hbar\overleftrightarrow{\Lambda}/2)[\mathrm{e}^{-\beta H}]_{\mathrm{w}}(\boldsymbol{q},\boldsymbol{p})\,, \\ 0 &= [H]_{\mathrm{w}}(\boldsymbol{q},\boldsymbol{p})\sin(\hbar\overleftrightarrow{\Lambda}/2)[\mathrm{e}^{-\beta H}]_{\mathrm{w}}(\boldsymbol{q},\boldsymbol{p})\,. \end{aligned} \tag{3.13}$$

We see immediately the absence of any dependence odd in $\hbar$, which is unlike billiards*). One way to solve this equation is to assume a solution of the form

$$[\mathrm{e}^{-\beta H}]_{\mathrm{w}}(\boldsymbol{q},\boldsymbol{p}) = \mathrm{e}^{-\beta[H]_{\mathrm{w}}(\boldsymbol{q},\boldsymbol{p})}\sum_{n=0}^{\infty}\left(\frac{-\hbar^2}{4}\right)^n \frac{A_n(\boldsymbol{q},\boldsymbol{p},\beta)}{(2n)!}\,, \tag{3.14}$$

*) When using the limit $n\to\infty$ of the potential $V(\hat{q}) = \hat{q}^{2n}$ as an approximation of the one-dimensional "billiard" with the wall located at $q = \pm 1$, one should pay attention to the fact tat the limits $n\to\infty$ and $E\to\infty$ (i.e. $\hbar\to 0$) cannot be interchanged.

where $A_0 = 1$ so that the classical result is recovered when $\hbar$ is put to zero. Then by grouping terms according to their power of $\hbar$ we find

$$-\frac{\partial A_n}{\partial \beta} = \mathrm{e}^{\beta H_w} \sum_{k=0}^{n-1} \binom{2n}{2k} \left[H_w \overleftrightarrow{\Lambda}^{2n-2k} \mathrm{e}^{-\beta H_w} A_k \right]. \tag{3.15}$$

The A_n are calculable recursively. Of course the specific recursion may simplify depending on the system as happens for Hamiltonians with low order polynomial potentials. The first correction, A_1, derived by Wigner [56] is given by

$$A_1(\boldsymbol{q},\boldsymbol{p},\beta) = \frac{1}{m}\left(\beta^2 \nabla^2 V(\boldsymbol{q}) - \frac{\beta^3}{3m}[m \nabla V(\boldsymbol{q}) \cdot \nabla V(\boldsymbol{q}) + (\boldsymbol{p} \cdot \nabla)^2 V(\boldsymbol{q})]\right). \tag{3.16}$$

This is not the only way to produce a solution to eq. (3.13). It so happens an exponentiated series in $\hbar$ of the form

$$[\mathrm{e}^{-\beta H}]_w(\boldsymbol{q},\boldsymbol{p}) = \exp\left[\sum_{n=0}^{\infty} \left(\frac{-\hbar^2}{4}\right)^n \frac{A'_n(\boldsymbol{q},\boldsymbol{p},\beta)}{(2n)!}\right] \tag{3.17}$$

can also be used. In fact, $A'_0 = -\beta H_w$ and A_1 is identical to the A'_1. For $n \neq 1$, however, the A'_n generated by eq. (3.17) are distinct from the A_n obtained through eq. (3.14) since the exponentiation groups and sums classes of terms.

To calculate the smoothed level density we calculate the number of terms needed in $[\mathrm{e}^{-\beta H}]_w(\boldsymbol{q},\boldsymbol{p})$, integrate over phase space and perform the inverse Laplace transform. For the quartic oscillators to two terms, the result for the integrated version is

$$\begin{aligned} \overline{N}(E) &= \frac{2K((1-\lambda)/2)}{3\pi} \frac{mE^{3/2}}{\hbar^2 a(\lambda)^{1/2}} - \frac{(b^{-1/2} + b^{1/2})(3+\lambda)}{24\sqrt{2(1+\lambda)}} + O(\hbar^2 E^{-3/2}), \\ K(z) &= \int_0^{\pi/2} \mathrm{d}\theta\, (1 - z \sin^2\theta)^{-1/2}, \end{aligned} \tag{3.18}$$

where $K(z)$ is a complete elliptic integral of the first kind. For our purposes the terms having an inverse energy dependence are unimportant so that this suffices. However, we are interested in the parity decomposition. Since the spectra are calculated for each of the four sequences (ϵ_1, ϵ_2) $(\epsilon_i = \pm 1)$ denoted by their component parity in (q_1, q_2), we add a symmetry decomposition to eq. (3.18). This is easily accomplished by using eq. (3.6) along with the Wigner transform of the parity operator, which is given by

$$[P_i]_w(\boldsymbol{q},\boldsymbol{p}) = \pi\hbar\delta(q_i)\delta(p_i) \qquad (i = 1,2), \tag{3.19}$$

so that the decomposed $\overline{N}(E)$ is

$$\begin{aligned} \overline{N}_{\epsilon_1,\epsilon_2}(E) = \frac{1}{4}\Bigg[&\frac{2K((1-\lambda)/2)}{3\pi} \frac{mE^{3/2}}{a(\lambda)^{1/2}\hbar^2} + \frac{\Gamma(\frac{1}{4})^2(\epsilon_1 b^{-1/4} + \epsilon_2 b^{1/4})}{6\pi^{3/2}} \frac{m^{1/2}E^{3/4}}{a(\lambda)^{1/4}\hbar} \\ &- \frac{(b^{-1/2} + b^{1/2})(3+\lambda)}{24\sqrt{2(1+\lambda)}} + \epsilon_1\epsilon_2 \frac{1}{4}\Bigg] + O(\hbar E^{-3/4}) \end{aligned}$$

$$= \frac{1}{4}\left[E^{3/2} + \frac{\epsilon_1 b^{-1/4} + \epsilon_2 b^{1/4}}{2\sqrt{6}\pi K^{1/2}((1-\lambda)/2)} E^{3/4} - \frac{(b^{-1/2} + b^{1/2})(3+\lambda)}{24\sqrt{2(1+\lambda)}} + \epsilon_1\epsilon_2 \frac{1}{4}\right] + O(E^{-3/4}) \,. \tag{3.20}$$

In the last equality, energies are measured in units of

$$\left[\frac{3\pi}{2K((1-\lambda)/2)} \frac{a(\lambda)^{1/2}\hbar^2}{m}\right]^{2/3},$$

which amounts to taking

$$a(\lambda)^{1/2} = \frac{2K((1-\lambda)/2)}{3\pi} \frac{m}{\hbar^2} \,. \tag{3.21}$$

In this way $\hbar_i = E_i^{-3/4}$ fixing the constant c_0 defined at the beginning of the section and $\overline{N}(E)$ is independent of λ to leading order*). This simplifies the scaling aspects for the quantum calculations described in the next subsection. Note that a decomposition for quantum statistics (for example, fermion statistics) is also easily produced in the same way again since the Wigner transforms of the permutation group elements by themselves are very simple (δ-functions). It would have been more difficult to produce the higher symmetry decomposition necessary for the $b = 1$ case in this simple way because the Wigner transform of the combined operations of permutation and parity no longer results in a δ-function form but instead an exponential phase with an $\hbar$ factor; the series solution then is insufficient so that a different approach is needed.

3.3. *The spectral calculations*

To calculate the spectrum we choose a matrix diagonalization technique since it is simple and works well with low order polynomial potentials.

In general the calculation starts by expressing the matrix element of the Hamiltonian $\hat{H}$ in a basis defined as the eigenvectors of some integrable (usually separable) $\hat{H}_0$. Then, truncating the basis at the dth vector and diagonalizing the finite matrix correctly gives the energy levels associated with eigenvalues of $\hat{H}$ which are almost contained in the truncated space. For anharmonic oscillators, the harmonic oscillator basis has been the usual choice [25, 27]. It is possible, however, to have a deeper understanding of the convergence by applying some simple semiclassical logic and when so understood to have a criterion for choosing the best suited basis (or equivalently $\hat{H}_0$) and how to truncate it. In this way we will be able to calculate extremely accurate and long sequences of levels.

*) The constant $a(\lambda)$ diverges logarithmically with $\lambda \to -1$ just as the classical phase space becomes non-compact. Equation (3.20) is then no longer valid. However, a modified approach taking advantage of eq. (3.17) is possible. With $V = aq_1^2q_2^2$, and introducing the scaled energy $\mathcal{E} = (16m^2/\hbar^4 a)^{1/3}E$, $\overline{N}(\mathcal{E})$ takes on the form

$$\overline{N}(\mathcal{E}) = \frac{\mathcal{E}^{3/2}\ln(\mathcal{E})}{2\pi} + \frac{C_0\mathcal{E}^{3/2}}{3\pi} + O(\mathcal{E}^{-3/2}\ln(\mathcal{E}^{3/2})),$$

where the first term corresponds to Simon's result ref. [49]. The second term is given in ref. [59], $C_0 = 5\ln 2 + 2\gamma - 4$ (where γ is Euler's constant).

Let $|n\rangle$ $(n \in N)$ denote the eigenvectors of $\hat{H}_0$ (with e_n the corresponding eigenenergy) and $|\alpha\rangle$ any eigenstate of $\hat{H}$ of interest $(\hat{H}|\alpha\rangle = E_\alpha|\alpha\rangle)$. One may express the overlap $|\langle n|\alpha\rangle|^2$ as the trace over the product of the two density operators, $\hat{\rho}_{nn}$ and $\hat{\rho}_{\alpha\alpha}$. Using eq. (3.6) we have

$$|\langle n|\alpha\rangle|^2 = \mathrm{Tr}(\hat{\rho}_{nn}\hat{\rho}_{\alpha\alpha}) = \frac{1}{(2\pi\hbar)^2}\int \mathrm{d}\boldsymbol{p}\,\mathrm{d}\boldsymbol{q}\,[\rho_{nn}]_{\mathrm{w}}[\rho_{\alpha\alpha}]_{\mathrm{w}}\,. \tag{3.22}$$

Roughly speaking, it is known that in the semiclassical limit the Wigner transform of an eigenstate with energy E of some quantum Hamiltonian is localized on the classical energy surface [28]. Thus, at this level of approximation, eq. (3.22) implies that the overlap between $|n\rangle$ and $|\alpha\rangle$ is null whenever the two energy surfaces $H_0 = e_n$ and $H = E_\alpha$ do not intersect. In practice, $|\langle n|\alpha\rangle|^2$ is not strictly zero but, to within fluctuations, decreases exponentially fast with the separation distance of the two energy surfaces measured as some function of $\hbar$. $|\alpha\rangle$ and E_α then converge in a calculation which includes in its truncated basis set all $|n\rangle$ whose $H_0 = e_n$ energy surfaces intersect $H = E_\alpha$. The best basis set is the one which has the minimum dimensionality required to make a set of $|\alpha\rangle$ of interest converge.

Now, say one wishes to calculate just a slice of the spectrum, which means finding $\{E_\alpha\}$ for $E_{\min} \le E_\alpha \le E_{\max}$. For the $\hat{H}$ treated here, it is always possible to find an energy surface $H_0 = e_{\max}$ that circumscribes $H = E_{\max}$ and an energy surface $H_0 = e_{\min}$ which inscribes $H = E_{\min}$. The basis then should consist of all $|n\rangle$ such that $e_{\min} \le e_n \le e_{\max}$. As a simple practical example, let $\hat{H} = \hat{p}^2/2 + \hat{q}^4$, $\hat{H}_0 = \hat{p}^2/2 + \omega^2\hat{q}^2/2$, and $E_\alpha \in [E_{\min} = 0, E_{\max}]$. To determine which harmonic oscillator basis to use (i.e., to fix ω), first calculate $e_{\max}$ as a function of ω. Eliminating p from the equation, we find

$$e_{\max} - E_{\max} = \tfrac{1}{2}\omega^2 q^2 - q^4\,. \tag{3.23}$$

For there to be only one intersection point, eq. (3.23) must be a perfect square. Therefore,

$$e_{\max} = E_{\max} + \omega^4/16\,. \tag{3.24}$$

To optimize the basis, one minimizes the dimensionality by setting the derivative of $\overline{N}_{H_0}(e_{\max})$ with respect to ω to zero. This gives

$$\omega^2 = 4E_{\max}^{1/2}/\sqrt{3} \quad \text{and} \quad e_{\max} = 4E_{\max}/3 \tag{3.25}$$

(the proportionality between $e_{\max}$ and $E_{\max}$ is due to the particular potential we use for $\hat{H}$ and $\hat{H}_0$). With this scaling the fraction of converged levels tends asymptotically toward

$$\frac{\overline{N}_H(E_{\max})}{\overline{N}_{H_0}(e_{\max})} = \frac{\Gamma(\frac{1}{4})^2}{6}\left(\frac{3}{\pi^2}\right)^{3/4} \approx 90\%\,. \tag{3.26}$$

For the 2-d coupled quartic oscillator usually a good choice of basis is to take $\hat{H}_0$ as a 2-d uncoupled quartic oscillator $\hat{H}_0 = \hat{\boldsymbol{p}}^2/2 + a_0(b\hat{q}_1^4 + \hat{q}_2^4/b)$. For λ not too close to -1, the H and H_0 energy surfaces will be fairly similar implying good convergence. Furthermore, they have the same scaling properties making the scaling choice of $\hat{H}_0$ energy independent. To calculate a slice of the $\hat{H}$ spectrum at highly excited energy E it turns out that arranging the two equal-energy surfaces $H = E$ and $H_0 = E$ to enclose equal volumes is best, which in this case equates the level densities. This explains our form for $a(\lambda)$ because a_0 can always be taken as $a(\lambda = 0)$ and thus

$\hat{H}_0$ is the same for all $\hat{H}$ we consider. As a final refinement, we have also taken account of the perturbation's diagonal matrix elements $\langle n|\hat{H}-\hat{H}_0|n\rangle$ before truncating the basis; we order the basis by the energies $(\hat{H})_{n,n} = \langle n|\hat{H}|n\rangle$. Basis states which are built in a highly one-dimensional way are very costly in energy and therefore moved up*).

We need to specify how to make use of the quartic oscillator basis, there being no simple closed form for the energies and matrix elements. First one solves the one-dimensional quartic oscillator in a harmonic oscillator basis with the frequency ω determined above. The fact that the harmonic oscillator is used disappears from the point of view of the two-dimensional calculations, it being just a computational aid for the $\hat{H}_0$ basis. The energies e_n and the matrix elements of $\{\hat{q}^2, \hat{q}^4\}$ calculated from the eigenvectors are stored for the two-dimensional calculations; the odd and even parity cases are calculated separately.

Let us now turn to the diagonalization of the two-dimensional coupled quartic oscillator in the uncoupled basis. To correctly obtain a slice of eigenvalues of $\hat{H}$ lying in the interval $[E_{\min}, E_{\max}]$, one needs to include in the truncated basis all states between the energies $e_{\min}$ and $e_{\max}$ of the inscribing surface $e_{\min} = H_0$ of $E_{\max} = H$ and the circumscribing surface $e_{\max} = H_0$ of $E_{\max} = H$, which, for $\lambda < 0$, comes at

$$e_{\min} = \frac{a_0}{a(\lambda)} E_{\min}, \qquad e_{\max} = \frac{a_0}{a(\lambda)(1+\lambda)} E_{\max}. \tag{3.27}$$

$d = \overline{N}_{H_0}(e_{\max}) - \overline{N}_{H_0}(e_{\min})$ then gives the dimensionality of the computed matrix. If $d_{\max}$ is the maximum dimensionality that can be diagonalized on the available computer, the number δ of levels that are converged for a slice starting at energy $E_{\min}$ is given (for each symmetry separately) by

$$\begin{aligned} \delta(E_{\min}, d_{\max}) &= \overline{N}_H(E_{\max}) - \overline{N}_H(E_{\min}) \\ &= \left(\frac{a(\lambda)(1+\lambda)}{a_0}\right)^{3/2} d_{\max} - [1-(1+\lambda)^{3/2}] E_{\min}^{3/2}. \end{aligned} \tag{3.28}$$

By patching together adjacent slices (with some small overlap; our estimates are optimistic being only attainable in the semiclassical limit) one may obtain sequences containing more than $d_{\max}$ levels. The maximum energy attainable is then $E_{\lim}(= E_{\min} = E_{\max})$ for which $\delta(E_{\lim}, d_{\max}) = 0$, which means that the $|\alpha\rangle$ are such that $E_\alpha \simeq E_{\lim}$ spread over $d_{\max}$ basis states. More specifically, for each parity sequence

$$d_{\max} = \frac{1}{4}\left(\frac{a_0}{a(\lambda)(1+\lambda)}\right)^{3/2} [1-(1+\lambda)^{3/2}] E_{\lim}^{3/2}, \tag{3.29}$$

and therefore the maximum number of levels that can be found using $d_{\max} \times d_{\max}$ matrices is

$$\overline{N}_H(E_{\lim}) = E_{\lim}^{3/2} = \frac{4 d_{\max}}{1-(1+\lambda)^{3/2}} \left(\frac{a(\lambda)(1+\lambda)}{a(0)}\right)^{3/2}. \tag{3.30}$$

(Of course, before this limit an increase of $d_{\max}$ will cost less than adding new slices.) In practical computations, we used $d_{\max} \simeq 5000$. The number of levels actually obtained for the different cases we have treated and the limit given in eq. (3.30) can be found in table 2.

*) This results from the fact that the $|n\rangle$ are EBK wave functions built on tori. At the level of approximation considered here, their Wigner transforms may be thought of as concentrated in a $(2\pi\hbar)^d$ volume surrounding the tori and, in fact, do not cover the energy surface uniformly.

Table 2
Complete list of computed quartic oscillators spectra: number of calculated levels converged to better than $10^{-2}D$, number of theoretically computable levels $\overline{N}_H(E_{\rm lim})$ [eq. (3.30) with $d_{\rm max} = 5000$] and number of spectral slices used.

λ	b	calculated	$\overline{N}_H(E_{\rm lim})$	# of slices
0.00	$\pi/4$	100 000	∞	1
−0.25	$\pi/4$	28 000	45 000	3
−0.35	$\pi/4$	22 000	29 000	3
−0.45	$\pi/4$	15 000	21 000	2
−0.60	$\pi/4$	9 000	12 000	1
$1/2\sqrt{2}$	$3\sqrt{2}/4$	8 000		1
1/4	3/2	6 000		1

To verify the accuracy of the one-dimensional calculation we make two checks against the asymptotic expansions for the energies $E_{{\rm qo},n}$ of the quartic oscillator given by [60]

$$E_{{\rm qo},n} = \pi^2\left(\frac{3(n+\frac{1}{2})}{\Gamma(\frac{1}{4})^2}\right)^{4/3} \sum_{k=0}^{\infty} c_k\,[9\pi(n+\tfrac{1}{2})^2]^{-k}, \tag{3.31}$$

where the first four WKB terms are

$$c_0 = 1, \qquad c_2 = \frac{5}{8} + \frac{11}{6}\left(\frac{\Gamma(\frac{1}{4})^2}{4\pi}\right)^4,$$
$$c_1 = 1, \qquad c_3 = \frac{11}{12} + \frac{341}{10}\left(\frac{\Gamma(\frac{1}{4})^2}{4\pi}\right)^4. \tag{3.32}$$

By $n = 40$, with the first four terms of eq. (3.31), the semiclassical energies are converged to better than 15 decimal places. One check on the matrix elements comes from a special case of the virial theorem, namely $E_{{\rm qo},n}/3 = \langle n|\hat{q}^4|n\rangle$, which we again compare to the asymptotic expansion for $E_{{\rm qo},n}$; there are also matrix element relations more restrictive than sum rules which also could have been used [61]. See fig. 6 for the actual errors. If $E_{{\rm qo},n}$ and the nth diagonal matrix element are good to 14 decimal places or better we assume the eigenstate has converged and the other matrix elements are also accurate to this level. In this way a basis of 180 harmonic oscillator functions allows accurate calculation of the first 126 quartic eigenstates (for each parity separately, 252 together).

For the two-dimensional calculation, a stringent test of the algorithm is to reproduce the $(\lambda, b) = (3, 1)$ spectrum, which is precisely equal to the $\hat{H}_0$ spectrum. We also have methods to numerically check the convergence of the routine for any value of λ. The first arises from the fact that the neglected states become important exponentially fast. With the levels above (below) missing, the downward (upward) pressure on the remaining levels is too small so that all of a sudden the levels deviate from their mean position by distances much larger than the fluctuations. This being exponentially quick we count back a couple of decades and to high precision we know where we have 10^{-2} precision (on the scale of a mean spacing); see fig. 7. In a similar vein, we calculate the best coefficients in the expansion of $\overline{N}(E)$ and compare to the exact. They again deviate at the same places in the spectra, but they give a slightly sharper view. Our second method comes from

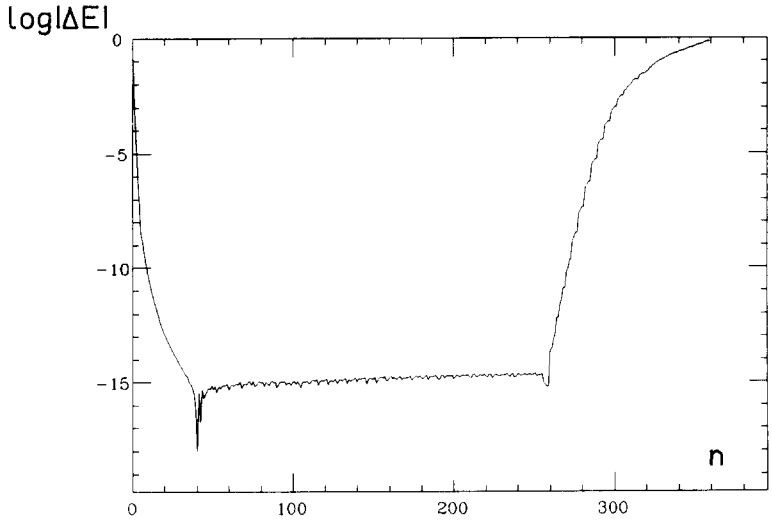

Fig. 6. Comparison of the one-dimensional quartic oscillator energies coming from a diagonalization in a well adapted harmonic oscillator basis (360 states taken) with the energies deriving from the first four terms in the semiclassical expansion [eqs.(3.31) and (3.32)]. Between $n = 0$ and $n = 40$, one sees the approach of the semiclassics to the actual energies. From $n = 40$ to $n = 260$, the diagonalization is converged to 15 decimal places and all states up to here may be used for the coupled quartic oscillators problem. Beyond $n = 260$, the exponentially fast failure to converge is seen.

realizing that the top of one slice gives an upper bound on the spectrum while the bottom of the next slice gives a lower bound; again see fig. 7. By subtracting the two we can identify the precision of every level extremely accurately; we also verified that there were essentially no crossings of the bounds. Oddly enough this is where we saw the first differences between chaotic and regular levels. In the spectral region between best convergence and nonsense the chaotic levels show a kind of noisy convergence that fluctuates from level to level superposed on the exponential increase in error. The regular sequences though, are fluctuation-free and sometimes less well converged than than the average chaotic level locally, at other times better. On average they are seen to converge about as well. This leads to our third method, which stems from the fact that the four matrices diagonalized are quite different; however, we shall see that there are regular levels quasidegenerate to such a degree ($< 10^{-9}$) that it is possible to see precisely how the convergence behaves by looking at the splitting of the degeneracies. For the most part the convergences are good to 10^{-5} to 10^{-6} (better for some regular levels) with the exception of levels near where the spectral slices were patched together, which are good only to $< 10^{-2}$.

We can envision ways to develop further these methods so as to be able to produce longer or more highly excited sequences. First of all, we could have, without any problem, approximately doubled the size of the matrices diagonalized from $\sim 5000 \rightarrow 10000$ since these matrices diagonalized extremely rapidly (10–15 quadriprocessor CPU minutes/matrix with a Cray-II). This would have doubled the number of levels easily attainable. Preliminary ideas indicate that it is quite probable that a kind of preconditioning of the matrices would have led to better convergence and perhaps another factor 2 increase in sequence length. So that if motivated to do so sequences of 100000 levels in certain interesting cases could have been obtained. These ideas could conceivably be applied to other polynomial potentials including perhaps ones of higher degrees of freedom.

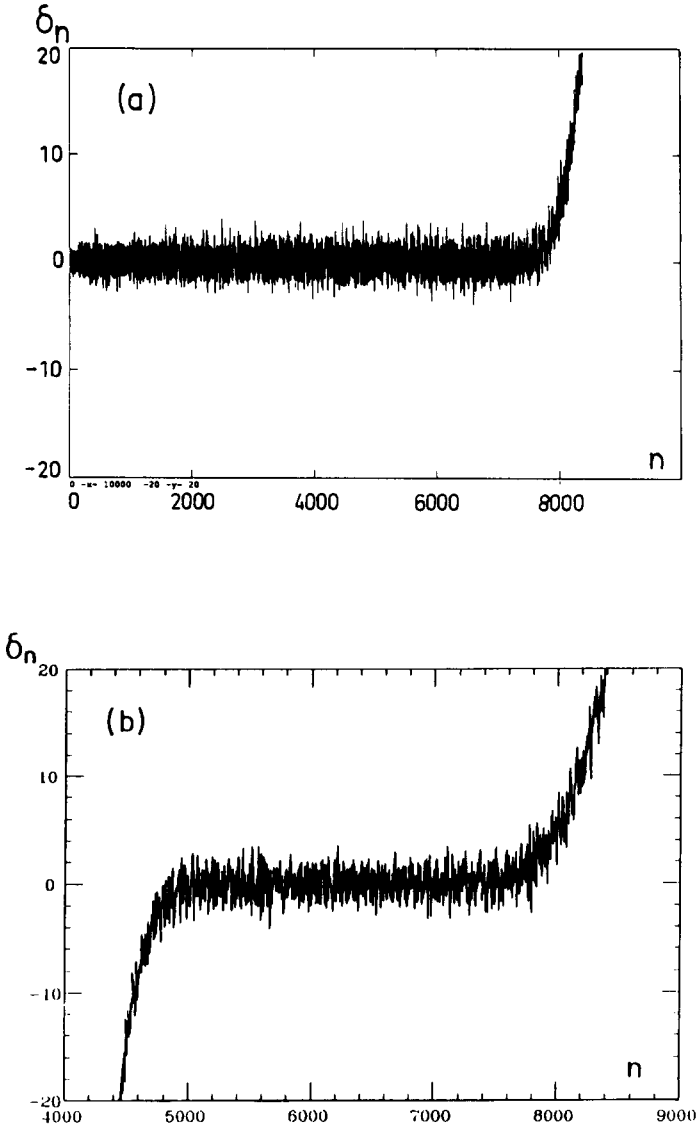

Fig. 7. Oscillatory part of the unfolded cumulative density of states, $\delta N = N(E) - \bar{N}(E)$, for the case $(\lambda, b) = (-0.25, \pi/4)$. The unfolding was performed with eq. (3.20). (a) The entire spectrum of reflection symmetry $(+,+)$ as patched together from the three slices that were used; (b) the result for just the uppermost slice of reflection symmetry $(+,-)$.

4. Regular states

We enter with this section into the heart of the matter, that of the relationship between a quantum system and its classical analog. For integrable systems, this is well understood since a standard EBK quantization scheme allows one to compute from the classical knowledge both the eigenenergies and their associated wave functions. This also includes KAM systems (i.e., the chaotic region is not widespread), for which there exists an extensive chemical physics literature (for a review see ref.

[8]). For the mixed systems we are interested in, the regular regions of phase space look very much as if they were part of such a regular system. It should therefore be possible, as Percival pointed out [40], to use the EBK quantization rules in such regions, and to extract from the global spectrum a set of levels which he refers to as being regular since they correspond to quantized invariant tori. We shall then adopt as definition that a regular eigenstate is one which is quantized on a single invariant torus and we shall continue to leave more vague the definition of a chaotic eigenstate.

This separation of the spectrum into a regular and an irregular part is more difficult to achieve than would appear at first sight. As is well known, quasi-integrable dynamics, as exemplified by what is termed KAM islands, has a much more complicated structure than integrable dynamics. For instance, it is not clear a priori how the quantization applies in places where instead of the expected invariant tori one finds either a chain of small subislands or cantori. Straightforward answers based on mathematical foundations should not be considered the final word on the subject since previous work indicates that a semiclassical quantization can often be used with fewer constraints than needed for the theoretical derivation of the EBK rules [8, 62, 63]. Our results will shed some light on these questions.

What we intend to do in this section is to perform this separation for a few cases of the quartic oscillators in a rather simple manner. The method of separation is not general but rather is applicable to systems with special symmetry properties. In fact, for certain ranges of the parameter λ, all invariant tori possess a duplicate somewhere in phase space, to which they are connected by one of the system's discrete symmetries. The induced quasidegeneracies will allow us to identify directly which eigenvalues in the spectrum are related to invariant tori. We will then return to the questions of resonances, and finally to the tunneling mechanism which causes the small splitting between quasidegenerate pairs. It will be shown that the presence of the neighboring chaotic sea noticeably modifies the way tunneling takes place.

We shall begin however with a presentation of a more typical utilization of the EBK quantization rules. Although this will not lead to the actual separation, we find it interesting to present it for two reasons. First of all, it will form the theoretical basis needed to understand what specific complications the KAM structure of the regular islands introduces in the EBK quantization scheme. Secondly, we shall use this standard EBK quantization as a reference to what is usually to be expected. The comparison between the results obtained in this first part and the final separation will give some insight into what distinguishes regular levels from chaotic ones.

4.1. EBK quantization

In a system with two degrees of freedom, as in our numerical example, the number of mutually independent closed curves which can be drawn on one invariant torus is two; see fig. 8. To each of these paths, C_1 and C_2, which are generally not trajectories, corresponds an action integral:

$$J_i = \oint_{C_i} \boldsymbol{p} \cdot \mathrm{d}\boldsymbol{q} \qquad (i = 1, 2)\,. \tag{4.1}$$

Then, in the semiclassical limit, if there are two integers n_1 and n_2 such that

$$\begin{pmatrix} J_1 \\ J_2 \end{pmatrix} = 2\pi\hbar \begin{pmatrix} n_1 + l_1/4 \\ n_2 + l_2/4 \end{pmatrix}, \tag{4.2}$$

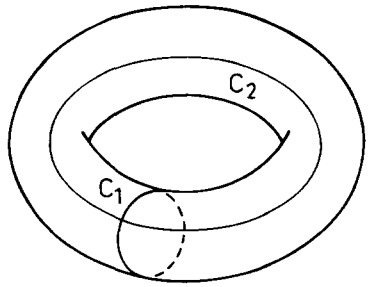

Fig. 8. A visualization of a two-torus and its two irreducible paths C_1 and C_2.

where l_1 and l_2 are the Maslov indices of C_1 and C_2, respectively (i.e. integer which counts the number of focal points through which C_1 or C_2 pass), the energy of the torus is an eigenvalue of the quantum Hamiltonian.

For a mixed system, invariant tori may be regarded as belonging to some KAM island. One of the paths on which the actions are calculated (say C_2) may be chosen along the general direction of the central periodic orbit C_p. At fixed energy, the corresponding action J_2 has thus a value close to $\oint_{C_p} \boldsymbol{p} \cdot \mathrm{d}\boldsymbol{q}$ (which is independent of the size of the island) for the whole island. The other path C_1 can be chosen transverse to the central orbit. J_1 thus varies from 0 (for the central orbit) to some maximum, which remains small if the island occupies a small proportion of the phase space.

When looking at a Poincaré section, it is most probable that one intersects a torus transversally. In all the cases we shall consider below, C_1 can be chosen as one of the curves which constitute the intersection of the torus with one of the planes $q_i = 0$ ($i = 1$ or 2). If, for instance, C_1 is included in the $q_2 = 0$ plane, the integral J_1 can just be written as

$$J_1 = \oint_{C_1} p_1 \, \mathrm{d}q_1 \tag{4.3}$$

since $\mathrm{d}q_2 = 0$. J_1 is then the area, in the Poincaré section, inside the trace of the torus. As C_1 is included in one of the planes $q_i = 0$ ($i = 1$ or 2), its Maslov index $l_1 = 2$, as any simple closed curve in a one-dimensional system. Thus, regular islands in Poincaré sections with area smaller than $\pi\hbar$ at the maximum energy considered will not support even a single regular level. For the quantum system, they will behave somewhat as if they were chaotic (or simply not there), assuming they are not surrounded by cantori that effectively enlarge them quantum mechanically.

To obtain all the regular levels, one has to compute the value of the actions J_1 and J_2 for each of the invariant tori and retain those which fulfill the quantization conditions. To make our presentation clearer, we shall begin with a simplified picture of the regular regions, in which we will consider them as containing only regular trajectories. We will thus forget, for a moment, all the complex inner structure due to the alternation of undestroyed and broken tori. Moreover we shall consider that in a Poincaré section in a particular energy surface, each island appears as a set of concentric curves, which means that it contains nothing resembling resonances or separatrices. In this approximate image, each point of a regular region lies in a torus defined by its two action integrals J_1 and J_2. We can thus perform a local canonical transformation from the $(\boldsymbol{q},\boldsymbol{p})$ variables to the action–angle ones $(\boldsymbol{\Theta},\boldsymbol{J})$ [with $\boldsymbol{J} = (J_1, J_2)$] in each regular island. This transformation cannot be made global for two immediate reasons. First of all, the action–angle variables are not

defined in the chaotic regions. Moreover two tori belonging to two different islands may correspond to the same value of J_1 and J_2. The transformation $(\boldsymbol{q},\boldsymbol{p}) \rightarrow (\boldsymbol{\Theta},\boldsymbol{J})$ is thus one to one for a single island, but not throughout all regular regions. We shall therefore focus on one particular regular island at a time, allowing us to uniquely define a torus by the values of its actions (J_1, J_2).

One now has to obtain the function $H(J_1, J_2)$ which leads to the eigenenergies E_{n_1,n_2} with quantum numbers (n_1, n_2) through eq. (4.2). This, strictly speaking, is equivalent to the knowledge of a one-parameter family of curves g^E defined in the (J_1, J_2) plane by the implicit relation

$$H(J_1, J_2 = g^E(J_1)) = E \ . \tag{4.4}$$

Each time a curve g^E lies on a point of the grid defined by eq. (4.2) $(n_1, n_2 = 0, 1, 2, \ldots), E = E_{n_1,n_2}$ is an eigenvalue of the quantum system. It remains to obtain the curves g^E. Practically, this would consist of measuring J_1 and J_2 for a large number of sampled tori on the E energy surface. As J_1 is actually the area inside a curve in the Poincaré section, it could be measured by a simple counting of pixels but this would be far too inaccurate. Also there is no direct way to numerically calculate J_2. It is thus convenient to introduce another set of variables describing a torus, namely (α, J), where α is the winding number of the torus and

$$J = J_2 + \alpha J_1 \ . \tag{4.5}$$

In a Poincaré section $\theta_2 = \text{const.}$, J appears as the action integral along a trajectory between two successive intersections with the section. One can also introduce the one-parameter family f^E such that $J = f^E(\alpha)$ for any torus (α, J) lying in the E energy surface.

Differentiating eq. (4.4) gives

$$\partial H/\partial J_1 + (g^E)' \partial H/\partial J_2 = 0, \tag{4.6}$$

which means that

$$(g^E)' \equiv \mathrm{d}J_2/\mathrm{d}J_1 = -\dot{\theta}_1/\dot{\theta}_2 = -\alpha \ . \tag{4.7}$$

The transformation from g^E to f^E (as well as the reverse one) is thus a Legendre transformation.

It is now quite easy to compute to a very good precision the couple (α, J) associated with a particular torus. This is accomplished by starting a trajectory from some point X of the torus lying in a Poincaré section, and by performing N iterations of the mapping $\mathcal{T}$. If s is such that $\mathcal{T}^s(X)$ corresponds to the closest approach to X after the N first iterations and r is the number of turns $\mathcal{T}^s(X)$ has made around the center of the island during the s iterations, then r/s is the best rational approximation to α with denominator $\leq N$. Other than a few exceptional regions near rationals with small denominators, this will generally lead to a precision of $O(N^{-2})$. (Our choice of $N = 1000$ gives α within $\sim 10^{-5}$.)

At the same time, the action

$$S = \int_X^{\mathcal{T}^s(X)} \boldsymbol{p} \cdot \mathrm{d}\boldsymbol{q} \tag{4.8}$$

taken along the trajectory connecting X and $\mathcal{T}^s(X)$ can be measured with a precision equal to that of our Runge–Kutta method. This can be done directly, by adding $\boldsymbol{p} \cdot \mathrm{d}\boldsymbol{q}$ at each step of integration. For a scaling Hamiltonian, whose potential fulfills eq. (2.4), S is given by $S = Et/(1/2 + 1/\mu)$

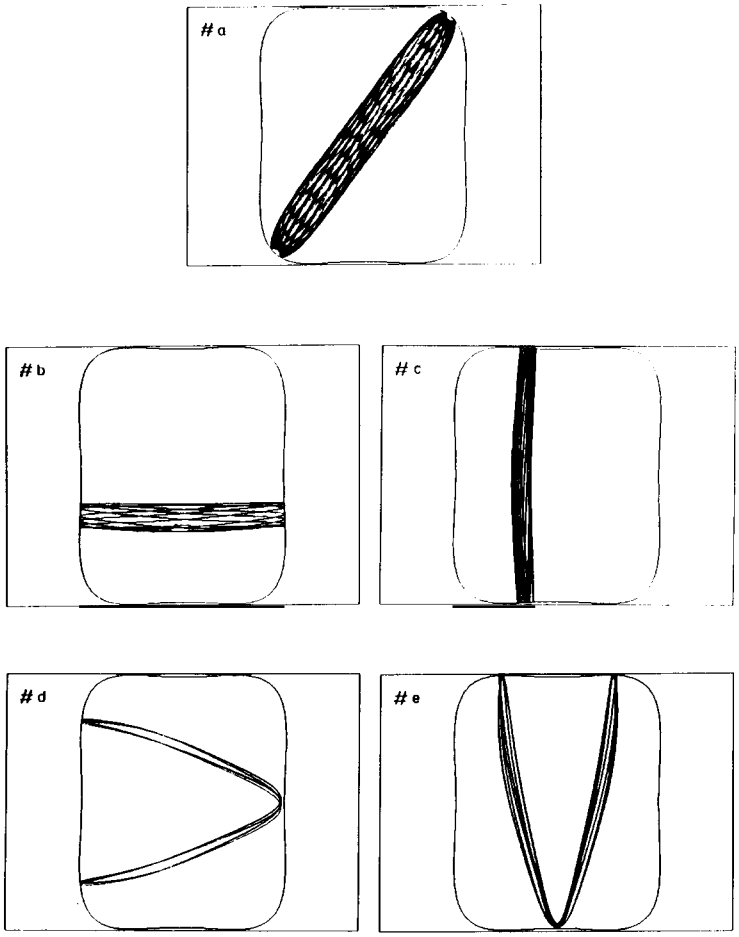

Fig. 9. Configuration space drawing of representative tori, one each coming from the islands $(a), (b), (c), (d), (e)$, respectively, for the case $(\lambda, b) = (-0.25, \pi/4)$. Their symmetric partners in $(a'), (b'), (c'), (d'), (e')$ are easily visualized (see also fig. 1).

$(\rightarrow 4Et/3$, for the quartic oscillators) since $\partial S/\partial E = t$ and S scales as $E^{(1/2+1/\mu)}$; t is the time needed to go from X to $T^s(X)$.

From the curves $J = f^E(\alpha)$, which are easily obtained with a good precision, one can construct g^E by repeated use of eq. (4.5) together with $\mathrm{d}J/\mathrm{d}\alpha = J_1$. There is of course some loss of precision δJ_1, during the first step, as for any numerical calculation of a derivative. This will however be somewhat compensated because one has the correct tangent to g^E. Thus, if J and α are accurate, the error comes from the second-order curvature term $\frac{1}{2}(\delta J_1)^2 (g^E)''$.

When considering scaling systems, such as the quartic oscillator, the computation of the curves g^E is greatly simplified since all g^E are related to $g^0 (= g^{E=1})$ through

$$g^E(J_1) = E^{(1/2+1/\mu)} g^0 (E^{-(1/2+1/\mu)} J_1) \rightarrow E^{3/4} g^0 (E^{-3/4} J_1) . \tag{4.9}$$

Recalling the grid defined by eq. (4.2) in the space (J_1, J_2), a point of the grid actually belongs to the regular island if it is the image, by a dilatation, of a point (J_1^0, J_2^0) of g^0, which means that

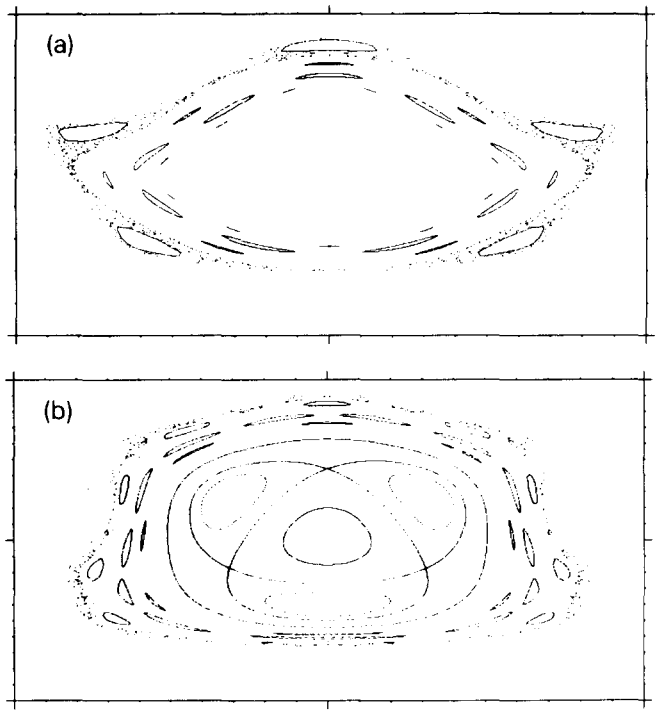

Fig. 10. Expanded view of island (a') showing some of its structure; (a) $q_2 = 0$ section for the case $(\lambda, b) = (-0.25, \pi/4)$, and (b) $q_1 = 0$ section for the case $(\lambda, b) = (-0.35, \pi/4)$.

the line going through the origin and the point of the grid intersects this curve. The quantization condition can be rewritten as

$$\begin{aligned} J_1^0(n_1, n_2) &= 2\pi\hbar(n_1 + \tfrac{1}{2})/E_{n_1,n_2}^{(1/2+1/\mu)}, \\ g(J_1^0(n_1, n_2)) = J_2^0(n_1, n_2) &= 2\pi\hbar(n_2 + \tfrac{1}{4}l_2)/E_{n_1,n_2}^{(1/2+1/\mu)}. \end{aligned} \tag{4.10}$$

We shall thus, loosely speaking, refer to the torus $(J_1^0(n_1, n_2), J_2^0(n_1, n_2))$ as a quantized torus, meaning here that one or more of its scaled analogs is an element of the grid. In fact a point of g^0 which quantizes for a given (n_1, n_2) will in general satisfy the same relation for an infinite number of couples since such a point of g^0 must satisfy the relation

$$J_2^0/J_1^0 = g^0(J_1^0)/J_1^0 = (n_2 + \tfrac{1}{4}l_2)/(n_1 + \tfrac{1}{2}) . \tag{4.11}$$

The fact that energy levels in very different places of the spectrum can correspond to exactly the same torus can be used to observe how the semiclassical limit is attained (we can equivalently think of this as fixing the energy $E = 1$ and finding the quantized values of $\hbar$).

As just shown, the variables (J_1, J_2) and (α, J^0) are related through a Legendre transformation. Depending on the physical circumstances one or the other of these pairs may enter more naturally. For completeness we reexpress the quantization conditions for scaling systems eq. (4.10) with the help of eq. (4.5) in terms of (α, J^0). This gives

$$E_{n_1,n_2}^{(1/2+1/\mu)} (\to E_{n_1,n_2}^{3/4}) = \frac{2\pi}{J^0}[(n_2 + \tfrac{1}{4}l_2) + \alpha(n_1 + \tfrac{1}{2})] . \tag{4.12}$$

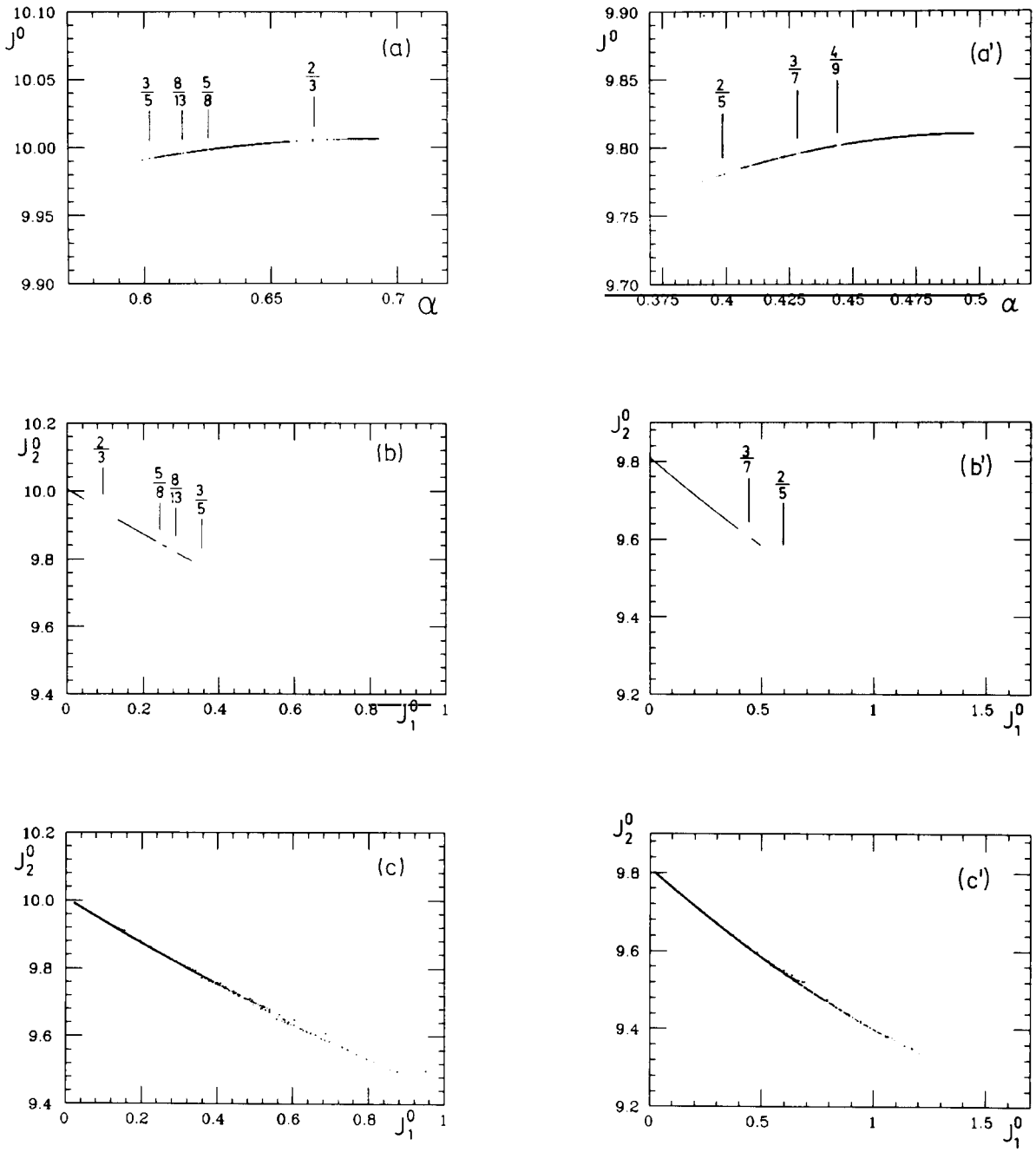

Fig. 11. Comparison of the classical and semiclassically derived actions of island (a). The unprimed figures are for the case $(\lambda, b) = (-0.35, \pi/4)$ and the primed for $(-0.25, \pi/4)$. (a) (α, J^0) which are obtained directly from the numerical integration of the classical equations of motion. (b) The derived actions (J_1^0, J_2^0) related to (α, J^0) by Legendre transformation. (c) The semiclassically derived actions via EBK and the quantum number assignments.

Let us now specialize to the quartic oscillator for the examples of $(-0.25, \pi/4)$ and $(-0.35, \pi/4)$. For $(-0.25, \pi/4)$, four sets of islands [labeled as $(a), (b), (c)$ and (d) on fig. 1] are large enough to support regular states below $E = 930$ ($\sim 28\,000$th level). Trajectories started from these islands are shown on fig. 9. For $(-0.35, \pi/4)$ only three islands [$(a), (b)$ and (c)] sustain regular levels. The corresponding trajectories show no essential differences with $(-0.25, \pi/4)$. In both cases, all Maslov indices l_1 associated to the paths C_1 are equal to 2 and the Maslov indices l_2 are equal to 4 for tori belonging to the islands $(a), (c)$ and (e), and 2 for those belonging to islands (b) and (d).

We have constructed the curves g^0 and f^0 for the main island [island (a)] for these two values of λ. Some remarks are in order: we know (Poincaré–Birkhoff theorem) that the simplified picture used until now for the the regular islands applies only for tori whose winding number α is sufficiently far from a rational. As a consequence, the curves g^0 and f^0 are only defined for a Cantor-like set of J_1^0 points, which are the only ones for which the EBK quantization rules hold rigorously; the remaining points originate either from small chaotic regions or from subisland chains (see fig. 10). However, depending on the density of initial conditions used, our numerical method gives a coarse grained equivalent. With our sampling choice, g^0 and f^0 appear as continuous curves where merely the largest resonances in fig. 10 are seen as gaps in fig. 11.

Ahead we shall first identify the regular levels and then assign the quantum numbers (n_1, n_2) through the EBK conditions. In so doing, a quantum curve, g^0_{qm}, will be constructed for the various regular islands allowing a fine comparison to be made to the classically constructed g^0. The problems of the resonances, which appear as gaps in g^0, and the complexity of the regular–chaotic region interface, will show differences between these two curves illustrating various effects due to the finite size of $\hbar$.

4.2. Dynamical quasidegeneracies

The actual separation of the regular levels from the rest of the spectrum is made possible here because of the discrete symmetry properties of the quartic oscillators. We have already mentioned in section 2 that for $\lambda \in [-1, \lambda^*]$, all the tori which correspond to the original structure are destroyed. The remaining invariant tori have a lower symmetry than the global one. They all thus have at least one exact replica which is its image by an element of the global symmetry group $\mathcal{G}_\tau$. As a consequence [64, 42] all the associated EBK wave functions and thus all the regular levels come in degenerate pairs (or perhaps higher degeneracy).*) When the exact eigenvalues are calculated, these degeneracies are slightly broken because of tunneling between tori (see section 4.5). As such effects are exponentially small, these levels remain remarkably close to each other, and we shall refer to them as quasidegenerate levels.

In practice, for all the cases we have treated, the rescaled tori large enough to quantize under our maximum energy have only one duplicate; one element of $\{P_1, P_2, P_1P_2\}$, which we generically call P, leaves them invariant. Thus, for a given torus τ associated with a wave function Ψ, among the four functions

$$\Psi^{\varepsilon_1,\varepsilon_2} = \tfrac{1}{4}(1 + \varepsilon_1 P_1)(1 + \varepsilon_2 P_2)\Psi \tag{4.13}$$

which belong to the sequences ($\varepsilon_1 = \pm 1, \varepsilon_2 = \pm 1$) two are non-zero and associated with quasidegenerate levels and the two remaining ones are null.

*) On the contrary, since all the significant chaotic regions are invariant under $\mathcal{G}_\tau$, no quasidegeneracies are expected for the chaotic states [65].

To know in which sequences the degenerate levels are to be found, we shall once again follow ref. [64]. Denoting, as usual, by C_1 and C_2 the two independent paths on which the quantization conditions are written, and by n_1 and n_2 the associated quantum numbers, we must first determine whether $P(\Psi(n_1, n_2))$ is equal to $\Psi(n_1, n_2)$ or to $-\Psi(n_1, n_2)$.

For any point r_0 of the torus, the phase difference between the contribution to $\Psi(n_1, n_2)$ of r_0 and $P(r_0)$ is

$$\Delta\phi = \frac{1}{\hbar}\int_C \boldsymbol{p}\cdot \mathrm{d}\boldsymbol{q} - \frac{\pi}{2}\mathrm{ind}(C), \tag{4.14}$$

where C is any path on τ joining r_0 to $P(r_0)$. As P is a canonical transformation, the phase $\Delta\phi'$ calculated on the symmetric path $P(C)$ to C is equal to $\Delta\phi$ also. And thus

$$2\Delta\phi = \frac{1}{\hbar}\int_{C+P(C)} \boldsymbol{p}\cdot \mathrm{d}\boldsymbol{q} - \frac{\pi}{2}\mathrm{ind}(C + P(C)). \tag{4.15}$$

Then, as $(C + P(C))$ is a closed path, it can be decomposed on C_1 and C_2 as

$$C + P(C) = a_1 C_1 + a_2 C_2, \tag{4.16}$$

where a_1 and a_2 are integers, which leads, using the quantization conditions, to

$$\Delta\phi = \pi(a_1 n_1 + a_2 n_2). \tag{4.17}$$

Thus, $\exp(\mathrm{i}\Delta\phi)$ is equal to $+1$ or -1 depending on whether $(a_1 n_1 + a_2 n_2)$ is even or odd. For all the tori we will consider, however, it happens that the path $(C + P(C))$ can be chosen equal to C_2, thus

$$\Delta\phi = \pi n_2, \tag{4.18}$$

$$P(\Psi_{n_1,n_2}) = (-1)^{n_2}\Psi_{n_1,n_2}. \tag{4.19}$$

The sequences in which the degenerate levels must be found then depend on P. In island (a) of the $\lambda = -0.25$ or -0.35 cases, for instance, P stands for P_1P_2. Thus for even n_2

$$P(\Psi_{n_1,n_2}) = \Psi_{n_1,n_2}, \qquad \Psi^{\varepsilon_1,\varepsilon_2}_{n_1,n_2} = \tfrac{1}{4}(1 + \varepsilon_1 P_1)(1 + \varepsilon_1\varepsilon_2)\Psi_{n_1,n_2}, \tag{4.20}$$

and the two eigenfunctions must belong to the $(+,+)$ and $(-,-)$ sequences to avoid $(1 + \varepsilon_1\varepsilon_2)$ being equal to 0. For odd n_2,

$$P(\Psi_{n_1,n_2}) = -\Psi_{n_1,n_2}, \qquad \Psi^{\varepsilon_1,\varepsilon_2}_{n_1,n_2} = \tfrac{1}{4}(1 + \varepsilon_1 P_1)(1 - \varepsilon_1\varepsilon_2)\Psi_{n_1,n_2}, \tag{4.21}$$

and the two eigenfunctions must belong to the $(+,-)$ and $(-,+)$ sequences. The same considerations can be used for any other regular region. For the main KAM islands of the $\lambda = -0.25$ and -0.35 cases, we summarize the results obtained in this way in table 3.

4.3. Separation of regular levels and quantum number assignments

To proceed further one compares two parity sequences, and one can indeed see at first glance that a large number of nearly degenerate levels occur. However, sometimes two unrelated levels are

Table 3
Symmetry of quasidoublets of the main KAM islands of the $(\lambda, b) = (-0.25, \pi/4)$ and $(-0.35, \pi/4)$ cases (see fig. 1).

Island #	n_2 even	n_2 odd	symmetry
$(a), (a')$	$(++), (--)$	$(+-), (-+)$	$P_1 P_2$
$(b), (b')$	$(++), (+-)$	$(-+), (--)$	P_1
$(c), (c')$ / $(d), (d')$	$(++), (-+)$	$(+-), (--)$	P_2

very close to each other just by statistical accident; our criterion for determining what is paired is that the spacing be $< 10\%$ of the mean level spacing, which implies, using a random superposition argument, that close to 15% of the spectrum could appear as fake pairs. One must therefore have a further way to filter the regular levels. This comes by realizing that the sequences $\{E^{3/4}_{n_1,n_2}\}$, where n_1 is constant and n_2 varies, are easily recognizable.

Locally the curve g^0 is well approximated by its tangent line and therefore, using eq. (4.12), the spacing

$$E^{3/4}_{n_1,n_2+1} - E^{3/4}_{n_1,n_2} \simeq 2\pi / J^0(J^0_1(n_1, n_2)) \tag{4.22}$$

remains nearly constant locally in the sequence. These sequences are easily associated with a particular KAM island via the spacing and J^0, although here the symmetry considerations alone usually suffice. Since the rescaled torus $\tau^0_{n_1,n_2+1}$ lies interior, in the Poincaré section, to $\tau^0_{n_1,n_2}$, the sequences continue to infinite energy as the tori approach the center of the KAM islands. Once the beginning of a sequence is found it can be followed right up through the entire spectrum, its degeneracy splittings tending to zero. Another way to produce a sequence, n_2 constant and n_1 varying leads to finite sequences (since one leaves the islands as n_1 increases) and the corresponding approximation of the type of eq. (4.22) works less well since typically $\alpha \gg J^0_1/J^0_2$. A third possibility, that of following the states all quantizing on a particular scaled torus, leads to infinite sequences, but it is too complicated to be of much help for making quantum number assignments; it is useful for studying the pure effects of decreasing $\hbar$.

Our filter of the regular levels is now so precise it will leave ambiguous no more than a few pairs per thousand levels. (There were some minor complications to resolve such as occasionally finding 3 or 4 levels nearly degenerate; these events were resolved by comparing the spacings pairwise and were flagged as special cases.) It is worth mentioning though that the filter can be made even more selective by using a very characteristic property of the quasidoublets, namely the real quasidegeneracies remain so for relatively large variation of the coupling λ (a quantum consequence of the KAM theorem). This is totally unlike the behavior of "statistical accidents", which will only be nearly degenerate (or degenerate) for one value of λ at the nearest approach. Thus the motion of the pair as a function of λ also exhibits a tell-tale sign. In fact, starting at $\lambda = 0$, two originally non-degenerate levels approach as λ is decreased to form a pair typically near $\lambda \simeq -0.05$. With rare exception, they remain paired until λ has decreased so much (perhaps $\lambda \simeq -0.40$) that the torus is completely broken; sometimes they remain paired beyond, long after the torus is gone. Obviously this in part depends on the torus. The maximum number of quasidegeneracies occurs near $\lambda = \lambda^*$.

So we extract the quasidegeneracy sequences from the full spectrum, and now wish to identify the quantum numbers for each of the regular levels. Again this is done without any need of the eigenfunctions; if $b = 1$, this would not be true for the one doubly degenerate sequence. It is easy to see that the sequence starting lowest in energy must be the $n_1 = 0$ one; the point at which $\pi\hbar$ just

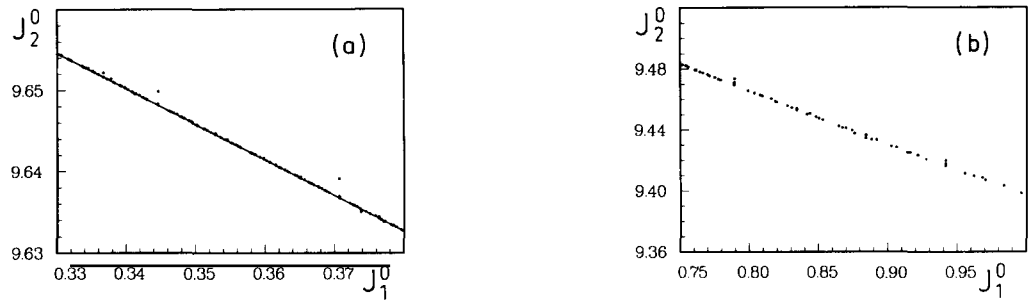

Fig. 12. Expanded view of two portions of figs. 11b′ and c′ superposed, each one corresponding roughly to a J_1^0 interval containing two successive points of the $n_1 = 0$ sequence; (a) at the interior of the classical island; (b) outside the classical island. The agreement between the classical line and quantum points is very precise when the first is defined. The points furthest from the classical line in (a), and from its extrapolation in (b) are in the $n_1 = 0$ sequence, where the semiclassics should and do work worst.

fits inside the KAM island area in a Poincaré map occurs at lower energy than $\frac{3}{2}\pi\hbar$, etc. The order of the appearance, in the spectrum, of the sequences easily determines n_1. To assign n_2, we recall eq. (4.12). E_{n_1,n_2} and n_1 are known very precisely and J^0 is approximately given by eq. (4.22). α is always close to $\frac{1}{2}$ in our mixed systems but it is not very crucial since n_2 is restricted to being odd or even depending on the symmetry considerations. Usually only one integer for n_2 comes close to satisfying eq. (4.12). The n_2 values for the rest of the members just come by counting up the sequence starting with the lowest n_2 value.

Once the quantum numbers $\{(n_1, n_2)\}$ of $\{E_{n_1,n_2}\}$ are known, one obtains through eq. (4.10) a set of couples $\{(J_1^0(n_1, n_2), J_2^0(n_1, n_2))\}$ which in the semiclassical approximation satisfy $H(J_1^0(n_1, n_2), J_2^0(n_1, n_2)) = 1$. By this means one constructs a curve g_{qm}^0 (which, loosely speaking, we shall refer to as a "quantum curve" since it is constructed from the quantum data) equivalent to the g^0 introduced in section 4.1. The resulting curves are shown on fig. 11 for the main island [island (a)] of the $\lambda = -0.25$ and $\lambda = -0.35$ cases. As expected, g_{qm}^0 precisely corresponds to g^0 wherever both are defined. An enlarged view of two small portions of a g^0 curve is given in fig. 12, in order to illustrate the quality of the correspondence. However, all missing segments due to resonances are interpolated, and the quantization seems to work well even for J_1^0 larger than the total area of the island. Visually, it seems that the quantum system has analytically continued g^0 along the most natural path through all the gaps and up to a J_1^0 that can be 2 or 3 times the classical maximum.*) We shall consider that quantization occurring beyond the maximum J_1^0 to be cantorus quantization [66]. However, we did not attempt to construct classically the cantori outside the island to confirm that they would lead to an extended g^0 curve similar to the quantum continuation. It would be an interesting, stringent quantitative test of these ideas to do so. It should be mentioned that the mechanism responsible for quantization above the maximum J_1^0 is most probably also responsible for the possibility of approximating the classical motion near "adiabatically stable" closed orbits by the motion of an integrable Hamiltonian, as done in ref. [67].

The quality (degree of splitting) of the quasidoublet sequences is however quite different depending on whether J_1^0 is inside (or close to) the regular region or distant from it . This is partially illustrated in fig. 13, where [continuing on with island (a)] the points of the grid $(n_1 + \frac{1}{4}l_1, n_2 + \frac{1}{4}l_2)$

*) For $\lambda = -0.25$, the maximum J_1^0 found was 1.20 despite the total area of the island being 0.66. For $\lambda = -0.35$, a J_1^0 equal to 0.9 was reached but little quantization occurred beyond 0.6, which is to compare with a total area of 0.37.

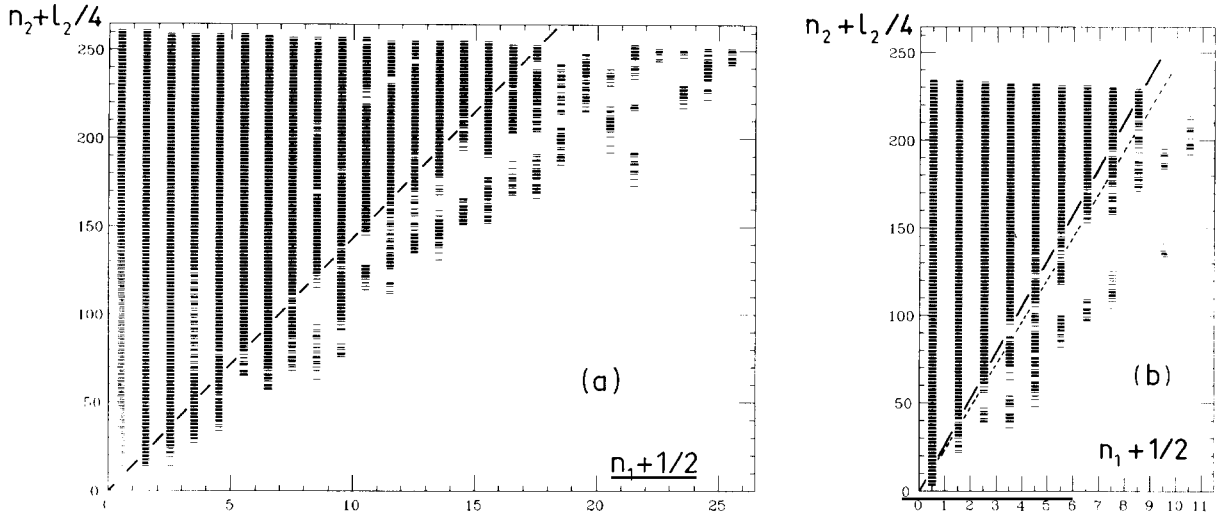

Fig. 13. Quantum numbers (n_1, n_2) of the regular states identified in and around island (a) as quasidoublets (each dash corresponds to a single doublet). The straight line locates the classical border of the KAM island and the lower right represents the exterior. (a) From the first 28 000 eigenvalues of the case $(\lambda, b) = (-0.25, \pi/4)$. (b) From the first 22 000 eigenvalues of the case $(\lambda, b) = (-0.35, \pi/4)$; the straight line corresponds to $J_1^0 = 0.37$ and the straight dotted line to $J_1^0 = 0.40$. See text for further explanation.

in the plane $(J_1/2\pi\hbar, J_2/2\pi\hbar)$ are shown for which a regular level has actually been found. On this picture, it is clearly seen that, with very rare exceptions, the sequences are nearly complete for the region of the plane $(J_1/2\pi\hbar, J_2/2\pi\hbar)$ corresponding to the interior of the classical island. Moreover, the sequences tend to remain complete to some distance beyond the classical boundary. However, further out, sequences start to break and become more and more fractured until they disappear.

For island (a) of the $\lambda = -0.35$ case, very few levels are missing for $J_1^0 \leq 0.4$ (see fig. 13b), whereas beyond this value, namely in the interval $0.4 \leq J_1^0 \leq 0.5$, about half of the levels are. This is reflected in the splitting of the corresponding quasidoublets. Typically, the splittings of interior levels are $10^{-4}D$–$10^{-7}D$ or less, those of boundary levels are $10^{-2}D$–$10^{-4}D$ and beyond $J_1^0 = 0.40$ they are $10^{-1}D$–$10^{-3}D$. The splittings do not, in most cases, increase smoothly from $10^{-7}D$ to $10^{-1}D$ as one goes from the center of the island to the maximum quantized J_1^0. Actually, fluctuations of several orders of magnitude exist between doublets for neighboring J_1^0. We shall return to this point at the end of this section.

The levels exterior to $J_1^0 = 0.40$ (i.e. 2% of the total number of levels) should therefore be regarded as being of intermediate status rather than being purely regular. When studying the statistical behavior of chaotic levels in the next section, we therefore only consider "regular" those levels with $J_1^0 \leq 0.40$. Note we have checked that the fluctuation measures to be discussed in the next section are by no means sensitive to this precise choice. The volume of the island is approximately

$$V = \int_{\text{island}} \mathrm{d}\boldsymbol{p} \cdot \mathrm{d}\boldsymbol{q}\, \Theta(E_0 - H) \simeq \tfrac{1}{2} J_1^0(\max) J_2^0(\max) , \tag{4.23}$$

where $J_1^0(\max)$ corresponds to the size of the island and $J_2^0(\max)$ to the action of the periodic

trajectory at the center of the island [$J_2^0(\max) = 10.01$]. Extending the value of $J_1^0(\max)$ from its classical value (0.37) to 0.40 increases the fraction of levels $f \simeq 2V/(2\pi)^2$ from $\sim 9\%$ to $\sim 10\%$.

Thus island (a) appears quantum mechanically as enlarged by 10–20% (for the $\lambda = -0.35$ case considered here and also for $\lambda = -0.25$) compared to its classical size. We would like to stress however that this is not always the case. The small islands behave in a significantly different way compared to the big ones. For islands (b), (c) and (d) for $\lambda = -0.25$ and (b) and (d) for $\lambda = -0.35$ there still exist a few levels which probably correspond to cantori just outside the classical islands. However, for both the quantizing tori not too deeply inside the islands and the cantori, the splittings are large and on average quite close to our maximum acceptable limit. In addition the sequences show some spacing irregularities as compared with the EBK expectation. In fact the quantum number assignments are, in some cases, more reliable outside of the big islands than inside the small ones. We strongly suspect that the small islands are providing another example of states of intermediate nature. They are either (de)localized on two or more quantizing tori and/or partly living in the chaotic region of the phase space. Moreover, a certain number of levels corresponding to tori interior to the classical small islands may be missing.*) Figure 14 illustrates one of the clearest cases, for which nearly half of the expected levels is lacking.**) At least for some small quantum numbers, there appear to be quantizing tori that do not give rise to a regular state. This is different from what happens for the big islands, for which the smallness of the quantum numbers is reflected simply by small displacements in energy compared to the EBK prediction (see again fig. 12 and caption). The image is thus that the small islands at our $\hbar$ are reduced in size quantum mechanically as opposed to being enlarged. In particular for island (c) of the $\lambda = -0.35$ case no quasidoublet has been identified although one expects some of them to be present. We believe that the nature of the regular–chaotic interface as described by classical dynamics (i.e. fast mixing beyond the border or, on the opposite extreme, presence of partial barriers) plays an important role in determining which of these possibilities occurs for a particular KAM island. Qualitatively, this argument is consistent with our experience in the quartic oscillators. As a consequence, the insistence on a strict correspondence between the definition of a regular state and an invariant torus is somewhat naïve. Presumably then, it is proper in some cases to associate regular states with other classical objects such as cantori while in other cases, even the existence of a torus satisfying the EBK conditions does not guarantee the existence of the corresponding regular state.

Let us now return to some of the difficulties encountered while doing the actual separation and quantum number assignments. A first delicate point consists of choosing properly the practical upper limit for the largest acceptable quasidegeneracy splitting. One would both like to get all actual quasidoublets (and thus increase the criterion), but yet not include so many fakes that their elimination is not feasible (which induces one to reduce the criterion). Our choice, 10%D, is a good compromise since increasing it adds a negligible number of true quasidoublets and yet the construction of the sequence can still be carried out easily. From the selected doublets, all sequences of length 3 or larger were extracted [J^0 in the proper range via eq. (4.22)]; small gaps in sequences were easy to adjust for.

At this point the quantum number assignments were usually straightforward, but some interrelated problems were encountered which depended on the KAM island under study, namely sequence crossings or "accidental degeneracies" and missing segments of sequences. First we discuss the sequence crossings. Consider two overlapping sequences of $\{E_{n_1,n_2}\}$ (n_1 fixed). They necessarily

*) Note that there is not necessarily a sharp distinction between those possible quasidoublet pairs which just fulfill our maximum splitting criterion and some which have been rejected.

**) Lack of levels from islands other than island (a) in the $\lambda = -0.35$ case compensates for the excess levels of island (a) in such a way that the total proportion of regular levels, $\sim 12\%$, is the same as the classical expectation.

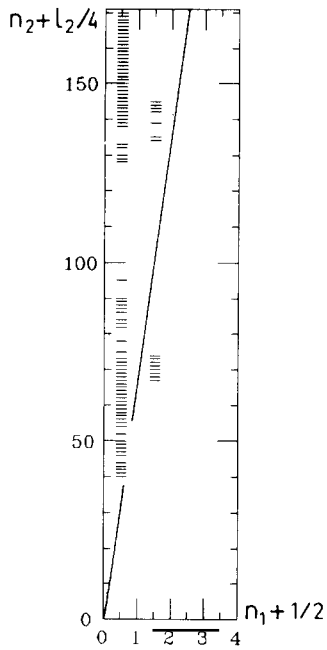

Fig. 14. Quantum numbers (n_1, n_2) of the regular states identified in and around island (b) as quasidoublets from the first 22 000 eigenvalues of the case $(\lambda, b) = (-0.35, \pi/4)$. The straight line locates the classical border of the KAM island and the lower right represents the exterior.

come from different regions of the curve g^0, so to speak, since their n_1 values are different. All of the curves g^0 from the various KAM islands have a gentle curvature so that the two sequences must have somewhat different spacings (though locally each sequence has nearly constant spacings). For certain pairs of n_1 values the sequences are close by somewhere in the spectrum and as one climbs (or descends) the sequences, the levels of the one with the slightly larger spacing overtake and pass the levels of the other sequence. This is what we call a sequence crossing. The crossing point is usually an accidental degeneracy in that two different quantizations accidentally lead to the same energy (therefore one finds four levels nearly degenerate); if the spacings are too different then it is possible to cross sequences without having a near-degeneracy (on the scale of a mean spacing). The accidental degeneracy splittings are much larger than the quasidegeneracy splittings.

In a sense accidental degeneracies are not really accidental in that with the knowledge of g^0 they are predictable. Starting with eq. (4.2), two different quantizations giving the same energy E satisfy

$$\Delta n_1/\Delta J_1^0 = \Delta n_2/\Delta J_2^0 = E^{3/4}/2\pi\hbar, \tag{4.24}$$

where Δ indicates differences. This implies

$$\Delta n_2/\Delta n_1 = \Delta J_2^0/\Delta J_1^0\,, \tag{4.25}$$

which means that the line connecting the two points on g^0 has a rational slope. Since n_1 at our energies never exceeds the low twenties, the differences ΔJ_1^0 cannot be infinitesimal. The curvature of g^0, then, is important. However, if making a limited expansion of $\Delta J_2^0/\Delta J_1^0$ around the point centered halfway between J_1^0 and $J_1^0 + \Delta J_1^0$, we find

$$\Delta J_2^0/\Delta J_1^0 \simeq -\alpha - \tfrac{1}{24}\alpha''(\Delta J_1^0)^2\,, \tag{4.26}$$

where the second term can usually be ignored. The centered point on g^0 has the same rational slope as the connecting line. Therefore two points equally spaced $\pm\Delta J_1^0/2$ from J_1^0 such that $\alpha = r/s = -\Delta n_2/\Delta n_1$ along with eq. (4.2) approximately give the sequence crossing point energy. Since $J_1^0(\alpha = r/s) \pm \Delta J_1^0/2$ do not necessarily quantize, the actual accidental degenerate energy occurs at the level in the n_1 sequence closest to that energy. In fact, for the quartic oscillators (and most other scaling systems), as $n_1 \to \infty$, the curvature can be ignored and the scaling is such that accidental degeneracies of infinite order coalesce slowly where α is rational. At a given energy, the smaller s, the higher order accidental degeneracy is possible.

There are now two possibilities. The first is that both sequences belong to a part of the classical curve or, otherwise said, are interior to the KAM island. Usually in this case the quasidegeneracies are excellent, giving no problem there. However, tunneling splits the two sequences near the accidental degeneracy if Δn_2 is even*) in such a way that, if one blindly (locally in the sequence, without knowledge of g^0) assigns n_2 quantum numbers, the tendency is to switch sequences at the crossing point and to start assigning false quantum numbers. This is easily seen after the fact when drawing the quantum curve g_{qm}^0. There will appear a kink in the sequence of points (J_1^0, J_2^0) and it will slowly veer away from g^0; assuming all the sequences are assigned quantum numbers, actually two of them will veer away from g^0 (one above g^0, the other below) at points separated by ΔJ_1^0 on g^0. This can be easily corrected if the curvature is not too weak. Also note that the quantum number assignments for the accidental degeneracies are dubious in that there are really two non-congruent quantized tori significantly contributing to each state there.

The second possibility, namely one sequence inside the KAM island and the other outside it, which here is the more frequent situation, arises because certain KAM islands quantize well beyond their chaotic boundaries when n_1 is not too large. This situation is complicated by the fact that the exterior sequences tend to be almost evanescent, disappearing and reappearing almost randomly as though they had a partial memory of a "nearby" more regular system. Of course the further to the exterior, the more tenuous, on average, the sequence. When both sequences seem well defined in that the quasidegeneracies are good and there are few missing levels, the tendency to switch sequences exists, as above, but is generally stronger. Still the quantum number assignments are fairly sensible once corrected. Sometimes the exterior sequence is more or less invisible, though predictable in that another sequence has extended g^0 to that region. Then one sees near the foreseen crossing point one of three cases: (i) no effect, (ii) for the exterior sequence a few isolated quasidegenerate pairs appearing like nearby "shadows" through the crossing region, or (iii) for the interior sequence a gap created where there should be none. We believe that cases (ii) and (iii) are examples of effects coming from levels that are of intermediate status being neither fully regular nor completely chaotic and not easily detectable by our method. Their relative abundance seems to tend to zero with increasing energy but they are always there to some extent in our spectra. We should remark that sometimes the quantum number assignments of parts of the exterior regions can be difficult. This is not only due to the gaps but g_{qm}^0 can get a little fuzzy there. For KAM island (a) for $\lambda = -0.25$, this was not a problem but for island (a) for $\lambda = -0.35$ it was.

The second problem, that of sequence gaps, also adds to the difficulty of assigning quantum numbers since n_1 can no longer be so easily determined for each subsequence. Usually this problem is solvable with some tedious work. They arise because within one sequence the quasidegeneracy splittings can vary locally by, say, three orders of magnitude; this was not true of all the KAM

*) If Δn_2 is odd, the n_1-fixed sequence crossing occurs such that the accidental degeneracy contains one level from each of the four $\{\epsilon_1, \epsilon_2\}$ representations; see discussion leading to eq. (4.21). If Δn_2 is even there are two levels each from two representations at the accidental degeneracy.

islands. This leads to occasional gaps in some sequences until splittings smaller than $O(10^{-5})$ (unit mean spacing) were attained. This tiny splitting comes well inside the KAM region. Some of these gaps can be associated with sequence crossing effects, but not all of them. Section 4.5 will show that this may be traced back to the way the chaos modifies the tunneling process between quasidegenerate states.

4.4. Resonances

Up to this point, it seems that the complexity of the motion inside the quantizing islands is completely ignored by the quantum system. The chaotic motion is so narrowly confined as to be effectively regular and even the largest resonances cause no difficulties. The g^0_{qm} curves simply interpolate the missing gaps in g^0, and almost all the possible quasidegeneracy pairs (n_1, n_2) are found (at least for the largest islands). At first glance the results are therefore quite satisfying. There remains however one puzzling feature. In island (a) $(-0.35, \pi/4)$, there is an $r/s = 2/3$ resonance which has an area such that it should, at least in principle, quantize directly somewhere beyond the 14 000th level in the spectrum (see fig. 10). Why no problems were encountered when quantum numbers were assigned in that region and what sense these quantum numbers have should be clarified.

Let us introduce $\{I_1, I_2, \tilde{\alpha}, I\}$, where I_1, I_2 are the action variables of tori belonging to some r/s resonance, $\tilde{\alpha}$ the associated winding number and $I = I_2 + \tilde{\alpha} I_1$. One knows that at sufficiently high energy quantum states will be labeled by quantum numbers (m_1, m_2) related via EBK to the actions (I_1, I_2). Quantum mechanically one expects some kind of smooth transition between the range of energy where the (n_1, n_2) we have been using are good quantum numbers and beyond, where the (m_1, m_2) are. However, it is not obvious, a priori, how the quantum system accomplishes this. The answer involves tunneling (uniformizations) such as the treatment by Ozorio de Almeida [68], which has as a consequence the well known relationship [44] between certain avoided crossings and resonances. Here, we forego any study of a uniformized semiclassical procedure and content ourselves with understanding how, at least from the point of view that we use to assign quantum numbers, a soft transition between the two families of quantum numbers is made possible by forming new sequences of states from the ones found ignoring the resonant structure. Including the tunneling, this transition will diminish the size of $\hbar$ for which a clear signal of the existence of the resonance will be seen as compared to the naive value expected from the size of the island.

Locating the (n_1, n_2) levels which may be reassigned (m_1, m_2) values follows easily by considering the grid of points (n_1, n_2) in the (J_1, J_2) plane. Those points included in the region bounded by two lines emanating from (0,0) and passing through the points of g^0 at either edge of the gap due to the resonance in question form the pool of candidate levels. To begin with, we shall use a simplified image in which inside the resonance both the curve g^0 and its analog $I_2^0 = \tilde{g}^0(I_1^0)$ are approximated by their tangent in the center of the resonance (i.e. at the origin for $\tilde{g}^0$). In this approximation, both J^0 and I^0 are everywhere equal to J^{0*} and I^{0*}, respectively, and thus the spacing of the n_1-fixed and m_1-fixed sequences are constant with

$$I^{0*} = sJ^{0*} = \oint \boldsymbol{p} \cdot \mathrm{d}\boldsymbol{q} \,, \tag{4.27}$$

where the integral is taken over the resonance's closed orbit. This means [see eq. (4.22)] that the spacing of the m_1-fixed sequences are s times smaller than those of the n_1-fixed ones. However,

since $\alpha = r/s$, eq. (4.12) implies that

$$\Delta E^{3/4} \equiv E^{3/4}_{n_1+\Delta n_1, n_2+\Delta n_2} - E^{3/4}_{n_1,n_2} \tag{4.28}$$

is precisely the spacing of the m_1-fixed sequence if

$$s\,\Delta n_2 + r\,\Delta n_1 = 1\ . \tag{4.29}$$

One may thus pool s neighboring n_1-fixed sequences $(n_1, n_1+1, \ldots, n_1+s-1)$ to construct an m_1-fixed one. Moreover, in this simplified image, all levels E_{n_1,n_2} appear "accidentally" degenerate with all $E_{n_1+\Delta n_1, n_2+\Delta n_2}$ when $s\,\Delta n_2 + r\,\Delta n_1 = 0$. There is thus an intrinsic ambiguity in the quantum number assignments and, in particular, in the choice between (n_1, n_2) and (m_1, m_2).

Let us now turn to a more realistic description with the help of fig. 15. In practice, because neither g^0 nor $\tilde{g}^0$ can be identified with their tangent in the center of the resonance, only a few levels, corresponding to the sequence crossings discussed in section 4.3, are actually nearly degenerate.*) As already stated [see eqs. (4.26) and (4.25)], $E_{n_1,n_2} = E_{n_1+\Delta n_1, n_2+\Delta n_2}$ not only requires that $\Delta n_2/\Delta n_1 = -r/s$ but also that the midpoint between (n_1, n_2) and $(n_1+\Delta n_1, n_2+\Delta n_2)$ [in the $(J_1/2\pi\hbar, J_2/2\pi\hbar)$ plane] is as close as possible to the line $\mathcal{L}_0$ corresponding to the center of the resonance. This can be visualized by drawing in the resonance's zone of the $(J_1/2\pi\hbar, J_2/2\pi\hbar)$ plane the lines $\mathcal{L}_k$ translated from $\mathcal{L}_0$ by k times the vector $(-s/2, r/2)$, where $k = \ldots, -1, 0, 1, \ldots$. The E_{n_1,n_2} such that (n_1, n_2) lies on $\mathcal{L}_k$ will be "accidentally" degenerate with E_{n_1-kr, n_2+ks} [(n_1-kr, n_2+ks) lying on $\mathcal{L}_{-k}$]. Moreover, I^0 and J^0 strictly speaking are not constant but remain very close to I^{0*} and J^{0*}. Therefore $\Delta E^{3/4}$ defined by eq. (4.28) is again the correct spacing for an m_1-fixed sequence under the condition eq. (4.29) provided one remains as close as possible to the center of the resonance and $\Delta n_1, \Delta n_2$ remain small.

Focusing now on the $r/s = 2/3$ case, the $m_1 = 0$ sequence is constructed starting from the lowest energy E_{n_1,n_2}, here around the 14 000th level, such that the resonance should quantize directly and such that (n_1, n_2) lies in the resonance zone. The three $n_1 =$ const. sequences which are closest to $\mathcal{L}_0$ are the three lying between $\mathcal{L}_{-1}$ and $\mathcal{L}_1$. In practice, it happens that at the bottom of the $m_1 = 0$ sequence they have $n_1 = 0, 1, 2$. Thus moving up in the $m_1 = 0$ sequence corresponds to $(\Delta n_1, \Delta n_2) = (-1, 1)$ when $n_1 = 1$ or 2, and to $(\Delta n_1, \Delta n_2) = (2, -1)$ when $n_1 = 0$. This lasts until the $n_1 = 0$ sequence goes beyond the line $\mathcal{L}_1$ (which corresponds to a sequence crossing between the $n_1 = 0$ and $n_1 = 3$ sequences), after which the same pattern is continued with the $n_1 = 1, 2$ and 3 sequences, and so on.

The $m_1 = 1$ sequence can then be constructed in essentially the same way by reassigning the levels corresponding to (n_1, n_2) lying between $\mathcal{L}_{-2}$ and $\mathcal{L}_{-1}$ and between $\mathcal{L}_1$ and $\mathcal{L}_2$. The main difference is that from time to time one has to hop from $\mathcal{L}_{-1}$ to $\mathcal{L}_1$, since the levels lying in between are already reassigned to the $m_1 = 0$ sequence. The succession of $(\Delta n_1, \Delta n_2)$ when moving up in the $m_1 = 1$ sequence is thus a little more complicated. Starting from a (n_1, n_2) close to $\mathcal{L}_{-2}$ one has (i) zero or one steps of $(-1, 1)$, (ii) a step of $(-4, 3)$ to pass over the levels already reassigned to $m_1 = 0$, (iii) one or zero steps of $(-1, 1)$ and (iv) a step of $(5, -3)$ to go from $\mathcal{L}_{+2}$ back to near $\mathcal{L}_{-2}$. The question arises now whether the spacings corresponding to the many different kinds of steps, especially the large ones, will be roughly equal, since we know that there is some curvature to g^0. However, this will not be the case. We recall that the lines $\mathcal{L}_k$ have been constructed so that they correspond to accidentally degenerate levels. Since all the large steps occur in the neighborhood

*) The degeneracies we are discussing now should not be confused with the quasidegeneracies existing for all regular levels here.

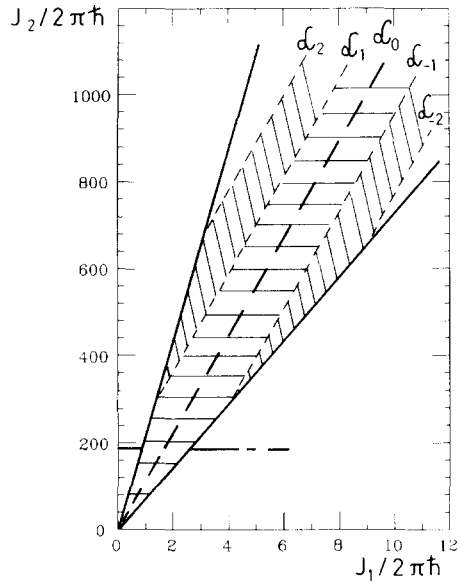

Fig. 15. Illustration in the $(J_1/2\pi\hbar, J_2/2\pi\hbar)$ plane of the reassignment from the (n_1, n_2) to the (m_1, m_2) quantum numbers for the $r/s = 2/3$ resonance in island (a) for the case $(\lambda, b) = (-0.35, \pi/4)$ (see also fig. 10b). The thick, almost (on this scale) horizontal line represents the curve g^E at the energy E where the resonance starts to quantize directly. The thick straight lines represent the border of the resonance and the thick dashed line its center. The $m_1 = 0$ ($m_1 = 1$) sequence lies in the horizontally (vertically) dashed region. See text for further explanation.

of some $\mathcal{L}_k$, one can regard them as being obtained from a small step from the almost degenerate partner near the line $\mathcal{L}_{-k}$. The curvature of g^0 therefore should only affect weakly the spacings.

Practically here it is not possible to see even the beginning of the $m_1 = 1$ sequence without going to much higher energies and even at the top of our spectra the sequences are better organized around the (n_1, n_2) quantum numbers. Except for tunneling effects at sequence crossings seen very low in the spectra, the spacings of the n_1-fixed sequence remain extremely steady. This implies small but noticeable irregularities in the spacings of the $m_1 = 0$ sequence. These irregularities are understandable because the tori on which this sequence is built are barely inside the islands of the resonance and tunneling effects will be strong. From what we have done it is then easily seen why the n_1-fixed sequence can be reobtained. Since only tiny energy displacements are actually required to make the (n_1, n_2) to (m_1, m_2) transition, they can be caused by very small matrix elements such as those provided by tunneling effects.

4.5. Chaos assisted tunneling

We now briefly discuss the behavior of the tunneling splittings of the quasidegenerate doublets. In doing so we closely follow the work of Tomsovic and Ullmo published elsewhere [43]. It has already been noted that the splittings were erratic and that their order of magnitude was not simply interpretable. This is the first clue that perhaps the chaotic region is playing a role in the tunneling that occurs between two islands. In this subsection, we shall follow up on this clue and expose the essential mechanism induced by the presence of chaos. The tunneling behavior will be shown to be drastically modified from the integrable or quasi-integrable case and to become extremely sensitive

to the variation of an external parameter.

In a standard treatment of a tunneling process, the only levels which enter are those which are nearly degenerate. For each doublet here, one is led to a two-level problem. For illustration, consider some particular doublet. One starts with two EBK wave functions Ψ_1 and Ψ_2, constructed on a torus T_1 and its symmetric partner T_2. The quantized energy is denoted by E. The Ψ_i $(i = 1,2)$ obey Schrödinger's equation asymptotically in $\hbar$, so that

$$\hat{H}\Psi_i = E\Psi_i + O(\hbar^2) . \tag{4.30}$$

In principle, it is possible to improve on this approximation to any order in $\hbar$ (see Maslov and Fedoriuk [69]) with only small modifications of the Ψ_i. However, the Hamiltonian projected on the space generated by the Ψ_i may still take on the form

$$\hat{H}\begin{pmatrix} \Psi_1 \\ \Psi_2 \end{pmatrix} = \begin{pmatrix} E & \epsilon/2 \\ \epsilon/2 & E \end{pmatrix}\begin{pmatrix} \Psi_1 \\ \Psi_2 \end{pmatrix} \tag{4.31}$$

as long as the admixing matrix element ϵ, which in this case is equal to the splitting ΔE, vanishes to any power in $\hbar$. This, for instance, is the case when

$$\Delta E = A e^{-S/\hbar} , \tag{4.32}$$

in which A and S are algebraic in $\hbar$. The usual treatment of tunneling, which has proven to apply for systems near integrability, always amounts in some sense to evaluating $\epsilon/2 = \langle \Psi_1 | \hat{H} | \Psi_2 \rangle$. This can be done in several ways for one-dimensional systems. For more degrees of freedom very few results exist, but the work of Wilkinson [70] gives a satisfactory image, which, although it is rigorously derived only for a limited class of Hamiltonians, should be relevant on a general footing. The main point we shall retain is that, to leading order, the splitting ΔE is given by an expression such as eq. (4.32), where S is the imaginary part of an action integral taken on a complex path. In other words, S is a purely classical quantity, and if one is able to tune $\hbar$ and to observe the splitting between states constructed on exactly the same tori, the data should gently fall on a line of slope -1 in a $\log \Delta E$ versus $1/\hbar$ plot. This has been done explicitly, and checked to be true, by Wilkinson for some nearly integrable systems [71].

With the quartic oscillators, one can in the same manner take advantage of the homogeneity of the potential to obtain a tuning of $\hbar$. As already pointed out, the quantizing tori indeed quantize for an infinite set of quantum numbers (assuming one rescales the energy). One may thus observe how the splitting changes keeping the classical mechanics strictly identical but for different values of $n_1 + 1/2$, which plays the role of $1/\hbar$. Figure 16 shows the results obtained for a set of three tori from the $(-0.25, \pi/4)$ case. For each of them there exist fluctuations of several orders of magnitude. A simple $\hbar$ dependence such as eq. (4.32) is excluded. Nor does any obvious indication of a predictable dependence on $\hbar$ exist. This behavior cannot be interpreted in terms of a two-level mechanism if A and S are to have a classical significance.

It is possible to obtain a clearer understanding of the tunneling by observing the variations of the splittings when an external parameter, here the coupling λ, is varied. In fig. 17, the splittings are shown for three tunneling pairs [associated with islands (a)] as a function of λ from before the islands' creation $(\lambda = 0)$ to well beyond their destruction $(\lambda = -0.60)$. In so doing, the quantum numbers (n_1, n_2) are fixed for each level thus defining via eq. (4.2) a one-parameter family of tori. As desired, with the variation of λ, $\hbar$ changes little for a given level; in the figure the three levels

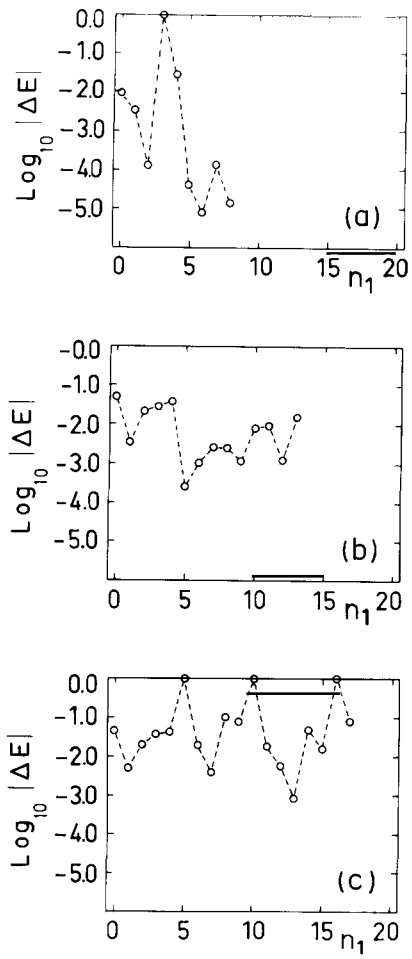

Fig. 16. Logarithm of the quasidegeneracy splittings (as always rescaled to unit mean spacing) for three tori versus n_1 [$(\lambda, b) = (-0.25, \pi/4)$]. The points are connected by dashed lines for easier viewing. A value zero indicates the pair was not located. (a) Torus $J_1 = 0.34$, (b) torus $J_1 = 0.53$, and (c) presumed cantorus $J_1 = 0.68$ just outside the 2/5 resonance.

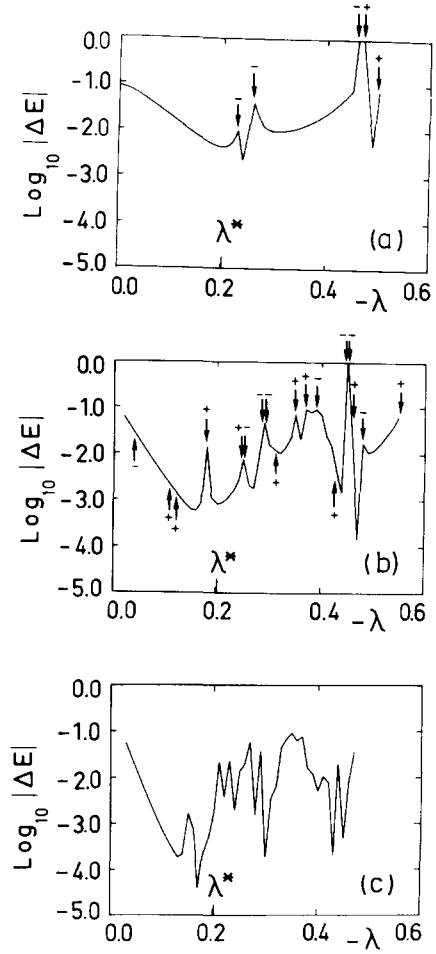

Fig. 17. Logarithm of the quasidegeneracy splittings for three cases of fixed quantum numbers (n_1, n_2) versus λ. $\hbar$ changes by a factor of three between figures (a) and (c). The arrows indicate the avoided level crossings, (+) occurring between the symmetry $(\epsilon_1, \epsilon_2) = (+, +)$ levels and (−) between the (−, −) ones. The (n_1, n_2) values are (a) (0, 14), (b) (0, 24), and (c) (1, 44).

shown are given in the order of decreasing $\hbar$ so to speak. At $\lambda = 0$, there are no resonances and no quasidegeneracies. As λ increases initially, resonances appear, some growing quite large. Yet the system remains quasi-integrable in the sense that the chaotic motion occupies a small fraction of phase space and is very much contained in narrow regions. In this regime, the splittings behave smoothly and they have no relation to the proximity of other levels. No visible effect occurs when a third regular state crosses the path of one of the states in the doublet. A quasidegenerate pair is rightfully considered as an isolated two-level tunneling system. Not surprisingly, we find that the exponential $\hbar^{-1}$ dependence given in eq. (4.32) is loosely satisfied. For example, compare figs. 17a and 17c, which were selected since they derive from exactly the same family of tori. Their

approximate factor 3 difference in the slopes of the initial roughly linear portion of the curves matches the factor 3 difference in $\hbar$ between their quantizations at any given value of λ.

Beyond the quasi-integrable regime (which effectively shrinks with $\hbar$), where one has a mixed system, the tunneling becomes affected by the non-integrability of the system. In distinction with the regular regime the splittings become extremely sensitive to the motion of the nearest chaotic levels. It is indeed quite instructive to compare the position of the extrema of ΔE with the places where the doublet's energy crosses that of the chaotic states. The number of crossings grows faster than the level density as $\hbar \to 0$ and they could only be marked on figs. 17a and 17b. Clearly, the peaks seen in the figure can mostly be associated with such a crossing. Near their tops, the difference in energy between a regular level and a chaotic crossing one dominates the splitting. This is a clear signature that in the vicinity of the peaks, the tunneling problem in its simplest form requires an extra level and is actually a three-level problem. Moreover, if one roughly evaluates the effect of the direct contribution, which would be found in the two-level scheme described above, by extrapolating the first part of the curve, the order of magnitude would be far too low to be of any relevance. Even the ranges of λ where the problem cannot be reduced to a three-level mechanism are presumably governed by a multi-level one.

The dynamical interpretation as exemplified in a three-level model is quite interesting. At first glance, it might have been anticipated that the effect of chaos would be to draw into the chaotic region a state initially localized in a KAM island. Instead, the major consequence of chaos is enhanced tunneling between islands by allowing transport across regions in phase space. Let the two EBK states be provided by some quantized torus in island (a) giving Ψ_1, and its symmetric partner in island (a') giving Ψ_2. Let us moreover specify the global phase of Ψ_2 by requiring that $\Psi_2 = \hat{P}_1 \Psi_1$. The initial state Ψ_1, even in the absence of direct coupling, will evolve into Ψ_2.

It is more convenient to work in the symmetric basis giving

$$\Psi_1 = (1/\sqrt{2})(\Psi^+ + \Psi^-), \qquad \Psi_2 = (1/\sqrt{2})(\Psi^+ - \Psi^-). \tag{4.33}$$

Ψ^+ and Ψ^- thus belong to the $(+,+)$ and $(-,-)$ sequences, respectively, if n_2 is even, and to the $(+,-)$ and $(-,+)$ sequences if n_2 is odd. We shall neglect the direct coupling between Ψ_1 and Ψ_2, which amounts to considering that the diagonal Hamiltonian matrix elements $\langle \Psi^+ | \hat{H} | \Psi^+ \rangle$ and $\langle \Psi^- | \hat{H} | \Psi^- \rangle$ are both equal to E ($\epsilon = 0$). Then, if for instance the chaotic state ϕ_c^+ belongs to the same symmetry class as Ψ^+, the three-level Hamiltonian appears in the simple form

$$\hat{H} \begin{pmatrix} \Psi^- \\ \Psi^+ \\ \phi_c^+ \end{pmatrix} = \begin{pmatrix} E & 0 & 0 \\ 0 & E & v \\ 0 & v & E_c \end{pmatrix} \begin{pmatrix} \Psi^- \\ \Psi^+ \\ \phi_c^+ \end{pmatrix}, \tag{4.34}$$

where the only admixing occurs between the chaotic and the regular symmetric (under $\hat{P}_1$) state through the tunneling matrix element v. Obtaining the time evolution of Ψ_1 is immediate—under the action of $\hat{U}(t) = \exp(-i\hat{H}t/\hbar)$, the antisymmetric component just picks up a phase $\exp(-iEt/\hbar)$ and the propagation of the symmetric, regular component follows from the standard treatment of the two-level problem. Assuming, for convenience, that $|v| \ll |E_c - E|$, there will be a weak oscillation of probability amplitude transfer from Ψ^+ to ϕ_c^+ and back of magnitude b ($\approx 2|v/(E_c - E)|$) and period t_0 ($\approx 2\pi\hbar/|E_c - E|$). At the end of each period, $\hat{U}(t_0)\Psi^+$ results in nothing more than an acquired overall phase $\exp[-i(E-\gamma)t_0/\hbar]$, where, relative to $\hat{U}(t_0)\Psi^-$, there is an extra phase fixed by $\gamma \approx v^2/(E_c - E)$. Thus after n periods,

$$\hat{U}(nt_0)\Psi_1 = e^{-iEnt_0/\hbar}(\Psi^- + e^{i\gamma nt_0/\hbar}\Psi^+). \tag{4.35}$$

As the relative dephasing of Ψ^+ and Ψ^- increases with time, the initial state is resonantly tunneling back and forth between Ψ_1 and Ψ_2 without ever fully appearing in the chaotic region. The image is that during each time step t_0, a small piece of a state on one torus breaks off and appears in the chaotic zone. By the end of the period t_0, that small piece has moved onto the symmetric partner torus. The total time to tunnel completely from one island to another is $2t_0/b^2$, which is just a simple combination of the squared amplitude and oscillation period.

In the more general situation, that is, if one does not select a value of the coupling such that one chaotic state plays a predominant role, the tunneling mechanism will involve many chaotic states. We strongly suspect that a detailed description of the individual splittings will be difficult to obtain. As suggested in the introduction as concerns chaotic motion, the statistical features may contain some very interesting properties. Although it is the next section that discusses in depth the ideas behind statistical modeling, we write down a zeroth order model which could be generalized or made clearer taking into account those aspects. The basic idea is that each regular state is independently, randomly, and weakly coupled to independent matrix ensembles modeling the chaotic states of the same symmetry. The model Hamiltonian would look like*)

$$\hat{H}\begin{pmatrix} \Psi^- \\ \mathcal{E}^- \\ \Psi^+ \\ \mathcal{E}^+ \end{pmatrix} = \begin{pmatrix} E & \{v\} & 0 & 0 \\ \{v\} & \text{GOE} & 0 & 0 \\ 0 & 0 & E & \{v'\} \\ 0 & 0 & \{v'\} & \text{GOE}' \end{pmatrix}\begin{pmatrix} \Psi^- \\ \mathcal{E}^- \\ \Psi^+ \\ \mathcal{E}^+ \end{pmatrix}, \tag{4.36}$$

where $\mathcal{E}^-$ and $\mathcal{E}^+$ represent the quantum Hilbert spaces of chaotic states with the same symmetry as Ψ^- and Ψ^+, GOE denotes a Gaussian Orthogonal Ensemble of random matrices, which will be thoroughly discussed in section 5, and $\{v\}$, $\{v'\}$ a random coupling with independent matrix elements (zero centered, normally distributed, and with equal variance v^2). The primes emphasize the independent nature of the ensembles and couplings. A very attractive problem would be to determine semiclassically the different parameters describing the model, particularly the behavior of the v, v', which correspond to classically forbidden transport processes, and to deduce from it definite quantitative predictions on the tunneling behavior. This we think is non-trivial but feasible, and we plan to look into it in the near future. In any case, the main qualitative features should remain the same as for the three-level problem. Namely, this should lead to enhanced tunneling with a great sensitivity to the variation of an external parameter, and without dissolution of a wave packet started in a regular region into the chaotic one.

The observed fluctuations of the quartic oscillators doublets' splitting thus find a natural interpretation in the multi-level mechanism we have introduced. Our discussion and results also are consistent with, and shed some light on the recent observations of Lin and Ballentine [72] for driven, double well oscillators. The scope of this new tunneling mechanism goes beyond the range of simple numerical experiments. Dynamical tunneling between symmetric regular states takes place in several simple molecular systems [73, 32, 6], and the characteristic features of the chaos assisted tunneling, such as the sensitivity to the variation of an external parameter, should allow one to detect it experimentally when the underlying classical motion is mixed. Additionally, it seems that some problems in condensed matter physics offer a good opportunity, perhaps the best one at the present time, to observe tunneling properties experimentally. The recent progress in molecular beam epitaxy allows one to design multilayer semiconductors with a high degree of control on their

*) We neglect here the inner structure of the chaotic region, which will be discussed in the next section.

specifications [74]. In particular they can be designed such that the vertical motion of the electrons takes place in wells. Experimental techniques probing the tunneling properties for such systems are already well developed (see, for instance, ref. [75]). If one is able to induce some chaos, by an intense laser pulse for instance as proposed by Lin and Ballentine, the tunneling properties should be drastically modified, in an experimentally observable manner.

5. Chaotic spectrum

We shall now concentrate on the part of the spectrum remaining after the removal of the regular levels. This shall be considered the "chaotic" spectrum. As discussed by Percival [40], these chaotic states are, in some sense, related to the classical chaotic phase space. There is no equivalent of EBK quantization there just as it fails in fully chaotic systems. As mentioned in the introduction, in such chaotic systems statistical characterizations of the spectra have been successful. By focusing attention on fluctuation properties new universal behavior has come to light. In 1983 Bohigas, Giannoni, and Schmit [14] conjectured that sufficiently chaotic systems had the fluctuation properties of the random matrix ensembles of Wigner and Dyson [16, 17]. For time reversal invariant systems such as the quartic oscillators the Gaussian or Circular Orthogonal Ensembles (GOE, COE) apply. Their spectra are remarkable in that they are very rigid implying a great deal of level repulsion. It is natural to apply the same random matrix ideas and the classification scheme of Percival to the chaotic parts of mixed systems. This along with the result that regular levels are Poisson distributed led to the Berry–Robnik surmise.

In fact, we are less concerned about the statistical properties of the regular levels for a large part because the classical knowledge may be used in a fairly complete way to give detailed information about the correspondence as we have just done in section 4. In cases such as ours, where the regular part of the spectrum may be removed, and where only one large chaotic region exists, the previous way of thinking is reduced to that of its essential postulate: the chaotic spectrum should have GOE fluctuations. It turns out that for the system we have studied this is not the case. Neither can the obtained fluctuations be mimicked by any independent superposition of spectra.

The GOE is basically constructed in such a way that it contains no information other than that time reversal invariance holds. In a sense, using a simple GOE to interpret the chaotic spectrum fluctuations amounts to considering the chaotic part of the classical phase space as a homogeneous, featureless object. However, we have seen, for the quartic oscillators with $\lambda = -0.35$ coupling, that an inner structure exists due to partial barriers. Moreover, similar behaviors, although perhaps even more complicated, should be found for most mixed systems; they may be missed if not explicitly searched for. We shall see that the classical information, concerning transport properties, can be translated into constraints on the matrix elements of the quantum evolution operator $\hat{U}(t) = \exp[-(\mathrm{i}/\hbar)\hat{H}t]$, and then from $\hat{U}(t)$ to the Hamiltonian itself. Once these constraints are expressed, a modeling using generalized random matrix ensembles will provide a prediction which agrees quite well in our test case.

5.1. *Association of a quantum subspace to a classical region*

Implicit in the classification scheme of Percival is that, if properly expressed, the Hamiltonian $\hat{H}$ or time evolution operator $\hat{U}(t)$ should appear in the semiclassical approximation as a block diagonal matrix, each block being associated with an isolated region of the classical phase space. In cases where a chaotic region of the phase space can be decomposed in nearly, but not completely,

isolated subregions, it is in the same way natural to consider that in some proper basis, $\hat{H}$ or $\hat{U}(t)$ for t not too long, should appear as a block diagonal matrix whose blocks are connected through small, but non-zero, matrix elements. The average size of these matrix elements, i.e. the quantum constraints, will be related to the flux connecting different subregions, i.e. to classical information. However, if those operators are expressed in no particular basis this peculiar form will not hold any more, although the corresponding information will still exist in a hidden way through matrix element correlations. In the following, we shall always assume that we are working in what we may call a relevant basis, that is any basis in which the constraints on the operators $\hat{H}$ or $\hat{U}(t)$ appear in a natural way. For instance, if the considered information were time reversal invariance (TRI) of systems without spin, the relevant bases are simply those in which all TRI Hamiltonians are simultaneously expressed as real symmetric matrices (in an arbitrary basis there is no reason why TRI Hamiltonians should be real). In the same way, when the system has some exact or model symmetry, relevant bases will be those corresponding to the appropriate irreducible representations. For our purposes, the relevant bases are those for which each vector will be unambiguously attached to a distinct region of the phase space. The set of vectors associated to one region will define a vector subspace which is more important physically than the bases themselves (as for TRI, there is an infinity of relevant bases, and physical results do not depend on the precise basis used).

When considering completely separated regions, it is sufficient to postulate explicitly or implicitly the existence of such relevant bases. Here, since we would like to actually relate the size of connecting matrix elements to classical flux, it is worthwhile to proceed a little further, and at least to characterize them in some way. Notice, however, that in no case will we need to explicitly construct a relevant basis. For this purpose, we shall introduce two different images, the first one based on the Weyl–Wigner calculus presented in section 3, the second on time-dependent EBK theory. Both images allow us to relate the admixing matrix elements of $\hat{U}(t)$ to the classical flux, although here we shall only present the derivation based on the first image, which is simpler. Thus, they are somewhat equivalent from a practical point of view. Since they give rise to different physical understanding, which may lead to a preference for one or the other depending on circumstances, we shall present both interpretations.

5.1.1. Weyl–Wigner image

Let us consider that the $2d$-dimensional phase space (d is the number of degrees of freedom) is partitioned into a certain number of $2d$-dimensional regions R_i which are nearly or even completely isolated under the classical motion generated by H. Let us consider moreover one region, say R, which extends only over a finite range of energy and thus has finite volume. Following simple intuition, since the Weyl formula

$$\overline{N}(E_R) \simeq \frac{1}{(2\pi\hbar)^d} \int \Theta(E_R - H_R)\, \mathrm{d}\boldsymbol{q}\, \mathrm{d}\boldsymbol{p} \tag{5.1}$$

holds for any Hamiltonian H_R, and since H_R can certainly be chosen such that R is the region of phase space such that $H_R(p,q) \leq E_R$, one may say that R is associated with the quantum subspace $\mathcal{E}_R$ generated by the eigenstates $|\psi_k\rangle$ [$k = 1, \ldots, \dim(\mathcal{E}_R)$] of the quantized $\hat{H}_R$ whose eigenvalues are smaller than E_R. The dimensionality of $\mathcal{E}_R$ is then

$$\dim(\mathcal{E}_R) \simeq \frac{1}{(2\pi\hbar)^d} \int_R \mathrm{d}\boldsymbol{q}\, \mathrm{d}\boldsymbol{p}\ . \tag{5.2}$$

Using the second equality of eq. (3.7), one may think of the Wigner transform $\rho_{kk}(\boldsymbol{q},\boldsymbol{p}) = [|\psi_k\rangle\langle\psi_k|]_{\mathrm{w}}(\boldsymbol{q},\boldsymbol{p})$ as a function taking the value 1 in some $(2\pi\hbar)^d$ cell of R and 0 elsewhere, the

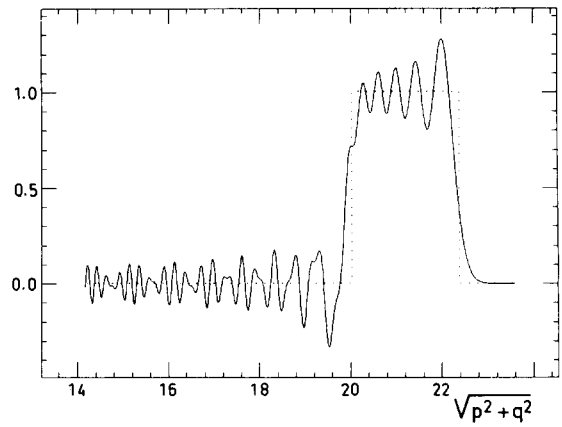

Fig. 18. Illustration, using the harmonic oscillator $\hat{H}(\hat{q},\hat{p}) = \frac{1}{2}(\hat{p}^2 + \hat{q}^2)$, of the relation between partial traces and volume integrals in restricted regions of phase space. The curvy line corresponds to the Wigner transform of eq. (5.3), where the summation extends from the 200th to the 250th eigenstate (energy domain between $\sqrt{401}$ and $\sqrt{501}$). The points correspond to the characteristic function eq. (5.5).

cells corresponding to different ρ_{kk} filling R without overlapping because of the third equality of eq. (3.7). This picture is, of course, very far from reality when applied to a single vector. When one considers the projector

$$\hat{P}_R = \sum_{k=1}^{\dim(\mathcal{E}_R)} \hat{\rho}_{kk} \tag{5.3}$$

it is however sensible to assume that the fluctuations of each particular ρ_{kk} will be washed out and that the previous image becomes more accurate. We shall therefore consider that the Wigner transform of $\hat{P}_R$ is simply the characteristic function χ_R of region R, i.e.,

$$[\hat{P}_R]_w(\boldsymbol{q},\boldsymbol{p}) \simeq \chi_R(\boldsymbol{q},\boldsymbol{p}), \tag{5.4}$$

$$\chi_R(\boldsymbol{q},\boldsymbol{p}) = \begin{cases} 1 & \text{if } (\boldsymbol{q},\boldsymbol{p}) \text{ belongs to } R, \\ 0 & \text{elsewhere}. \end{cases} \tag{5.5}$$

In fig. 18 we confirm how well this works for the Wigner transforms of a projector of a group of harmonic oscillator eigenstates. As long as the eigenstates belonging to an energy range of at least $\hbar^{2/3}$ are included, only a small residual oscillation appears superposed on $\chi_R(\boldsymbol{q},\boldsymbol{p})$.

We may implement the classical energy conservation, which means that each classical feature is to be considered at one particular energy. Quantum mechanically speaking, one expects the behavior of the spectrum around some energy E to be related only to the classical motion around that energy. We shall thus consider in the following the intersection of regions R_i with an energy slice $H \in [E - \Delta E/2, E + \Delta E/2]$ rather than the total region itself. This implicitly supposes that the Hamiltonian expressed in a relevant basis appears as a bordered matrix: the matrix elements between two vectors whose mean energies are too far apart on the classical scale should be close to zero. We shall thus consider that the Wigner transform of any basis state whose mean energy is equal to E is localized on the classical energy surface $H = E$. Therefore, in the Weyl–Wigner image, relevant bases are characterized by the fact that

(i) the Wigner transform of any state is localized on one classical energy surface;

(ii) the Wigner transform of a projector onto any subspace associated to a region R_i is the characteristic function χ_{R_i}.

We suspect that these requirements can be fulfilled in the limit $\hbar \to 0$, although some care must be exercised as to the details of the classical phase space one wishes to resolve. For finite $\hbar$, the main postulate made here is that the departure from the above description will not be relevant as far as one is concerned with the statistical properties of the spectrum. See the work of Ozorio de Almeida [1] and Berry [76] which may place these intuitive ideas on a firmer foundation.

5.1.2. Maslov image

One may also deal with relevant bases from another point of view. Since we shall only introduce it to help physical understanding, we shall restrict ourselves here to a brief description, and refer to ref. [77] for a more detailed account.

The basic semiclassical tool, in this picture, is the time-dependent EBK approximation for multidimensional systems developed by Maslov [69, 39, 78]. The first aim of this semiclassical approach is to give a construction which associates a quantum wave function ψ to each Lagrangian torus $\mathcal{T}$ of the classical phase space which fulfills the conditions eq. (4.2). Note that this association is of a purely geometrical nature and is made without any reference to a particular Hamiltonian. Then, if one introduces some dynamics through a quantum Hamiltonian $\hat{H}(\hat{p}, \hat{q})$ and its classical limit $H(p, q)$, one can also associate a wave function $\psi(t)$ to each image $g^t\mathcal{T}$ of $\mathcal{T}$ by the Hamiltonian flow g^t. $\psi(t)$ (which is calculated only by a classical propagation of $\mathcal{T}$) is, in the semiclassical approximation [i.e. to $O(\hbar^2)$], a solution of the time-dependent Schrödinger equation. This can be summarized with the following diagram:

$$\begin{array}{lccc} & t = 0 & & t \\ \text{classical} & \mathcal{T} & \longrightarrow & g^t\mathcal{T} \\ & \downarrow & & \downarrow\, O(\hbar^2) \\ \text{quantum} & \Psi & \longrightarrow & \hat{U}(t)\Psi \end{array}$$

Thus, if one is able to build an orthonormal basis $\{\psi_\alpha^i\}$ of the quantum vector space such that

(i) each state ψ_α^i is obtained from a classical torus $\mathcal{T}_\alpha^i$ through the Maslov construction,

(ii) each torus $\mathcal{T}_\alpha^i$ thus defined is completely interior to one of the regions R_i, and

(iii) each torus $\mathcal{T}_\alpha^i$ wanders in a small range of energy on the classical scale,

the set $\{\psi_\alpha^i\}$ may be used as a relevant basis. In this way one may obtain a semiclassical approximation of the evolution operator $\hat{U}(t)$ by expressing the matrix elements $\langle\psi_\alpha^i|\hat{U}(t)|\psi_\beta^j\rangle = \langle\psi_\alpha^i|\psi_\beta^j(t)\rangle$. Moreover, it can be easily shown that the scalar product of two wave functions constructed on tori which have no point in common is zero in the stationary phase approximation. Thus, if two regions R_i and R_j are completely disconnected, all $\langle\psi_\alpha^i|\psi_\beta^j(t)\rangle$ are virtually zero since $g^t\mathcal{T}_\beta^j$ never intersects $\mathcal{T}_\alpha^i$. In the same way, if R_i and R_j are only slightly connected, the probability that $g^t\mathcal{T}_\beta^j$ intersects $\mathcal{T}_\alpha^i$ is small and the matrix elements connecting block i to block j are also small. They can be evaluated to give the same result that we shall obtain with the Weyl–Wigner image. Finally, (iii) implies that all quantum features of $\hat{U}(t)$ are related to the classical motion near a specific energy.

Constructing a basis which satisfies (i) and (ii) is, in a sense, equivalent to finding an integrable Hamiltonian H_0 which respects the boundaries of the regions R_i. For a one degree of freedom

system (say time dependent and periodic to allow chaos), this is actually trivial. For more degrees of freedom, we know of no proof at the present time that such an H_0 can be found and here its existence, which is the only result we need, not its actual construction, is to be considered as a sensible postulate which need only be fulfilled in an approximate way. Concerning (iii), note that, since a Lagrangian torus included in an energy surface of H is an invariant torus, the $\mathcal{T}_\alpha^i$ cannot be required to have zero extension in energy.

One interesting feature of relevant bases considered from the Maslov image is that each matrix element of $\hat{U}(t)$ is separately accounted for. The mean square value in each connecting block thus leads, as previously stated, to the same result as one may obtain from the Weyl–Wigner image. However, at least from an intuitive point of view, both the homogeneity of the repartition of the matrix elements inside each block and their decorrelation, which we shall postulate when introducing random matrix theory, can here be understood as deriving from the chaotic behavior of classical motion. Indeed, for two regions R_i and R_j (including the case $i = j$) for which at a time t a complete mixing is obtained, and connected through a Markovian-like process (if $i \neq j$), the probability that the image under g^t of some torus $\mathcal{T}_\beta^j$ intersects a torus $\mathcal{T}_\alpha^i$ will be the same for all α and β, giving a uniform value to the expectation of the $|U_{\alpha\beta}^{ij}|^2$ (for fixed i and j). Moreover, the decorrelation of the motion of distinct tori will naturally lead to the decorrelation of the matrix elements. As a consequence of the homogeneity and independence of matrix elements of the evolution operator, the Hamiltonian matrix can be regarded as having these same properties.

Finally, although all bases which satisfy (i), (ii) and (iii) are a priori equally good relevant bases, some of them (i.e. those for which in each R_i the $\mathcal{T}_\alpha^i$ form a pattern resembling a single resonance) appear as more natural. If moreover R_i is a chaotic region surrounding a KAM island, the basis which corresponds to the part of g_{qm}^E outside of the island (recall fig. 11) may be called the preferred relevant basis. It is only easily defined as far as g_{qm}^E is (and thus may not exist if g_{qm}^E does not extend the classical KAM limit), but its existence seems to underlie the quantum motion.

5.2. *Relation between flux and matrix elements*

From now on, we shall consider that all operators are expressed in some relevant basis $\{|i,\alpha\rangle\}$, where i labels the region to which $|i,\alpha\rangle$ is associated and α is a sublabel defining the precise state under consideration. Let us also denote by E_α^i the mean energy

$$E_\alpha^i = \langle i,\alpha|\hat{H}|i,\alpha\rangle \tag{5.6}$$

of $|i,\alpha\rangle$. We do not know how to calculate precisely in a semiclassical manner all the matrix elements. Neither do we suspect that this is truly possible or the interesting thing to do. However, the mean square behavior and other similar average properties are essential. We therefore introduce, for any operator $\hat{A}$, the local expectation value defined as

$$\langle\hat{A}\rangle_E = \frac{1}{N_{E,\Delta E}} \sum_{E_\alpha^i \in [E-\Delta E/2, E+\Delta E/2]} \langle i,\alpha|\hat{A}|i,\alpha\rangle \ , \tag{5.7}$$

where N_{E,Δ_E} is the number of levels whose mean energies lie in the interval $[E-\Delta E/2, E+\Delta E/2]$. In this definition, one implicitly assumes the independence of the average from the choice of ΔE to within a range, infinitesimal classically yet infinite on the scale of the density of states.

Denoting by $\hat{P}_E$ the projector

$$\hat{P}_E = \sum_{E_\alpha^i \in [E-\Delta E/2, E+\Delta E/2]} |i,\alpha\rangle\langle i,\alpha| \ , \tag{5.8}$$

the expectation value eq. (5.7) can be written as

$$\langle \hat{A} \rangle_E = \frac{1}{N_{E,\Delta E}} \mathrm{Tr}[\hat{A}\hat{P}_E] \,. \tag{5.9}$$

5.2.1. Admixing matrix elements of $\hat{U}(t)$

The operator whose matrix elements are naturally related to the classical motion is the time evolution operator $\hat{U}(t)$. Considering a time t sufficiently long that the interior of each nearly disconnected classical region is completely mixed, and yet sufficiently small that the relative volumes of phase points exchanged between neighboring regions are small, $\hat{U}(t)$ is a block diagonal matrix whose blocks are connected through small admixing matrix elements which we now evaluate. Namely, we are interested in the expectation value

$$\begin{aligned} \langle \hat{U}(t)\hat{P}_j\hat{U}^\dagger(t)\hat{P}_k \rangle_E &= \frac{1}{N_{E,\Delta E}} \mathrm{Tr}[\hat{U}(t)\hat{P}_j\hat{U}^\dagger(t)\hat{P}_k\hat{P}_E] \\ &= \frac{1}{N_{E,\Delta E}} \int \frac{\mathrm{d}\boldsymbol{q}\,\mathrm{d}\boldsymbol{p}}{(2\pi\hbar)^d} [\hat{U}(t)\hat{P}_j\hat{U}^\dagger(t)\hat{P}_k\hat{P}_E]_{\mathrm{w}}(\boldsymbol{q},\boldsymbol{p}) \,. \end{aligned} \tag{5.10}$$

Since we are only concerned with the leading term in $\hbar$, the Wigner transform of an operator product may be approximated with the product of the individual Wigner transforms. Thus one can write

$$\frac{1}{N_{E,\Delta E}} [\hat{U}(t)\hat{P}_j\hat{U}^\dagger(t)\hat{P}_k\hat{P}_E]_{\mathrm{w}}(\boldsymbol{q},\boldsymbol{p}) = [\hat{P}_j]_{\mathrm{w}}(\boldsymbol{q},\boldsymbol{p},t)\,[P_k]_{\mathrm{w}}(\boldsymbol{q},\boldsymbol{p})\,\frac{[\hat{P}_E]_{\mathrm{w}}(\boldsymbol{q},\boldsymbol{p})}{N_{E,\Delta E}} + \mathrm{O}(\hbar^2) \,, \tag{5.11}$$

where $[\hat{P}_j]_{\mathrm{w}}(\boldsymbol{q},\boldsymbol{p},t) = [\hat{U}(t)\hat{P}_j\hat{U}^\dagger(t)]_{\mathrm{w}}(\boldsymbol{q},\boldsymbol{p})$ is the Wigner transform of $\hat{P}_j$ after it has evolved under the quantum motion during a time t. Now eq. (3.10) applies for each of the vectors $|i,a\rangle$ and thus for $\hat{P}_j$. Continuing on with leading order in $\hbar$, this means that $[\hat{P}_j]_{\mathrm{w}}(\boldsymbol{q},\boldsymbol{p},t)$ evolves to $\mathrm{O}(\hbar^2)$ like a fluid density under the classical law of motion. Since $[\hat{P}_j]_{\mathrm{w}}(\boldsymbol{q},\boldsymbol{p},0) = [\hat{P}_j]_{\mathrm{w}}(\boldsymbol{q},\boldsymbol{p})$ is taken as $\chi_{R_j}(\boldsymbol{q},\boldsymbol{p})$, $[P_j]_{\mathrm{w}}(\boldsymbol{q},\boldsymbol{p},t)$ is equal, at this level of approximation, to the characteristic function $\chi_{g^tR_j}$, which takes the value one inside the image g^tR_j of region R_j under the Hamiltonian flow and zero outside.

The effect of $[\hat{P}_E]_{\mathrm{w}}/N_{E,\Delta E}$ is just to select the energy E at which the classical features must be considered. We have assumed that the Wigner transform of a vector $|i,\alpha\rangle$ of the relevant bases is localized around the classical energy surface $H = E_\alpha^i$, thus $[\hat{P}_E]_{\mathrm{w}}(\boldsymbol{q},\boldsymbol{p})$ may be regarded as null outside the energy range $H(\boldsymbol{q},\boldsymbol{p}) \in [E - \Delta E/2, E + \Delta E/2]$. Since moreover this slice is supposed to contain many states, all particular features of the $[|i,\alpha\rangle\langle i,\alpha|]_{\mathrm{w}}$ are smoothed away, and with the same logic as in section 3.3, $[\hat{P}_E]_{\mathrm{w}}(\boldsymbol{q},\boldsymbol{p})$ may be regarded as equal to one if $H(\boldsymbol{q},\boldsymbol{p}) \in [E - \Delta E/2, E + \Delta E/2]$ and to zero elsewhere. Since moreover ΔE is supposed to be infinitesimal on the classical scale, one may write

$$[\hat{P}_E]_{\mathrm{w}}(\boldsymbol{q},\boldsymbol{p}) = \delta(E - H)\,\Delta E \tag{5.12}$$

and thus

$$\langle \hat{U}(t)\hat{P}_j\hat{U}^\dagger(t)\hat{P}_k \rangle_E \simeq \frac{1}{(2\pi\hbar)^d \bar{\rho}(E)} \int \mathrm{d}\boldsymbol{q}\,\mathrm{d}\boldsymbol{p}\,\chi_{g^tR_j}(\boldsymbol{q},\boldsymbol{p})\chi_{R_k}(\boldsymbol{q},\boldsymbol{p})\delta(E - H) \,. \tag{5.13}$$

The numerator of the right hand side of eq. (5.13) is thus simply the Liouville measure at energy E of the overlap of g^tR_j and R_k. For time t sufficiently short that the probability of return is

negligible*), the left hand side of eq. (5.13) is t times the flux, Φ_{jk}, connecting region j to region k, and thus

$$\langle \hat{U}(t)\hat{P}_j\hat{U}^\dagger(t)\hat{P}_k\rangle_E \simeq \frac{\Phi_{jk}(E)t}{(2\pi\hbar)^d\bar{\rho}(E)} \,. \tag{5.14}$$

5.2.2. Admixing matrix elements of $\hat{H}$

To facilitate the connection with the theory of transitions [79] in random matrix theory, which we shall discuss in the next subsection, and which has been developed using the Gaussian ensemble framework, we now translate what is known about $\hat{U}(t)$ to information on $\hat{H}$ itself. To obtain a theoretical prediction for the chaotic spectrum fluctuations which may be compared to spectral data, we therefore have to relate the expectation value eq. (5.10) to the size of the connecting matrix elements of the Hamiltonian operator expressed in a relevant basis.

Let us first split the Hamiltonian matrix into two pieces,

$$\hat{H} = \hat{H}_0 + \hat{H}_1 \,, \tag{5.15}$$

where $\hat{H}_0$ is purely block diagonal, and $\hat{H}_1$ contains only the small block non-diagonal connecting matrix elements. This induces for $\hat{U}(t)$ a natural separation into

$$\hat{U}(t) = \hat{U}_0(t) + \hat{U}_1(t) \,, \tag{5.16}$$

where $\hat{U}_0(t)$ is defined as

$$\hat{U}_0(t) = \exp\left[-(\mathrm{i}/\hbar)\hat{H}_0 t\right] \,. \tag{5.17}$$

Note both $\hat{U}(t)$ and $\hat{U}_0(t)$ are unitary matrices but $\hat{U}_1(t) = \hat{U}(t) - \hat{U}_0(t)$ is most likely not.

To evaluate the size of the matrix elements of $\hat{H}_1$ which correctly gives the expectation values $\langle \hat{U}(t)\hat{P}_j\hat{U}^\dagger\hat{P}_k\rangle_E$ ($= \langle \hat{U}_1(t)\hat{P}_j\hat{U}_1^\dagger(t)\hat{P}_k\rangle_E$ since $\hat{U}_0$ is purely block diagonal) we shall start from the equality

$$\hat{U}(t) = \hat{U}_0(t) - \frac{\mathrm{i}}{\hbar}\int_o^t \mathrm{d}\tau\, \hat{U}_0(t-\tau)\hat{H}_1\hat{U}(\tau) \,, \tag{5.18}$$

which can be verified by differentiating both members and by noting that for $t = 0$ eq. (5.18) is obviously true. Neglecting any contribution of $\hat{H}_1$ beyond first order, one simply finds

$$\hat{U}_1(t) \simeq -\mathrm{i}\int_0^t \frac{\mathrm{d}\tau}{\hbar}\hat{U}_0(t-\tau)\hat{H}_1\hat{U}_0(t) \,. \tag{5.19}$$

We now choose a particular relevant basis, namely $\{|\mathcal{E}_\alpha^i\rangle\}$, in which $\hat{H}_0$ is diagonal and where the subscript i indicates that $|\mathcal{E}_\alpha^i\rangle$ belongs to the vector space associated with region R_i. The $|\mathcal{E}_\alpha^i\rangle$ are related to any relevant basis $|i,\alpha\rangle$ by a block diagonal orthogonal transformation which leaves the mean squared matrix element of the off-diagonal blocks invariant. In this basis, one obtains

*) This implies that the time t must be much smaller than Φ_{jk}/V_j and Φ_{jk}/V_k, where the volume $V_i(E)$ equals $V_i(E) = \int_{R_i} \mathrm{d}\boldsymbol{q}\,\mathrm{d}\boldsymbol{p}\,\delta(E-H)$.

$$\langle \hat{U}_1^\dagger(t)\hat{P}_j\hat{U}_1(t)\hat{P}_k\rangle_E$$
$$= \frac{1}{\hbar^2}\int_0^t\int_0^t \mathrm{d}\tau_1\,\mathrm{d}\tau_2\,\langle \hat{U}_0^\dagger(\tau_2)\hat{H}_1\hat{U}_0^\dagger(t-\tau_2)\hat{P}_j\hat{U}_0(t-\tau_1)\hat{H}_1\hat{U}_0(\tau_1)\hat{P}_k\rangle_E$$
$$= \frac{2}{\hbar^2}\int_0^t \mathrm{d}\tau\,(t-\tau)\frac{1}{N_{E,\Delta E}}$$
$$\times \sum_{\substack{\mathcal{E}_\alpha^k\in[E-\Delta E/2,E+\Delta E/2]\\ \mathcal{E}_\beta^j\in[0,\infty[}} \exp[-(\mathrm{i}/\hbar)(\mathcal{E}_\alpha^k-\mathcal{E}_\beta^j)\tau]|\langle\mathcal{E}_\alpha^k|\hat{H}_1|\mathcal{E}_\beta^j\rangle|^2\,. \tag{5.20}$$

Note that no statistical assumption has yet been made to obtain eq. (5.20). To proceed further we suppose that all statistical quantities concerning the particular system ($\hat{H} = \hat{H}_0 + \hat{H}_1$) considered are the same as their average values taken over some matrix ensemble. This ensemble is taken such that all matrix elements of $\hat{H}_1$ are independently chosen from each other and from the eigenvalues of $\hat{H}_0$, and the mean square matrix element is constant and chosen as v_{jk}^2 in each block connecting space j to space k. Also, the mean density of levels

$$\overline{\overline{\rho^i(E)}} = \overline{\overline{\sum_\alpha \delta(E-\mathcal{E}_\alpha^i)}}$$

(where the double bar means ensemble averaging) can be taken equal to the smoothed density $\bar{\rho}^i(E)$ of the ith block of the actual Hamiltonian since $\hat{H}_1$ is weak.

Besides the simplifications introduced by this "statistical postulate", its physical relevance may be understood from two different points of view. On the one hand, it is possible to think of each particular matrix of the ensemble as representing slices of spectra sufficiently far one from each other that they behave independently (i.e., a local diagonalization of one slice does not essentially change the matrix elements around the other) and yet sufficiently close that the classical behavior at their respective energies is similar. On the other hand, the ensemble introduced presumably possesses the ergodicity property of the Wigner–Dyson ones [80], which means that any of its elements (and in particular the actual $\hat{H}$ under consideration) almost certainly behaves like the ensemble average. It is most probable that both these arguments should enter into a justification of the introduction of such an ensemble.

Thus, using the independence of the $\langle\mathcal{E}_\alpha^j|\hat{H}_1|\mathcal{E}_\beta^k\rangle$ from the eigenvalues of $\hat{H}_0$, and

$$\overline{\overline{|\langle\mathcal{E}_\alpha^j|\hat{H}_1|\mathcal{E}_\beta^k\rangle|^2}} = v_{jk}^2 = \text{const.},$$

one obtains

$$\overline{\overline{\langle \hat{U}_1^\dagger(t)\hat{P}_j\hat{U}_1(t)\hat{P}_k\rangle_E}}$$
$$= \frac{2}{\hbar^2}\frac{v_{jk}^2}{N_{E,\Delta E}}\int_0^t \mathrm{d}\tau\,(t-\tau)\int_0^\infty \mathrm{d}y \int_{E-\Delta E/2}^{E+\Delta E/2} \mathrm{d}x\,\bar{\rho}^j(y)\bar{\rho}^k(x)\exp[-(\mathrm{i}/\hbar)(x-y)\tau]\,. \tag{5.21}$$

Since ΔE is infinitesimal on the classical scale, $\bar{\rho}^k(x)$ can be set equal to $\bar{\rho}^k(E) = f_k(E)\bar{\rho}(E)$ [where $f_k(E)$ is the relative volume of region R_k at energy E] in the interval $[E-\Delta E/2, E+\Delta E/2]$. The integration on x thus leads to

$$\int_{E-\Delta E/2}^{E+\Delta E/2} \mathrm{d}x\, \mathrm{e}^{-(\mathrm{i}/\hbar)x\tau} = \Delta E\, \mathrm{sinc}(\Delta E\, \tau/2\hbar)\mathrm{e}^{-(\mathrm{i}/\hbar)E\tau} \tag{5.22}$$

[where sinc $u = \sin(u)/u$]. This basically means that as soon as

$$\Delta E\, \tau/\hbar > 2\pi \tag{5.23}$$

the unit circle is uniformly covered, leading to a center of gravity at O. The oscillations that exist in the sinc function for $\Delta E\, \tau/\hbar > 2\pi$ are due to the sharp cut made in energy and therefore have no physical significance. Since ΔE is assumed large on the quantum scale, the only contribution of the integration over τ comes from the neighborhood of $\tau = 0$. On may thus extend the time integral from t to infinity, and drop the τ in $t - \tau$.

Therefore, one obtains

$$\begin{aligned} \overline{\overline{\langle \hat{U}_1^\dagger(t)\hat{P}_j\hat{U}_1(t)\hat{P}_k\rangle_E}} &\simeq \frac{2\pi t}{\hbar}\frac{v_{jk}^2}{N_{\overline{E,\Delta E}}}\int_0^\infty \mathrm{d}y \int_{E-\Delta E/2}^{E+\Delta E/2} \mathrm{d}x\, \bar{\rho}^j(y)\bar{\rho}^k(x)\delta(x-y) \\ &\simeq \frac{2\pi}{\hbar} t f_j f_k \bar{\rho}(E) v_{jk}^2 \,. \end{aligned} \tag{5.24}$$

This equation may be regarded as a statistical version of Fermi's Golden Rule. There are however some slight differences in its domain of applicability. To bègin with, it does not concern the transition amplitude from a discrete level to the continuum spectrum (with almost constant coupling). Only averages between discrete levels are obtained and not one particular transition amplitude. A second difference stems from the smoothing over a range of energy ΔE, which allows the extension of the time integral in eq. (5.21) to infinity not because t is presumed large but because ΔE is. In the limit when ΔE contains an infinite number of levels [$\Delta E \to \infty, \bar{\rho}(E) = \text{const.}$], the time integral in eq. (5.21) would also lead to a delta function even for arbitrarily small t. Note however that eq. (5.24) [and also eq. (5.14)] is valid only for a range of "intermediate" times. On the one hand, t must be sufficiently long so that the matrix elements of $\hat{U}(t)$ are shared homogeneously inside each block, which in particular implies that $\hat{U}(t)$ cannot be approximated by $1 - (\mathrm{i}/\hbar)\hat{H}t$. A classical analog may be that t must be sufficiently long so that the motion inside each region R_i is completely mixed, and thus

$$g^t(x) \neq x + J\nabla H\, t, \qquad J = \begin{pmatrix} -1 & 0 \\ 0 & 1 \end{pmatrix}.$$

On the other hand, t must be sufficiently short, depending on the size of $\hat{H}_1$, so that the approximation eq. (5.19) holds. Basically, it is equivalent to the constraint on t needed for eq. (5.14) to be valid, i.e., the probability that a classical point in phase space changes regions twice during t is negligible.

Let us now introduce the dimensionless transition parameter

$$\Lambda_{jk} \equiv v_{jk}^2/D^2\,, \tag{5.25}$$

where $D = 1/\bar{\rho}(E)$ is the local mean spacing. Λ_{jk} appears naturally in quantum perturbation theory when $\hat{H}_0$ is perturbed by $\hat{H}_1$ and, as will be discussed in the next section, it is also the relevant parameter in random matrix transitions. Since eq. (5.24) can be used in the same range of t as eq. (5.14), one obtains the transition parameter–flux relation

$$\Lambda_{jk} = \frac{1}{4\pi^2} \frac{\Phi_{jk}(E)}{(2\pi\hbar)^{d-1} f_j f_k} , \tag{5.26}$$

in which time no longer enters since both sides are related to instantaneous properties, i.e. to the Hamiltonian. This relation is crucial for describing quantitatively a wide variety of phenomena involving spectral statistics, localization of wave functions, suppression of chaos, etc.

Some care has to be exercised when applying eq. (5.26) to a particular quantum system. The above derivation of the Lambda–flux relation eq. (5.26) has assumed for simplicity that no regular fraction of the spectrum, and no exact symmetries, were present. One can easily check that regular levels are correctly disposed of if, as done in table 1, the f_i's represent relative chaotic volumes, i.e., $\sum_i f_i = 1$ [the D in the r.h.s. of eq. (5.25) being then the local mean spacing of chaotic states.] However, if the system possesses exact symmetries, the Hilbert space decomposes into a certain number of subspaces labeled by exact quantum numbers (ϵ_i), $i = 1, \ldots, n$, each of which contains (locally in energy) only a fraction $g(\epsilon_i)$ of the states. Each sequence, to be treated separately, has thus a mean spacing equal to $g(\epsilon_i)D$. For the quartic oscillators in the generic case, ϵ_1 and ϵ_2 are the parity numbers associated to $\hat{P}_1$ and $\hat{P}_2$, and $g(\epsilon_1 = \pm 1, \epsilon_2 = \pm 1) \simeq 1/4$ for each of the four sequences.

Without entering into the details, one can see, by following the previous derivation step by step, that, when considering a sequence $(\epsilon_1, \ldots, \epsilon_n)$, one must formally replace v_{jk}^2 by $v_{jk}^2(\epsilon_i)$, and D by $D(\epsilon_i)$ in eq. (5.25) as

$$D \longrightarrow D(\epsilon_i) = D/g(\epsilon_i) , \tag{5.27}$$

$$v_{jk}^2 \longrightarrow v_{jk}^2(\epsilon_i) = v_{jk}^2/g(\epsilon_i) . \tag{5.28}$$

Equation (5.28) can be understood intuitively as expressing the fact that the semiclassical propagation of a state $|j, \alpha\rangle$ does not depend on its symmetry properties, and, therefore, the average sum of square matrix elements $\|\hat{P}_k \hat{U}(t)|j, \alpha\rangle\|^2$ remains the same as if no symmetry was present. For Λ_{jk} this leads to

$$\Lambda_{jk} \longrightarrow \Lambda_{jk}(\epsilon_i) = g(\epsilon_i)\Lambda_{jk} . \tag{5.29}$$

For the quartic oscillators the $\Lambda_{jk}(\pm, \pm)$ are thus equal to one quarter of the result given by eq. (5.26).

5.3. Random matrix modeling

5.3.1. Traditional aspects

By random matrix theory (RMT) we mean the construction of matrix ensembles with respect to some measure, such as the volume element in the matrix element space, and the subsequent analysis to characterize and to determine their statistical properties. For example in the GOE, the matrix elements are chosen as independent zero-centered Gaussian random variables all with the same variance except for the diagonal elements, which have twice the variance. The ensemble is

invariant under orthogonal transformations and each member is diagonalizable by an orthogonal transformation. Along with the other classical ensembles, it has the additional property of being strongly ergodic or, in other words, as the dimensionality $d \to \infty$, almost all members of the ensemble have the fluctuation properties of the ensemble [80].

In order to be more quantitative in what follows we now introduce some standard quantities which allow one to measure these fluctuations. It is possible to express the measures as functions of a hierarchy of exact k-point correlation densities, R_k, which give the probability density of finding distinct levels at k specific points in the spectrum or in an ensemble of spectra. All information about spectral fluctuations can be expressed as functions of these correlations. Often the correlation functions can be considered as locally translationally invariant, which is the case here. The "center of mass" coordinate may then be removed, reducing the number of variables from k to $k-1$. It is then sensible, to start with, to restrict one's attention to two-point correlation measures; these will depend solely on the variable r giving the distance between two points in the spectrum. Once R_2 is specified, the higher order correlations, R_k $(k > 2)$, are constrained; it is an open question as to precisely how constrained they are and to which extent they contain some new information [81]. In this paper, we restrict ourselves to two-point measures, which already contain clear signatures of the properties under discussion.

To be a little more precise, assuming translational invariance, $R_2(r)$ is defined as the probability density of finding a level at a distance r from a given level. It is related to Dyson's cluster function, $Y_2(r)$, as

$$Y_2(r) = 1 - R_2(r)\,. \tag{5.30}$$

Depending on the situation, we will use the more convenient of these two functions. A nice feature of using exact two-point measures comes from the fact that the uncorrelated superposition of spectra results in a very simple form for the measures. For example [80],

$$Y_2^{\text{mixed}}(r) = \sum_{i=1}^{n} f_i^2 Y_2^i(f_i r)\,, \tag{5.31}$$

where there are n spectra superposed and f_i is the relative measure of the ith spectrum.

Perhaps the most often considered two-point measures are $\Sigma^2(r)$ and $\overline{\Delta}_3(r)$. $\Sigma^2(r)$ is the variance of the number of levels in an interval of length r. In terms of R_2 (Y_2), it is given by

$$\Sigma^2(r) = r - r^2 + 2\int_0^r \mathrm{d}s\,(r-s)R_2(s) = r - 2\int_0^r \mathrm{d}s\,(r-s)Y_2(s)\,. \tag{5.32}$$

Related to $\Sigma^2(r)$ through integration [80], $\overline{\Delta}_3(r)$ measures the deviation of $N(E)$ from the best straight line. It is perhaps most useful with short sequences or when the integrity of the data suffers and we shall therefore not make use of it here, since it carries no new information.

Another set of often considered measures are not exact two-point functions. They are the nth nearest neighbor spacing distributions, $\rho_n(r)$, and in particular, the nearest neighbor spacing distribution $\rho_0(r)$. These may be expressed as functions depending on all the k-point correlation functions. For the most part only $\rho_0(r)$ is used and usually just to demonstrate the extent of the short range level repulsion. This information is contained in measures definable in terms of $R_2(r)$, which contains information about level correlations at all ranges of r. It is however somewhat

hidden in a function like $\Sigma^2(r)$, which for small r behaves $\sim r$ [see eq. (5.32)]. We shall therefore use the measure $\hat{R}_2(r)$ defined by

$$\hat{R}_2(r) = \int_0^r \int_0^r R_2(r_1, r_2)\, dr_1\, dr_2 = 2\int_0^r (r-s) R_2(s)\, ds = \Sigma^2(r) - (r - r^2) \tag{5.33}$$

to characterize the short range fluctuations, say $r < 1$. Introduced in ref. [81], it is a pure two-point function and as convenient as $\rho_0(r)$ or its integrated version.

It would be desirable, of course, to consider directly $R_2(r)$ since all two-point measures follow from it. However, for a given spectrum the result is a series of δ-functions, and one must decide how to histogram the results, etc. Even this is not as satisfactory as calculating $\Sigma^2(r)$, for which the statistical significance can be thought of as being enhanced by the smoothing effect of integration. Note that $\Sigma^2(r)$ can be thought of as being Y_2 doubly integrated, in that

$$d^2\Sigma^2(r)/dr^2 = -2Y_2(r)\,. \tag{5.34}$$

But in integrating twice, the essential r-dependence of R_2 is being hidden. It is important not to lose this information here since in the r-dependence lies the essential trademark of the generalized ensemble fluctuations (see section 5.3.2). Also note that highly integrated measures at different r give more and more highly correlated results, thus tending to deviate statistically in one direction from theoretical expectations. To strike a balance we shall thus calculate both $\Sigma^2(r)$ and the integral

$$I(r) = \int_{-r}^{+r} Y_2(s)\, ds \tag{5.35}$$

of Y_2 at large r ($r \leq 5$), and $\hat{R}_2$ at small r ($r \leq 1$). For exact results, which will be needed for comparison later on, see appendix A.

5.3.2. Generalized ensembles

We may think of the Random Matrix Theory summarized to this point as belonging to the traditional subject matter, i.e. the measures, the canonical ensembles, etc. However, an interesting, more contemporary branch of RMT is beginning to emerge [79, 82, 83] and, as will be seen in what follows, this is precisely what is needed here. Consider a spectrum or ensemble of spectra with any level statistics whatsoever. The question is: how do the fluctuation properties change when a weak interaction in the form of one of the canonical ensembles is added to it? Depending on the strength of the interaction, there will be a transition in the fluctuations toward those of the perturbing canonical ensemble. Viewed globally the transitions are discontinuous as the dimensionality tends to infinity. However, there is a local viewpoint, the physically interesting one, which permits a smooth parametrization of the transitions. It is the transition parameter introduced in eq. (5.25) which governs such transitions in what we shall call generalized ensembles.

To see how such ensembles naturally arise, let us go back to the image of two very chaotic billiards placed side by side and connected through a small hole. In the limit where the hole is closed, the two billiards are independent, and the complete spectrum may be modeled by the uncorrelated superposition of two properly weighted GOE spectra. Or equivalently, to make closer contact with

the relevant basis point of view, the actual Hamiltonian may be modeled by the following block diagonal GOE:

$$\begin{pmatrix} \mathrm{GOE}_1 & 0 \\ 0 & \mathrm{GOE}_2 \end{pmatrix}.$$

At the opposite extreme, if the hole is very large, one expects a full GOE matrix. In between, one knows that in relevant bases the Hamiltonian appears as a block diagonal matrix whose blocks are connected through small off-block-diagonal matrices whose mean square matrix elements are semiclassically related through eq. (5.26) to the flux connecting the two billiards. With the assumption, in a sense implicitly made in the two limiting cases, that the matrix elements behave in such bases as zero-centered independent Gaussian variables, one naturally comes to associate to the two slightly connected billiards an ensemble constructed as a two-block diagonal GOE plus a very weak GOE-like coupling in the off-diagonal blocks. This could be thought of as the basic constituent with which more complicated ensembles, such as will be needed for the quartic oscillators, will be constructed. Due to the invariance of the off-diagonal blocks under orthogonal transformations which act on the diagonal blocks, the ensemble is equivalent to the random superposition of two weighted GOE spectra plus a weak perturbing GOE. Unfortunately, there does not yet exist simple closed forms for the rapid transition in level statistics from two GOE spectra to one, although below we describe its general qualitative features.

Another example of a transition problem we shall briefly discuss is that of Poisson plus a weak GOE, in short Poisson + GOE(v^2), where v^2 denotes the variance of the GOE matrix elements. This ensemble has the advantage that some perturbative results are known which display the essential features of transitions in the kinds of ensembles introduced here. We will use it to guide our intuition on the behavior of the previous example, which, for our purposes, is the physically relevant one. Moreover, when the ensemble for the mixed system requires many block diagonal GOEs weakly interacting among themselves, the ensemble may in certain circumstances be approximated by a Poisson + GOE(v^2) ensemble (at least as far as the short range fluctuations are concerned). The Poisson spectrum may be thought of in this case as the limit of an infinite number of superposed GOE spectra.

The transitions in fluctuation properties for both of these examples of generalized ensembles are governed by the BBGKY hierarchical equations for R_k [79],

$$\frac{\partial R_k}{\partial \Lambda} = \sum_{j=1}^{k} \frac{\partial}{\partial r_j}\left\{ \Delta_k^{\beta} \frac{\partial}{\partial r_j}\left(\frac{R_k}{\Delta_k^{\beta}}\right) - \beta \int_{-\infty}^{\infty} \mathrm{d}r_{k+1} \frac{R_{k+1}}{r_j - r_{k+1}} \right\}, \tag{5.36}$$

where r is a distance in mean spacings, $\Delta_k^{\beta} = \prod_{i<j} |r_i - r_j|^{\beta}$ ($\beta = 1$ for the GOE), and Λ is the transition parameter $\Lambda = v^2/D^2$, with v^2 the variance of the perturbing ensemble and D the mean level spacing. Other applications of eq. (5.36) include fundamental symmetry breaking such as time reversal breaking [79]. For our purposes, the value of these equations comes from the fact that the transition parameter is rigorously shown to govern the transition. To be more precise, this means that once the initial ensemble is specified (i.e., in our first example, for instance, once the relative density of levels of each block is fixed) fixing Λ will uniquely specify all the R_k correlation functions and thus all the spectral fluctuation properties.

We now have a complete prescription for constructing the ensembles accounting for weakly broken, isolated transport barriers. It incorporates the Liouville measures of the selected regions,

which set the unperturbed ensemble characteristics, and the connecting fluxes, which set the weak interaction part of the ensemble. So there are block diagonal GOEs with dimension proportional to the relative density of states for each diagonal block (associated to a classical region) of the Hamiltonian expressed in relevant bases, plus off-diagonal couplings characterized by the Λ_{jk} given in eq. (5.26) between block j and block k. Once again, we stress that, once these characteristics of the matrix ensemble are fixed, all of its statistical properties are*). Thus, since both Λ_{jk} and f_j are related to classical quantities which can be computed from the classical motion, in our model the classical behavior completely determines the predictions of the quantum fluctuation properties. Although the ensembles are specified, there are no existing analytic predictions for their statistics, and we shall eventually need Monte-Carlo simulations to compare the actual fluctuations of our test case with those of the relevant matrix ensemble.

The hierarchical equations are difficult to solve exactly (even for the stationary solutions, $\Lambda \to \infty$, which correspond to the canonical random matrix ensembles) and to the authors' knowledge, solutions of exactly soluble problems have always been found first by other methods. They are however convenient for generating perturbative solutions to various orders in Λ. Quite often the perturbation solution of the hierarchical equations is sufficient for a particular application (as in time reversal breaking) and it usually demonstrates the essential transition. For R_2 the lowest order solution comes by inserting in eq. (5.36) R_3 equal to its unperturbed ($\Lambda = 0$) form [79]. The resulting equation can then in principle be solved by the method of quadratures [84], or one can use directly a form of degenerate perturbation theory [85].

All of the transitions described by eq. (5.36) have important general features. The transition toward classical ensemble fluctuation properties is essentially completed for $r^2 \ll c_0\Lambda$, where the constant is typically about 10, being π^2 for TR breaking and 16 for Poisson + GOE(v^2). On the other hand, the transition has essentially not started in the opposite regime of r. It is this feature which is quite opposite to what happens by superposing spectra. Therefore in the case $(-0.35, \pi/4)$, the quantum signature of the classical transport will be fluctuation properties of the GOE at small r and more like the superposition of five GOEs at large r (there are five main isolated zones in the chaotic region). For the Poisson + GOE(v^2) the lowest order solution to eq. (5.36), in the infinite dimensional limit, is [85]

$$R_2(r,\Lambda) = (\pi/8\Lambda)^{1/2} r \mathrm{e}^{-r^2/16\Lambda} I_0(r^2/16\Lambda), \tag{5.37}$$

where $I_0(x)$ is the Bessel function $J_0(\mathrm{i}x)$. Equation (5.37) shows the discontinuous transition to linear level repulsion. However, the integral of the $Y_2(r,\Lambda)$ function remains zero

$$\int_{-\infty}^{\infty} Y_2(r,\Lambda)\,\mathrm{d}r = 0\,, \tag{5.38}$$

just as for the Poisson ensemble, whereas the integral for the GOE equals 1. In other words, the nearby levels are pushed away creating a kind of excess density just beyond the distance to which they moved and little happens at long distance.

5.4. *The spectral fluctuations*

We are now almost ready to turn to the practical application and testing of these ideas with regard to the spectral fluctuations of the quartic oscillators. However, first we must digress a little to discuss

*) We are assuming that what is true for the two-block case, generalizes for the many-block case.

an important limitation on the ensemble theory. It is well known that there exists a connection between periodic orbits and induced oscillations in the density of states, which implies that the spectral fluctuations could depend specifically on details of the system through the properties of these orbits. Indeed, the fluctuation measures involving long range correlations amongst widely separated levels are highly system dependent. This was seen by Seligman et al. [25] and Casati et al. [86], and a theory in terms of the shortest periodic orbits was given by Berry [21]. The essential idea is that the shortest orbits bound the longest lengths of the oscillations in the spectrum leading to a leveling off of the fluctuations beyond a certain range in the spectrum; it is often referred to as "the saturation of the fluctuation measures".

According to the general wisdom, the exponential proliferation of orbits with increasing action serves as an underlying basis for statistical or ensemble modeling as long as shorter range fluctuations are studied. See Berry [21], and Hannay and Ozorio [22] for a much more comprehensive view of this. Because our interest here does not lie with this problem, throughout section 5 we have been implicitly assuming that we are considering fluctuations on scales well away from such non-universal features. It turns out that having 20 000 or more levels in our spectra is crucial in helping us avoid the saturation regime when we test the random matrix modeling that we propose.

We show here two examples of what we mean by saturation in order to demonstrate clearly what is happening. In fig. 19 a typical subtracted Poisson spectral staircase, $N(E) - \overline{N}(E)$, is plotted versus an integrable quartic oscillator one. It is almost difficult to see how the integrable system could be talked about as though Poisson statistics are relevant. Perhaps because of the immense Poisson fluctuations, it seems easy to accept that the saturation effects are so striking, but even in fig. 20 they are evident in the comparison of a GOE with a chaotic system. In the figures it is clear that the quartic oscillator spectra are missing components in the longest wavelength domain.

To be slightly more specific, we define the saturation point r_s as the point where the number variance $\Sigma^2(r)$ takes on its first maximum. Since the slope of $\Sigma^2(r)$ does not magically jump to 0 at r_s, saturation effects might be seen well before this point. This can be clearly seen on fig. 21, for the integrable example. A bit of a surprise for us was the fact that our mixed systems saturated at far smaller r_s than either the integrable or fully chaotic cases. However, the shortest periodic orbit does not change sufficiently to account for this difference. This suggests that focusing too closely on the shortest periodic orbit is insufficient for mixed systems. One possible explanation is that the Lyapunov exponents are certainly smaller in the mixed case's chaotic region. This implies roughly speaking a weaker exponential proliferation of the periodic orbits as a function of the period T. It is plausible that this delays (as a function of T) the applicability of the reasoning used by Hannay and Ozorio [22] in deriving a sum rule for the periodic orbits requiring a kind of uniform exploration of phase space (since the period of the shortest closed orbit may not be related any more to the characteristic periods for which closed orbits can be considered as uniform). And thus, following the ideas of Berry, saturation may occur at shorter range than that naively expected from the shortest periodic orbit. This matter should be further explored. As a practical matter, we will calculate the statistics at short range ($r \leq 5$) only including the highest levels and then saturation does not pose serious problems, though we can detect a tiny residual effect even at the highest reaches of our spectra.

For the $(-0.35, \pi/4)$ case, we are now able to compare the random matrix ensemble predictions with the actual spectral fluctuations. The first step in the process of calculating a spectral fluctuation measure is the unfolding of the spectrum. That is, any secular level density change is removed and the mean spacing is set equal to one. It can be easily verified that the mapping of the spectrum $\{E_i\}$ to $\{E_i'\}$ via $\{E_i'\} = \overline{N}(E_i)$ performs this operation beautifully [15]. For this we use the analytic result eq. (3.20) applied individually to each of the four parity sequences. In our case, a

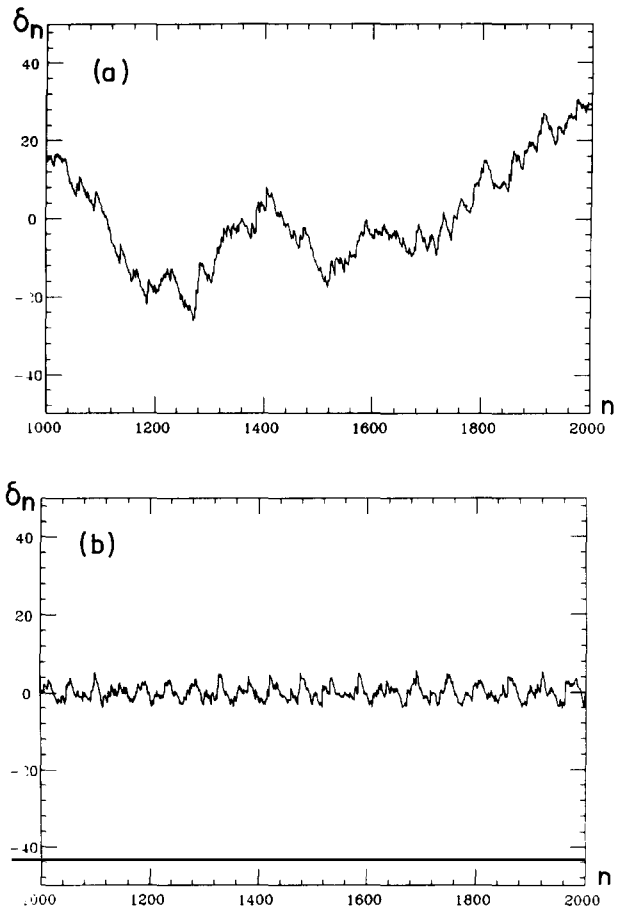

Fig. 19. Oscillatory part of the unfolded cumulative density of states, $\delta N = N(E) - \overline{N}(E)$, for a slice [1000–2000] of 1000 levels. (a) From a Poissonian spectrum with centroid adjusted. (b) From the uncoupled quartic oscillators $(\lambda, b) = (0, \pi/4)$, reflection symmetry $(+,+)$; the unfolding was performed using eq. (3.20).

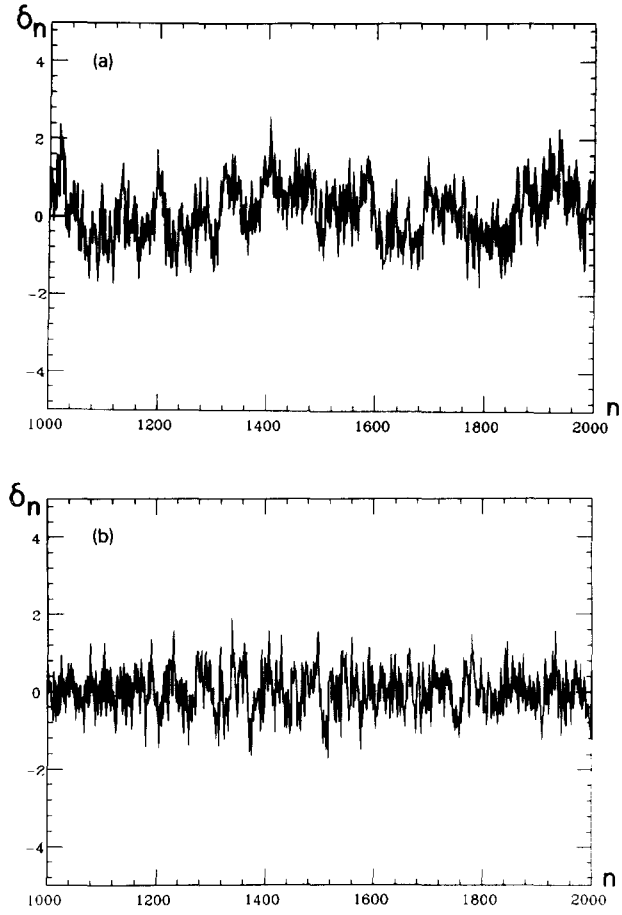

Fig. 20. Oscillatory part of the unfolded cumulative density of states, $\delta N = N(E) - \overline{N}(E)$, for a slice [1000–2000] of 1000 levels. (a) From a 5000-dimensional GOE matrix; the spectrum was unfolded analytically using Wigner's semicircle law. (b) From the coupled quartic oscillators for the case $(\lambda, b) = (-0.60, \pi/4)$, and reflection symmetry $(+,+)$; the unfolding was performed using eq. (3.20).

further correction is needed since the regular levels were removed. After checking that the number removed was to a high degree independent of the energy, it was sufficient to simply multiply by the remaining fraction of levels. As a technical matter, we have devised new methods for calculating the measures $\hat{R}_2(r), I(r)$ and $\Sigma^2(r)$ in a more statistically significant way, enabling us to make more precise comparisons. The details will be published elsewhere [87].

Turning now to the random matrix predictions, there exist no analytic results to tell us what the precise fluctuations of the appropriate ensemble are. We use the classical information given in table 1 to fix the parameter of the Monte Carlo as given in table 4; for those regions (j,k) not connected by a classical flux $v_{jk} = 0$. We construct 100 matrices of dimensionality 400. In doing so we paid careful attention to adjusting the diagonal block matrix element variances such

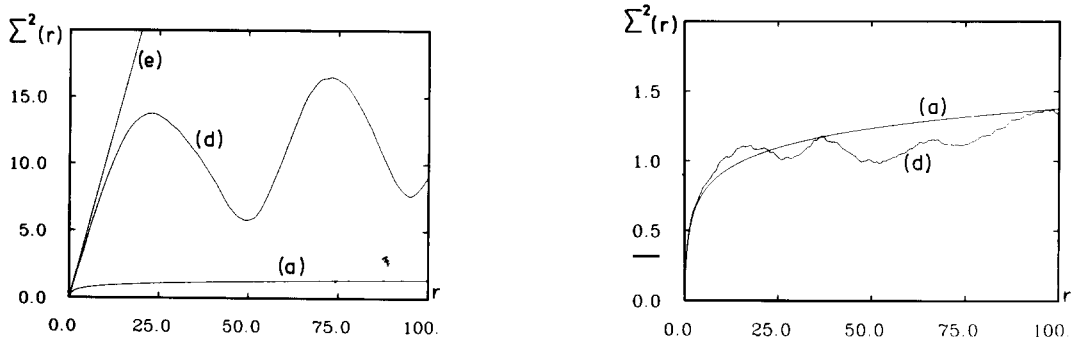

Fig. 21. A plot of the number variance $\Sigma^2(r)$ versus r for a slice [4600–5800] containing 800 levels, illustrating saturation effects. Left: curve (d) from the uncoupled quartic oscillators for the case $(\lambda, b) = (0, \pi/4)$. Right: curve (d) from the coupled quartic oscillators for the case $(\lambda, b) = (-0.60, \pi/4)$. For the sake of comparison, the GOE (a) and Poisson (e) results are also drawn.

that each individual block, once diagonalized, had a semicircular level density of identical radius to the others. This assured that the unperturbed ensemble ($\Lambda_{jk} = 0$) had, on average, constant relative densities everywhere in the spectrum. Since the value of Λ varies across the spectrum (due to the semicircular density) we used only the middle half of the spectra for fluctuation calculations; we adjusted for the 10–20% variation of Λ in this regime. Note that intermediate ensembles once diagonalized do not necessarily have semicircular level densities; this is clear from the fact that the perturbation affects differing regions on the semicircle differently. This was also accounted for.

In fig. 22 we compare the results for the quartic oscillators $(-0.35, \pi/4)$, the Monte Carlo, and various relevant theoretical curves; see the caption of fig. 22 for details. First we give $\Sigma^2(r)$, which is the more statistically significant measure. We see that the quartic oscillator behaves very much like the theoretical prediction. Both curves follow the GOE at short range and both move away toward the superposition curve at longer range. We consider the agreement excellent.

To best see the r dependence of the quartic oscillators' statistics, we give a plot of the $I(r)$ curves. The point at which the fluctuations start to break with the GOE curve to move toward the

Table 4

Values of the transition parameters Λ_{jk} [see eq. (5.26) and table 1] for the case $(\lambda, b) = (-0.35, \pi/4)$ used in the Monte-Carlo calculation of the fluctuations. Regions 1 and 2, and 6 and 7 are grouped together because their connecting Λ's are rather large ($\Lambda_{12} = 2.4$, $\Lambda_{67} = 1.7$) and regions 1 and 7 contain very few states. Taking these structures into account does not modify the fluctuation result. The values are for an average energy of $\bar{E} = 706$ corresponding to the 16 000th to the 22 000th level. The effects of the reflection symmetries, which has been accounted for, reduces the values by a factor 4 [see eq. (5.29)].

	Λ_{jk}
(1+2)↔3	0.6
3↔4	1.05
4↔5	0.65
5↔(6+7)	0.4

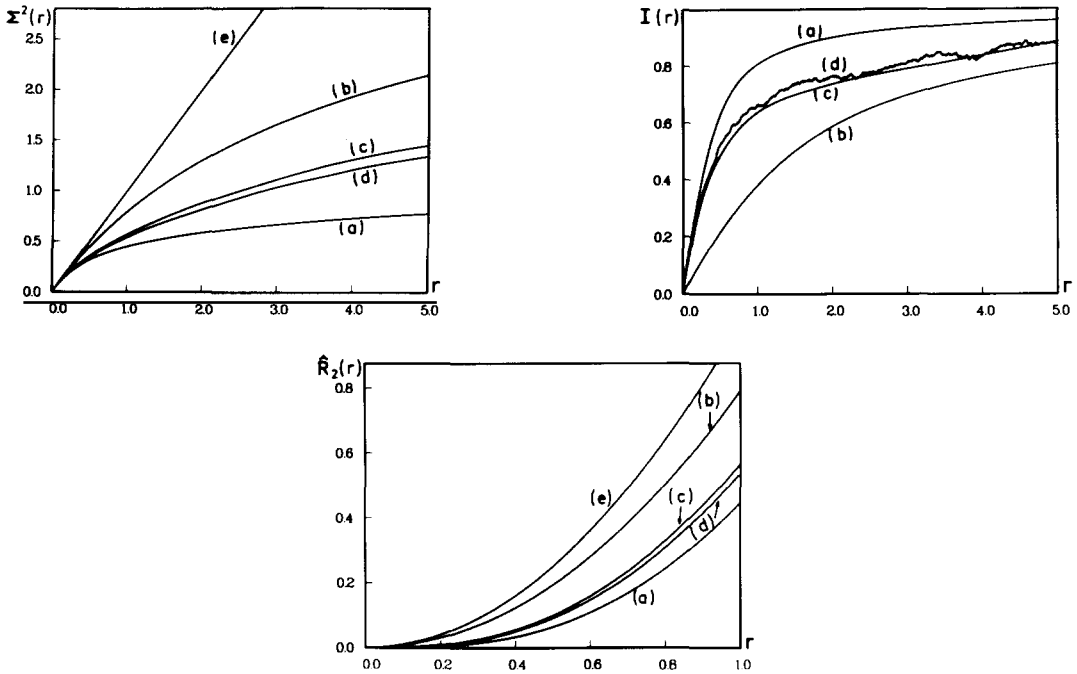

Fig. 22. Results for the spectral fluctuations and comparison with different models. Top left: number variance $\Sigma^2(r)$. Top right: integral of the two-level cluster function [see eq. (5.35)]. Bottom: the measure $\hat{R}_2(r)$ [see eq. (5.33)]; notice the difference in abscissa. (a) One GOE; (b) five GOE blocks weighted according to the fraction of total phase space volume (see table 1); the blocks are decoupled; (c) from the theory presented in this paper, namely like (b) but with blocks coupled by the Λ_{jk} as given in table 4; (d) from the 16 000th to the 22 000th eigenenergies of the coupled quartic oscillators, case $(\lambda, b) = (-0.35, \pi/4)$; the regular levels ($\sim$ 12%) have been subtracted out; (e) from a Poissonian spectrum, for the sake of comparison. See text for further explanation.

superposition curve is quite clear. Lastly, in order to concentrate more fully on the level repulsion, we include the $\hat{R}_2(r)$ plot; the lower the curve the greater the repulsion.

Despite the excellent general agreement, it is clear that the Monte Carlo consistently overestimates the quartic oscillators' fluctuations to a small but significant degree. This implies the couplings amongst blocks determined by Λ_{jk} are slightly too small. To have an idea of the magnitude of the discrepancy, we performed some additional Monte-Carlo calculations. We find that increasing the non-zero Λ_{jk} by a constant 25% or so aligns the theory and data perfectly (since Λ_{jk} contains the matrix element variances this only implies an underestimation of 10–15% of the magnitude of the matrix elements). We remind the reader that, because the Φ_{jk} connect only neighboring regions, nearly 4/5 of the possible coupling matrix elements were taken to be exactly zero. This may be a bit too extreme. It seems plausible that quantum dynamically a new kind of tunneling process might exist allowing a very weak but direct transport amongst other regions (blocks $i \leftrightarrow j$). We have not yet attempted to work out a semiclassical theory for the magnitude of the forbidden Λ_{jk}, which would presumably be exponentially small in $\hbar$. It would be very interesting to know if therein lie the reasons for the small deviations as opposed to stemming from the various approximations required to derive eq. (5.26). For then an extended theory (also covering saturation) could possibly be quantitatively applied to physical systems whose $\hbar$ need not be nearly as small as is the case in fig. 22.

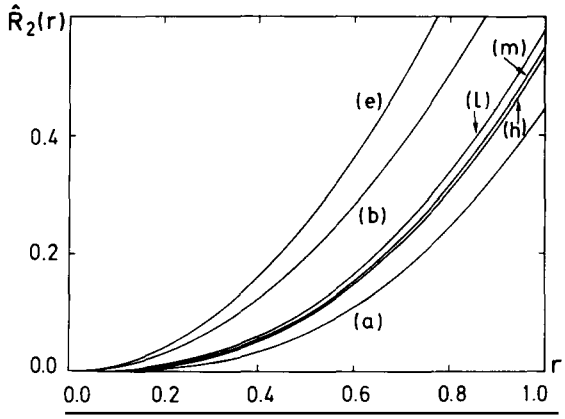

Fig. 23. Plot of the measure $\hat{R}_2$ to illustrate, for the case $(\lambda, b) = (-0.35, \pi/4)$, the energy dependence predicted by the theory. (ℓ) From the 3900th to the 6000th level; (m) from the 8500th to the 11 600th level; (h) from the 17 400th to the 22 000th level. (a), (b) and (e) as in fig. 22.

As a final test of the theory, we have looked for the energy ($\hbar$) dependence of the transition parameter–flux relation. This is a somewhat difficult effect to see largely because as we drop lower in the spectrum saturation becomes a problem even at scales as short as 1–2 mean spacings, but the effect itself is more prominent at longer range. So in fig. 23, we only show the short range measure $\hat{R}_2(r)$ for a low, middle and high energy regime; $\hbar$ decreases by a factor two in going from low to middle and again from middle to high. The correct trend is reproduced nicely.

6. Localization of chaotic eigenstates

The study of chaotic eigenfunctions of bounded systems began in earnest with the numerical studies of McDonald and Kaufman [30] on the eigenfunctions of the stadium billiard. They noted, among other things, that many of the states were quite complicated, roughly giving the impression of randomness. A random wave function in this context is a Gaussian random function of position [29] resulting from a random superposition of fixed wavelength plane waves. These functions are also marked by a rapid decay of correlations with distance between their intensities determined at two different points [29]; some of the surprising properties of these states are discussed by O'Connor et al. [88]. In 1984, Heller [31] showed that this statistical image was insufficient. Also in conjunction with the stadium, he discovered the "scarring" of eigenfunctions by the least unstable periodic orbits. Using short time semiclassical dynamics, he derived a non-classical, enhanced intensity above the random expectations that had to be found near these orbits in at least some of the eigenfunctions (interesting advances were later added by Bogomolny [89]). Heller identified the parameter determining the magnitude of the scarring to be $2\pi/\xi\tau$, where ξ is the Lyapunov exponent describing the local instability of nearby orbits and τ is the period of the closed orbit [31]. This enhancement can be considered as a form of eigenfunction localization with a semiclassical basis. For highly chaotic systems, scarring as understood in this way is a rather weak form of localization.

Given that the short time dynamics of a single orbit and its environs has an impact on the properties of chaotic eigenstates, it is natural to ask whether the collective tendency of the orbits

to cross slowly from certain regions to others in phase space, with the associated time scales, also has consequences for the chaotic eigenstates. This is the spirit of the study of Geisel, Radons, and Prange [90], on the effect of cantori on quantum states. Here, our goal is to search for a relationship between the eigenstate properties, wave packet dynamics, and the classical quantities describing the diffusion process, i.e. the connecting fluxes and the volumes of subregions. In principle, the statistical model, involving generalized random matrix ensembles, constructed in the previous section is suited just as well for this purpose as it is for describing the spectral fluctuations. We expect therefore that the same model will describe the statistical nature of the eigenfunctions to a similar degree as has already been demonstrated for the energy levels. Recall that the generalized ensembles specifically excluded system dependent saturation effects. This led to a restriction that the spectral fluctuation measures of interest were understood to be in the short range, "universal" regime. Similarly, the ensembles cannot account for scarring since the statistical postulates of the ensembles specifically exclude information about features such as short periodic orbits. Therefore, any localization due to transport barriers is distinct from scarring, will turn out to have different $\hbar$-behavior and, in general, the interplay of both mechanisms should be sought in order to understand chaotic eigenstates. To simplify this section we will focus on isolating barrier localization effects. Scarring effects (see ref. [67] for a nice discussion of scarring in coupled quartic oscillators) and their interplay with barrier localization will be left for future work. This is already a rather large subject, and we will only discuss and verify a few of the possible types of behavior. Once done, we will speculate a little as to what connections exist between our work and the more standard subject matter of localization.

6.1. *A semiclassical mechanism of localization*

The generalized ensembles generate predictions whether the Λ_{ij} are large or small. For this section though, we find it preferable to concentrate on the perturbative regime where leading behavior can be derived analytically in a straightforward way. Although the calculation and the cases looked into will be geared for this, we expect that the ensembles will work as well or better beyond the perturbative domain as they do in it. We start by considering the behavior for a simpler case than is found for the quartic oscillators. Assume an ensemble constructed as a GOE of large dimension except that it is restricted to take on a two by two block diagonal form. Let its matrix elements be of variance one and let the blocks have relative dimensionalities f_1 and f_2. To this ensemble, a weak GOE perturbation is added of variance v_{12}^2 [in shorthand 2GOE (1) + GOE(v_{12}^2)]. Consider an eigenstate $|\mathcal{E}_\alpha^j(v_{12}^2)\rangle$ of a particular member Hamiltonian of the full ensemble, which can be followed back with $\Lambda_{12} \to 0$ [see eq. (5.25)] to an unperturbed eigenstate $|\mathcal{E}_\alpha^j(0)\rangle$ belonging to the vector subspace j ($j = 1, 2$) of the unperturbed member. For sufficiently small Λ_{12}, $|\mathcal{E}_\alpha^j(v_{12}^2)\rangle$ is mainly localized in the vector subspace j. Indeed, using a degenerate perturbation method, one can write the mean square projection of $|\mathcal{E}_\alpha^j(v_{12}^2)\rangle$ into the vector space k ($\neq j$) as

$$\Gamma_{jk} \equiv \overline{\overline{\sum_\beta |\langle \mathcal{E}_\alpha^j(v_{12}^2)|\mathcal{E}_\beta^{k\neq j}(0)\rangle|^2}} \simeq \frac{1}{2}\sum_\beta \left[1 - \left(1 + 4\frac{|\langle \mathcal{E}_\alpha^j(0)|\hat{H}|\mathcal{E}_\beta^k(0)\rangle|^2}{[\mathcal{E}_\alpha^j(0) - \mathcal{E}_\beta^k(0)]^2}\right)^{-1/2}\right], \tag{6.1}$$

where, as before, the double bar means ensemble averaging and α, β label individual states within their respective subspaces. The above approximation can be understood as coming from a separate contribution of the different states $|\mathcal{E}_\beta^k(0)\rangle$. One then uses the exact two by two diagonalization result for each term and finally sums all the individual contributions. When all levels are distant, the r.h.s. summation of eq. (6.1) is equal to the usual perturbation result except for higher order

corrections. It moreover matches smoothly with the degenerate perturbation result when one level $\mathcal{E}_\beta^k(0)$ comes close to $\mathcal{E}_\alpha^j(0)$. The rarity of three or more levels being found nearly degenerate leads also to higher order corrections and can be ignored. One may then use the exact two by two matrix diagonalization between any pair of levels to account for their admixing whether they are nearly degenerate or not. This avoids the necessity of matching the treatment of a nearly degenerate pair to the treatment of a well separated pair. To perform the ensemble average, the interaction matrix element $\langle \mathcal{E}_\alpha^j(0)|\hat{H}|\mathcal{E}_\beta^k(0)\rangle$ is accounted for with a Gaussian weighted integration whose variance is v_{jk}^2. The sum over β is replaced by an integration over the two-point probability density $R_2(r)$.*) By interchanging ensemble averaging and integration, $R_2(r)$ takes on the form of a constant, f_k, because the unperturbed levels of j,k are superposed independently with no correlations between them. This gives ($\Lambda_{jk} = v_{jk}^2/D^2$)

$$\Gamma_{jk} \simeq \frac{1}{\sqrt{2\pi}} \int_{-\infty}^{\infty} d\omega\, e^{-\omega^2/2} \int_{-\infty}^{+\infty} ds\, \frac{f_k}{2} \left(1 - \frac{|s|}{\sqrt{s^2 + 4(v_{jk}^2/D^2)\omega^2}}\right) = 2f_k\sqrt{\frac{2\Lambda_{jk}}{\pi}}, \tag{6.2}$$

valid for $\Lambda_{jk} \ll 1$.*) As expected, because of the ensemble averaging, Γ_{jk} is independent of α. This result also holds for ensembles such as the one constructed for the quartic oscillators for which there are more than two diagonal blocks provided the blocks j and k ($j \neq k$, $j,k = 1,2,\ldots$, total number of blocks), are directly connected by admixing. For those j,k not directly admixed, it is necessary to go to higher and higher orders of perturbation theory until a link is established between the two. The more barriers to be crossed, the weaker the projection and the higher the order in Λ.

For the system that the ensemble models, Λ_{jk} is the quantum equivalent of a flux Φ_{jk} connecting two classical regions R_j and R_k. One finally has using the Λ–Φ relation, eq. (5.26),

$$\Gamma_{jk} \simeq \left(\frac{2}{\pi^3} \frac{f_k \Phi_{jk}}{(2\pi\hbar)^{d-1} f_j}\right)^{1/2}. \tag{6.3}$$

When exact symmetries are present, the resulting modification of the Λ_{jk} discussed in section 5.2.2 has to be taken in account. For the quartic oscillators with $b \neq 1$ this reduces the Γ_{jk} by a factor 2 [see eq. (5.29)]. To the extent that the eigenstates of the unperturbed ensemble are considered to be completely localized in one classical region, eq. (6.3) gives the average intensity of the eigenstates of the full ensemble $|\mathcal{E}_\alpha^j(v^2)\rangle$ which has spread into region R_k. Thus partial transport barriers give rise to a mechanism which blocks the spreading of eigenfunctions and leads to what we shall call "semiclassical" localization. This is because the localization is most naturally interpreted by a semiclassical analysis of the partial barriers.

In the perturbative regime covered here, the classical flux $\Phi \ll \hbar$. It is not obvious how far this condition can be pushed without encountering problems. Strictly speaking, no restrictions were

*) $R_2(r)$ may be expressed simply as a sum over the nth nearest neighbor spacing distributions $\rho_n(r)$, $R_2(r) = \sum_{n=0}^{\infty} \rho_n(|r|)$.

*) For completeness, note that for the Poisson + GOE(v^2) ensemble, a similar result can be obtained concerning how rapidly as a function of Λ the unperturbed ($\Lambda = 0$) eigenstates are spread over the neighboring states. In the same way as above one obtains

$$\overline{\overline{|\langle \mathcal{E}_\alpha(v^2)|\mathcal{E}_\alpha(0)\rangle|^2}} = 1 - \overline{\overline{\sum_{\beta\neq\alpha} |\langle \mathcal{E}_\alpha(v^2)|\mathcal{E}_\beta(0)\rangle|^2}} = 1 - 2\sqrt{2\Lambda/\pi}\,.$$

made in the derivation of the A–Φ relation requiring the flux to be larger than some fraction of $\hbar$. However, we suspect that there is a point below which classically forbidden transitions would become the dominant processes. Other considerations which should be pursued have to do with extending the theory beyond the perturbative regime and investigating multiple barriers. Although exact calculations often appear to be intractable, good approximation schemes exist which should be applicable [18]. We leave this for future work.

Semiclassical localization also has manifestations in the properties of long time wave function propagation. This can be illustrated by propagating any initial state ψ^j which is contained within a single vector subspace associated to one of the chaotic subregions. If the barriers are effective, ψ^j will not democratically explore the weakly connected regions even in the infinite time limit. One quantity which expresses this property is the long time average of the intensity of $\psi^j(t)$ projected into the subspace k,

$$\Delta_k^j = \lim_{T\to\infty} \frac{1}{2T} \int_{-T}^{+T} \|\hat{P}_k \psi^j(t)\|^2 \, \mathrm{d}t , \tag{6.4}$$

where again $\hat{P}_k$ is the appropriate projector. Δ_k^j can roughly be interpreted as the fraction of time a wave packet started in region j will spend in region k. It more precisely corresponds to the fraction of the state intensity that lives in region k. If the mixing is strong and complete, then as $T \to \infty$, $\Delta_k^j \to f_k$ [32], which is the classical expectation. Now, let us assume that $\Gamma_{jk} (k \neq j)$ is small ($\Gamma_{jk} \ll 1$) and higher order contributions like $\Gamma_{jk}\Gamma_{kl}$ are negligible. Since Δ_k^j is independent of the particular state taken as ψ^j, it is convenient to chose the initial state as some unperturbed eigenstate $|\mathcal{E}_\alpha^j(0)\rangle$. Inserting the identity $\sum_{l,\gamma} |\mathcal{E}_\gamma^l(v^2)\rangle\langle\mathcal{E}_\gamma^l(v^2)|$,

$$\hat{P}_k \hat{U}(t) |\mathcal{E}_\alpha^j(0)\rangle = \sum_l \left(\sum_\gamma \hat{P}_k \exp[-(\mathrm{i}/\hbar)\mathcal{E}_\gamma^l t] |\mathcal{E}_\gamma^l(v^2)\rangle\langle\mathcal{E}_\gamma^l(v^2)|\mathcal{E}_\alpha^j(0)\rangle \right) . \tag{6.5}$$

The integration over t in the r.h.s. of (6.4) kills all the non-diagonal terms as $T \to \infty$, so that

$$\Delta_k^j = \sum_l \left(\sum_{\beta,\gamma} \overline{\overline{|\langle\mathcal{E}_\beta^k(0)|\mathcal{E}_\gamma^l(v^2)\rangle|^2 \, |\langle\mathcal{E}_\gamma^l(v^2)|\mathcal{E}_\alpha^j(0)\rangle|^2}} \right) . \tag{6.6}$$

The leading order contributions to Δ_k^j are given by the terms such that $(l,\gamma) = (j,\alpha)$ or (k,β). Then, since

$$\overline{\overline{|\langle\mathcal{E}_\beta^k(0)|\mathcal{E}_\beta^k(v^2)\rangle|^2}} \simeq \overline{\overline{|\langle\mathcal{E}_\alpha^j(v^2)|\mathcal{E}_\alpha^j(0)\rangle|^2}} \simeq 1 , \tag{6.7}$$

neglecting correlations amounts to approximating Δ_k^j by

$$\sum_\beta \left(\overline{\overline{|\langle\mathcal{E}_\beta^k(v^2)|\mathcal{E}_\alpha^j(0)\rangle|^2}} + \overline{\overline{|\langle\mathcal{E}_\beta^k(0)|\mathcal{E}_\alpha^j(v^2)\rangle|^2}} \right) = 2\Gamma_{jk} . \tag{6.8}$$

This equality relies on the reverse transformation matrix (from the perturbed to the unperturbed basis), being the transposed of the direct one. However, although eq. (6.7) remains true on the average, $|\langle\mathcal{E}_\beta^k(0)|\mathcal{E}_\beta^k(v^2)\rangle|^2$, say, may be significantly lower than one. This occurs, for instance, when

some unperturbed level $\mathcal{E}_\alpha^j(0)$ is very close to $\mathcal{E}_\beta^k(0)$ (closer than v_{jk}). These events, although rare in the perturbative regime, give rise to the main contribution to Γ_{jk}. Therefore, the contribution due to correlations in the evaluation of

$$\sum_\beta \overline{\overline{|\langle \mathcal{E}_\beta^k(0)|\mathcal{E}_\beta^k(v^2)\rangle|^2 |\langle \mathcal{E}_\beta^k(v^2)|\mathcal{E}_\alpha^j(0)\rangle|^2}} \quad \text{and} \quad \sum_\beta \overline{\overline{|\langle \mathcal{E}_\beta^k(0)|\mathcal{E}_\alpha^j(v^2)\rangle|^2 |\langle \mathcal{E}_\alpha^j(v^2)|\mathcal{E}_\alpha^j(0)\rangle|^2}}$$

is also of order Γ_{jk} and should be included. Neglecting as before all contributions involving more than two levels, one obtains with the same kind of reasoning

$$\sum_\beta \overline{\overline{|\langle \mathcal{E}_\beta^k(0)|\mathcal{E}_\beta^k(v^2)\rangle|^2 |\langle \mathcal{E}_\beta^k(v^2)|\mathcal{E}_\alpha^j(0)\rangle|^2}} \simeq \sum_\beta \overline{\overline{\left(1 - |\langle \mathcal{E}_\beta^k(v^2)|\mathcal{E}_\alpha^j(0)\rangle|^2\right) |\langle \mathcal{E}_\beta^k(v^2)|\mathcal{E}_\alpha^j(0)\rangle|^2}}$$
$$= f_k \sqrt{\tfrac{1}{2}\pi \Lambda_{jk}} = \tfrac{1}{4}\pi \Gamma_{jk} .$$

The other term gives the same contribution, so that one finally obtains

$$\Delta_k^j \simeq 2\left(\tfrac{1}{4}\pi \Gamma_{jk}\right) , \tag{6.9}$$

valid for $j \neq k$. Also, using $\hat{P}_j = 1 - \sum_{k \neq j} \hat{P}_k$,

$$\Delta_j^j = 1 - \sum_{k \neq j} \Delta_k^j . \tag{6.10}$$

Thus, with the exception of the small leakage due to the Γ_{jk}, any initially localized state just "rattles around" within the subregion it started. This quantum behavior is in contrast with the classical evolution of a Liouville density, which eventually spreads uniformly over the whole chaotic region, not just a subregion. Clearly, the partial transport barrier semiclassical localization, depending on the flux, provides a mechanism for the "quantum dynamical suppression of classical chaos".

To observe such effects, we shall for convenience consider Gaussian initial wave packets which take on the form

$$\psi_{q_0 p_0} = \left(\pi\sigma^2\right)^{-1/2} \exp\left(-\frac{(q - q_0)^2}{2\sigma^2} + \frac{i p_0 \cdot (q - q_0)}{\hbar}\right) . \tag{6.11}$$

Slightly more general forms also exist but are not needed here (see also ref. [32]). The Wigner transform of $\psi_{q_0 p_0}$ is given by

$$[\psi_{q_0 p_0}]_w(q,p) = 4 \exp\left(-\frac{(q - q_0)^2}{\sigma^2} - \frac{\sigma^2 (p - p_0)^2}{\hbar^2}\right) . \tag{6.12}$$

With the centroid q_0, p_0 well within some phase space region, say the jth, and the variance σ^2 adjusted to balance the uncertainties in q and p, $[\psi_{q_0 p_0}]_w(q,p)$ will be virtually null outside region j. This [see the semiclassical definition of $\hat{P}_j$, eq. (5.4)] ensures that $\psi_{q_0 p_0}$ belongs to the Hilbert subspace j. Some care must be exercised in constructing such a wave packet. In particular, σ^2 has to scale as $E^{-1/4}$ if one desires to change the wave packet energy in a manner adapted to the classical scaling properties.

Since the semiclassical localization is occurring in "quantum" phase space it is difficult to display that a propagated wave packet is just bouncing around within one subregion by looking at it in

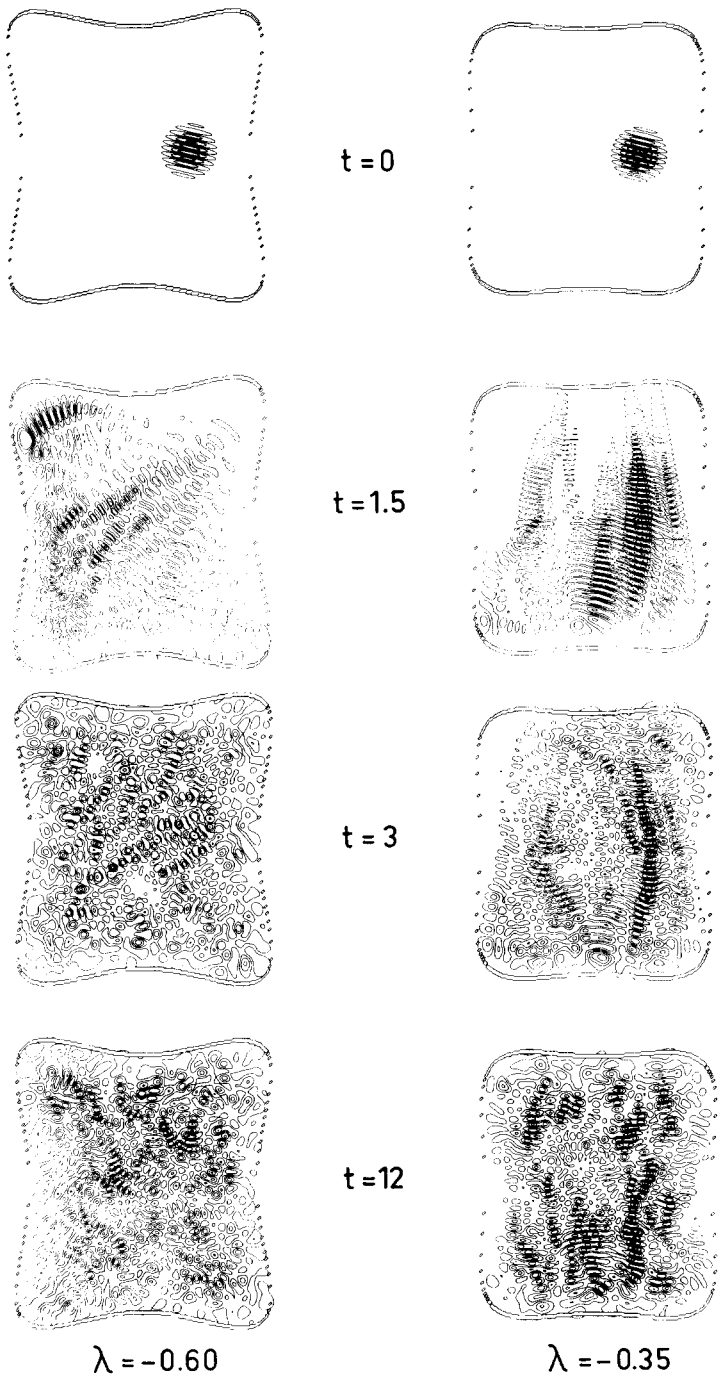

Fig. 24. Propagation, in configuration space, of a wave packet for two different values of the quartic oscillators' coupling λ. The state originally belongs to region (6+7) (see fig. 5) and has a mean energy $E = 100$. Time is measured in units of the period of the central closed orbit of island (a). For $(\lambda, b) = (-0.60, \pi/4)$ (left column), the classical phase space may be regarded as structureless. For $(\lambda, b) = (-0.35, \pi/4)$ (right column), partial barriers described in section 2.4 are present.

configuration space. The same difficulties would have occurred with eigenstates. Indeed, fig. 24, which shows the evolution of a wave packet launched for the quartic oscillators with two different values of the coupling, does not present striking differences when λ is modified. In the first case, $(\lambda, b) = (-0.60, \pi/4)$, there are no significant barriers, nor substantial regular motion and the wave packet rapidly spreads to fill the whole available phase space. The propagated state quickly assumes many of the features of a Gaussian random state. In the second case, essentially the same wave packet is launched, but this time for a coupling $(\lambda, b) = (-0.35, \pi/4)$. Recall that there are five significant chaotic subregions for this coupling as well as a few amply sized KAM regions. The initial conditions and variance of the wave packet were selected to fit the Gaussian inside chaotic region numbered (6 + 7) (see fig. 5). The wave packet again spreads rapidly, and at first sight it appears roughly similar to the one evolving under the $\lambda = -0.60$ coupling. By concentrating on the nodal patterns and turning points, it is however already possible to tell that there is very little momentum in the horizontal direction. None of the rest of the phase space structure is visible in this crude way.

By placing "probe" Gaussians amongst the various regions, labeled as k, the sharp differences between the two time evolutions become readily apparent. The correlation functions

$$c_{jk}(t) = \langle \psi^k_{q_0' p_0'}(0) | \psi^j_{q_0 p_0}(t) \rangle \tag{6.13}$$

can be used to measure the communication between regions. Note that here c_{jk} depends in principle not only on the labels j and k but also on the precise wave packets used. In fig. 25, the absolute value of four correlation functions are plotted against time for the same two couplings as for fig. 24. For $(\lambda, b) = (-0.60, \pi/4)$ (without structure), one observes that after an early transient period the $c_{jk}(t)$ are nearly indistinguishable statistically speaking. There is fairly uniform communication. This is to be contrasted with the second case $(\lambda, b) = (-0.35, \pi/4)$, whose phase space structure guided the choice of probe Gaussians (same probe for both λ values). Among the four probes, the first was chosen to belong to region (6 + 7), as was the initial propagated Gaussian, in order to serve as a reference intensity. Their initial overlap was arranged to be almost zero. The second is in region 5 being just across a single barrier. The third was placed in region (1 + 2) so that all four significant barriers had to be crossed. Finally, the last was put inside KAM island (a), which is inside region 5. The barriers have a sharp effect and each successive $c_{jk}(t)$ becomes weaker and weaker. We also see that for this system, it is easier to cross four barriers than to cross one barrier and tunnel into KAM island (a).

Beyond qualitative arguments, the statistical model can be used to quantitatively predict the long time averages of the absolute squares of these correlation functions. Some care must be taken, however, because it is necessary to account for the energy spread of the wave packet. Its shape is easily determined by simple semiclassical considerations. The spectrum of $\psi_{q_0 p_0}$, namely

$$S_{q_0 p_0}(E) \equiv \sum_n |\langle \psi_{q_0 p_0} | \mathcal{E}_n \rangle|^2 \delta(E - \mathcal{E}_n) \tag{6.14}$$

(the $|\mathcal{E}_n\rangle$ generically denote all the eigenstates, i.e. the $|\mathcal{E}^l_\beta(v^2)\rangle$), is the Fourier transform of the autocorrelation function

$$a_{q_0 p_0}(t) = \langle \psi_{q_0 p_0}(0) | \psi_{q_0 p_0}(t) \rangle .$$

The global smooth envelope $\bar{S}_{q_0 p_0}$ of the spectrum of $\psi_{q_0 p_0}$ is thus obtained by Fourier transforming the initial decay of $a_{q_0 p_0}(t)$. Since one only needs $a_{q_0 p_0}(t)$ for times short enough that the mean

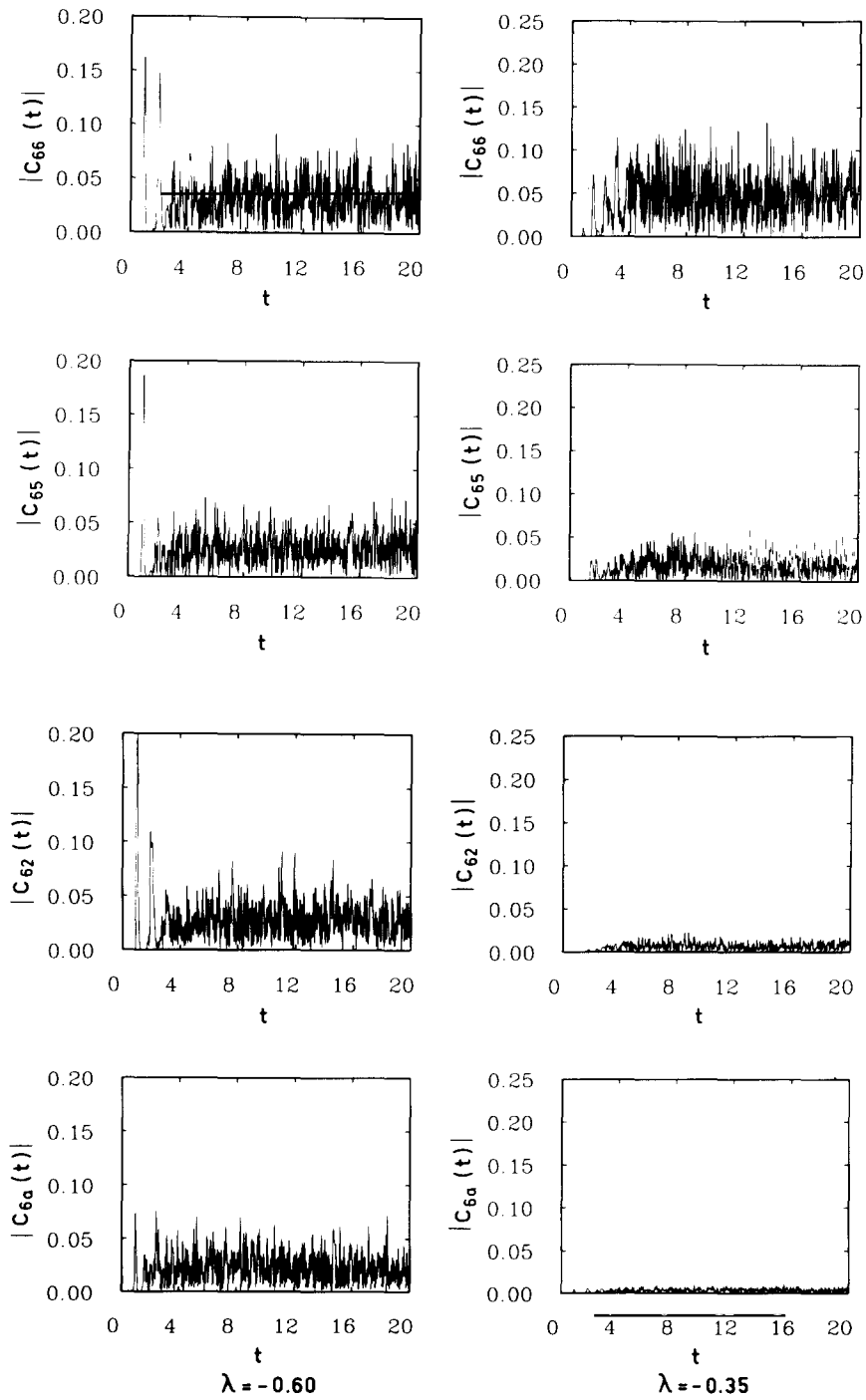

Fig. 25. Absolute value of the correlation functions $c_{jk} = \langle \psi^k(0)|\psi^j(t)\rangle$ [see eq. (6.13)], where the moving packet ψ^j corresponds to the one displayed in fig. 24. At $t = 0$ it is launched from region (6+7). The probe packets belong to (top) region (6+7), (second) region 5, (third) region (1+2), (bottom) island (a). See text and the caption of fig. 24 for further explanation. As in fig. 24, time is measured in units of the period of the central closed orbit of island (a).

position of the wave packet has moved less than a few σ, its dispersion properties can usually be neglected. This is called a frozen Gaussian approximation by Heller [91]. Thus one can use

$$\psi_{\boldsymbol{q}_0\boldsymbol{p}_0}(t) = \psi_{\boldsymbol{q}_t\boldsymbol{p}_t}\,, \tag{6.15}$$

where $(\boldsymbol{q}_t,\boldsymbol{p}_t) = g^t(\boldsymbol{q}_0,\boldsymbol{p}_0)$ (the classical flow). If the initial $(\boldsymbol{q}_0,\boldsymbol{p}_0)$ is not close to a turning point, the variations of the potential can be neglected (free motion) so that

$$a_{\boldsymbol{q}_0\boldsymbol{p}_0}(t) = \exp\left(-\frac{\boldsymbol{p}_0^2}{4\sigma^2}t^2 - \frac{\mathrm{i}}{\hbar}E_0 t\right) \qquad [E_0 = H(\boldsymbol{q}_0,\boldsymbol{p}_0)]\,, \tag{6.16}$$

$$\overline{S}_{\boldsymbol{q}_0\boldsymbol{p}_0}(E) = \frac{1}{2\pi\hbar}\int \mathrm{e}^{(\mathrm{i}/\hbar)Et} a_{\boldsymbol{q}_0\boldsymbol{p}_0}(t)\,\mathrm{d}t \simeq \frac{\sigma}{\pi^{1/2}\hbar\|\boldsymbol{p}_0\|}\exp\left(-\frac{\sigma^2}{\boldsymbol{p}_0^2}\frac{(E-E_0)^2}{\hbar^2}\right)\,. \tag{6.17}$$

For wave packets, the interesting quantity related to Δ_k^j is

$$C_{jk} = \lim_{T\to\infty}\frac{1}{2T}\int_{-T}^{T}\mathrm{d}t\,|c_{jk}(t)|^2\,. \tag{6.18}$$

To compute it, we start by decomposing $\psi^k_{\boldsymbol{q}'_0\boldsymbol{p}'_0}$ and $\psi^j_{\boldsymbol{q}_0\boldsymbol{p}_0}$ in the unperturbed basis, giving

$$|\langle\psi^k_{\boldsymbol{q}'_0\boldsymbol{p}'_0}(0)|\psi^j_{\boldsymbol{q}_0\boldsymbol{p}_0}(t)\rangle|^2 = \sum_{\alpha,\beta}|\langle\mathcal{E}^k_\beta(0)|\psi^k_{\boldsymbol{q}'_0\boldsymbol{p}'_0}\rangle|^2\,|\langle\mathcal{E}^j_\alpha(0)|\psi^j_{\boldsymbol{q}_0\boldsymbol{p}_0}\rangle|^2\,|\langle\mathcal{E}^k_\beta(0)|\hat{U}(t)|\mathcal{E}^j_\alpha(0)\rangle|^2\,. \tag{6.19}$$

On the scale of the energy span of the envelopes $\overline{S}^l$ ($l = j$ or k), the unperturbed energies $\mathcal{E}^l_\gamma(0)$ can be regarded as residing on top of the perturbed ones $\mathcal{E}^l_\gamma(v^2)$. Indeed, in the perturbative regime they have moved less than a mean spacing. The dispersion of a state should never be larger than $\sqrt{\Lambda}$ mean spacings even at $\Lambda \simeq 10$, at which point mixing is completed. One can therefore use $\overline{S}^l(E)$ to describe the smooth energy behavior of $\overline{S}^l(E; v^2 = 0)$. This gives

$$\overline{|\langle\mathcal{E}^l_\gamma(0)|\psi^l\rangle|^2} = \overline{S}^l(\mathcal{E}^l_\gamma)/\bar{\rho}_l(\mathcal{E}^l_\gamma)\,. \tag{6.20}$$

It also implies that $|\langle\mathcal{E}^k_\beta(0)|\hat{U}(t)|\mathcal{E}^j_\alpha(0)\rangle|^2$ is virtually null whenever $\mathcal{E}^k_\beta(0) \not\approx \mathcal{E}^j_\alpha(0)$ (on the same scale as before).

Assuming time average and local smoothing in energy are equivalent to ensemble averaging, and that the terms in the r.h.s. summation of eq. (6.19) are uncorrelated*), C_{jk} can be written as

$$\begin{aligned} C_{jk} &= \int\int \mathrm{d}\mathcal{E}^k\,\bar{\rho}_k(\mathcal{E}^k)\,\mathrm{d}\mathcal{E}^j\,\bar{\rho}_j(\mathcal{E}^j)\,\frac{\overline{S}^k(\mathcal{E}^k)}{\bar{\rho}_k(\mathcal{E}^k)}\,\frac{\overline{S}^j(\mathcal{E}^j)}{\bar{\rho}_j(\mathcal{E}^j)}\,\Delta_k^j\,\frac{\delta(\mathcal{E}^k-\mathcal{E}^j)}{\bar{\rho}_k(\mathcal{E}^k)} \\ &= \frac{\Delta_k^j}{f_k\bar{\rho}_c}\int \mathrm{d}E\,\overline{S}_k(E)\overline{S}_j(E)\,. \end{aligned} \tag{6.21}$$

*) The matrix elements of $\hat{U}(t)$ certainly are independent of the way in which $\psi^j_{\boldsymbol{q}_0\boldsymbol{p}_0}$ and $\psi^k_{\boldsymbol{q}'_0\boldsymbol{p}'_0}$ are expressed in the unperturbed basis. However, if $j = k$, $|\langle\mathcal{E}^{j=k}_\alpha(0)|\psi^j_{\boldsymbol{q}'_0\boldsymbol{p}'_0}\rangle|^2$ and $|\langle\mathcal{E}^j_\alpha(0)|\psi^j_{\boldsymbol{q}_0\boldsymbol{p}_0}\rangle|^2$ may not be uncorrelated if the classical trajectory initiated at $(\boldsymbol{q}_0,\boldsymbol{p}_0)$ passes near $(\boldsymbol{q}'_0,\boldsymbol{p}'_0)$ at a short enough time such that $\psi^j_{\boldsymbol{q}_0\boldsymbol{p}_0}(t)$ has kept its Gaussian original form. This would invalidate eq. (6.21) for C_{jj}. However, if $\psi^j_{\boldsymbol{q}'_0\boldsymbol{p}'_0} = \psi^j_{\boldsymbol{q}_0\boldsymbol{p}_0}$, a simple argument leads to a result equivalent to eq. (6.21) for the time average of the absolute square of the autocorrelation function (see, for instance, ref. [92]), i.e., as for the GOE, the projection of an eigenvector on a fixed, real vector is a Gaussian variable x, and therefore $\langle x^4\rangle = 3\langle x^2\rangle^2$.

($\bar{\rho}_c = f_c\bar{\rho}$ is the density of chaotic states.) In the last expression, it has been assumed that the level density, $\bar{\rho}(E)$, and the transition parameter, Λ_{jk}, are constant over the energy domain of $S_j(E)$ and $S_k(E)$. Since the wave packets under consideration have been taken with the same energy E_0, one finally finds

$$C_{jk} = \frac{1}{\pi^{1/2}\hbar\bar{\rho}_c(E)\sqrt{\boldsymbol{p}_0^2/\sigma^2 + \boldsymbol{p}'^2_0/\sigma'^2}}\frac{\Delta_k^j}{f_k} \tag{6.22}$$

$$\simeq \frac{1}{\pi^{1/2}\hbar\bar{\rho}_c(E)\sqrt{\boldsymbol{p}_0^2/\sigma^2 + \boldsymbol{p}'^2_0/\sigma'^2}}\left(\frac{\Phi_{jk}}{2\pi f_j f_k (2\pi\hbar)^{d-1}}\right)^{1/2},$$

where $\boldsymbol{p}_0$, σ^2 and $\boldsymbol{p}'_0$, σ'^2 are the initial momentum and variance of the wave packets ψ^j and ψ^k. The last form, valid for $j \neq k$, has been added to emphasize again the connection with the classical flux and exhibits the exchange symmetry between j and k which must exist. Equations (6.21) and (6.22) should be compared to the result expected when no structure is present in phase space, which is given by [32]

$$C_{jk} = \frac{1}{\bar{\rho}}\int \mathrm{d}E\,\overline{S}_k(E)\overline{S}_j(E) \simeq \frac{1}{\pi^{1/2}\hbar\bar{\rho}(E)\sqrt{\boldsymbol{p}_0^2/\sigma^2 + \boldsymbol{p}'^2_0/\sigma'^2}}. \tag{6.23}$$

Notice that in eq. (6.23) j and k just specify the wave packets. The relative effect of the partial barriers is thus the term Δ_k^j/f_k, which for the quartic oscillators behaves as $E^{3/8}$ in the perturbative regime.

To compare exact (quantum) results to the above prediction, we shall use different wave packets than the ones drawn previously in fig. 24. Indeed, when looking qualitatively at localization effects, it was convenient to locate initially the wave packet in region (6+7) thereby ensuring a maximum number of barriers to be crossed before reaching region (1+2). However, the ratios flux/volume are such that the barriers separating regions 6 and 7 can hardly be treated by a perturbative approach, even at the energy $E = 100$ considered. For a quantitative check of the perturbative result we shall therefore use a moving wave packet located initially in region 5, and probes contained in regions 1 to 7. To take explicitly into account the symmetries of the problem we shall completely symmetrize (i.e. by $\hat{P}_1$, $\hat{P}_2$ and $\hat{T}$) these packets. Then the wave packets will belong to the same symmetry class, here $(+,+)$, and will be real up to a global phase. Except for the lowering of the Λ's discussed in section 5.2.2, the effects of symmetries will be correctly disposed of by taking $\bar{\rho}_c$ in eq. (6.22) as the density of chaotic states in the considered sequence (one quarter of the total one). Finally, choosing the evolving packet in the largest region gives more flexibility to avoid effects due to short closed orbits, which as we shall see, is quite crucial at the rather low energy considered here.

That the closed orbits affect the quantum evolution can be seen by looking at the short time behavior of autocorrelation functions (recall that until now, we were essentially concerned with long time limits). For Gaussian packets such as (6.11), two characteristic times have to be considered [32]. The first one t_1^* ($\simeq \sigma/\|\boldsymbol{p}_0\|$) characterizes the initial decrease, which, as we have seen, fixes the global envelope of the wave packet spectrum. The second t_2^*, which is still very short since it depends logarithmically on $\hbar$, measures the time during which the packet keeps its Gaussian original form. For $t < t_2^*$ the autocorrelation function appears as a succession of soft bumps associated to recurrences, that is, to times (if any) for which the centroïd returns classically near to its initial position. Between these recurrences, the autocorrelation function remains close to zero, until the

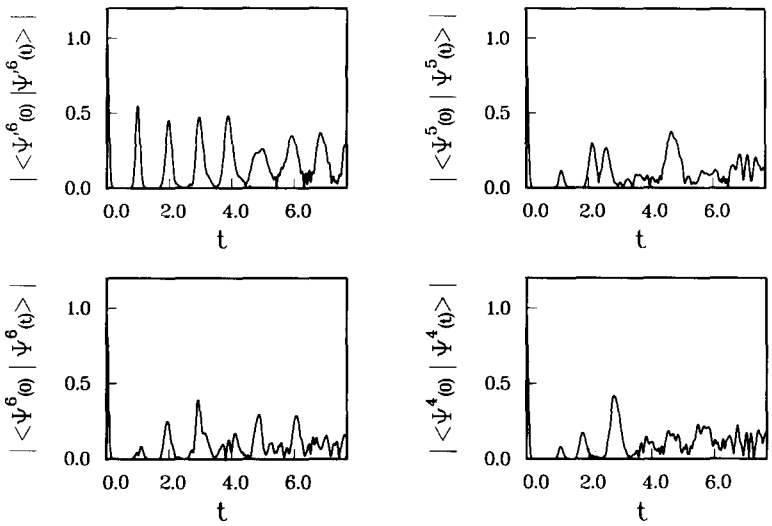

Fig. 26. Short time autocorrelation ($t < t_2^*$), in the quartic oscillators with $(\lambda, b) = (-0.35, \pi/4)$, of the symmetrized wave packets $\Psi^{6'}$ (top left), Ψ^6 (bottom left), Ψ^5 (top right), and Ψ^4 (bottom right), whose parameters are given in table 5. A clear difference exists between $|\langle\Psi^{6'}(0)|\Psi^{6'}(t)\rangle|$, showing sharp recurrences regularly spaced, which is the signature of strong scarring, and the other functions. In fact, except for $\Psi^{6'}$, these short time autocorrelation functions have been used to select in table 5, by successive trials, states as spared as possible from the effects of closed orbits. For time scale guidance, the period of the shortest orbits is $T \simeq 2$ at $E = 100$.

kind of noisy structure which characterizes the dissolution of the wave packet in phase space takes over. One may compare in fig. 26 some autocorrelation functions of wave packets. For Ψ^4, Ψ^5 and Ψ^6 a few recurrences exist, but they are neither sharp nor regularly spaced. On the contrary $|\langle\Psi^{6'}(0)|\Psi^{6'}(t)\rangle|$ shows clear, strong recurrences. They appear moreover with an almost fixed period since the time intervals between the four first extrema fall in the range $\Delta t = 0.98 \pm 0.01$. This can be traced back to the presence of a closed orbit which is stable for $\lambda = -0.25$ (the central elliptic orbit of island (e), see fig. 1), but has turned hyperbolic, through a period doubling process, by $\lambda = -0.35$. As shown by Heller [31], such behavior of the short time autocorrelation function implies what he has termed scarring, that is, enhanced intensity of some of the eigenstates in the neighborhood of a closed trajectory. And any feature of the eigenstates must in some way affect the long time evolution of the wave packet, which we are interested in here.

The Markovian modeling of the classical motion which underlies our treatment of localization as well as spectral statistics specifically excludes features such as scarring. This is meaningful in the asymptotic regime since only the neighborhood of the less unstable short orbits are affected, and the concerned relative volume becomes negligible as energy increases. However, because of computer time limitations, and to remain as close as possible to the perturbative regime, the quantum calculations presented in this section correspond to a rather intermediate energy ($E = 100$) for which it turns out that a good part of the phase space is affected by scarring. One may note that this latter effect is significantly enhanced by the discrete symmetries (shorter, less unstable symmetric orbits). This may in part explain why the random matrix modelization for spectral statistics worked poorly in the lower part of the spectrum. For simplicity we shall test the localization result using wave packets as little affected by scarring as possible. We have thus propagated wave packets for small times, and eliminated the ones showing the presence of a closed orbit (except $\Psi^{6'}$). The parameters defining the ones finally retained are described in table 5.

Table 5
Parameters of the wave packets used for a quantitative comparison of the semiclassical prediction and the quantum results (see table 6). The labeling of the different regions is as in fig. 5. The states are obtained by symmetrization, by $\hat{P}_1$, $\hat{P}_2$, and $\hat{T}$, of the Gaussian expression eq. (6.11). $q_1(\max) = [bE/a(\lambda)]^{1/4}$ ($q_2(\max) = [E/ba(\lambda)]^{1/4}$) is the maximum q_1 (q_2) in the $q_2 = 0$ ($q_1 = 0$) Poincaré section, $p(\max) = \sqrt{2E}$ is the maximum momentum, and σ_0^2 is equal to $E^{-1/4}$. The packets considered correspond to $E = 100$. Ψ^5 serves as propagated packet, and the other ones as probe Gaussians.

	region	$\frac{q_1}{q_1(\max)}$	$\frac{q_2}{q_2(\max)}$	$\frac{p_1}{p(\max)}$	$\frac{p_2}{p(\max)}$	$\frac{\sigma^2}{\sigma_0^2}$
Ψ^1	1	0	0.404	0.987	0	1
Ψ^2	2	0	0	0.987	0.158	1
Ψ^3	3	0	0.385	0.935	0.321	1
Ψ^4	4	0	0.800	0.768	0	0.25
Ψ^5	5	0.514	0	0.561	0.784	1
Ψ^6	6	0.670	0	0	0.894	1
$\Psi^{6'}$	6	0.533	0	0.237	0.929	1
Ψ^7	7	0.248	0	0	0.998	1
Ψ^a	island (a)	0	0	0.629	0.777	1

To calculate the quantum values of the time averages C_{jk} ($j = 5$, $k = 1, \ldots, 7$) [see eq. (6.18)], Ψ^5 has been propagated for a long enough time t_f ensuring that transient phenomena have vanished. Actually t_f is about 300, which insures that it is much larger than not only the breaktime $2\pi\hbar/D$ ($\simeq 20$ at $E = 100$), but also the times $2\pi\hbar/v_{jk}$ (< 70 at $E = 100$) ($v_{jk} = \Lambda_{jk}^{1/2} D$) which in ensembles treated perturbatively characterize the transport among regions. In addition, it has been verified that the numerical values of the C_{jk} are well converged. The correctness of the Ψ^5 propagation is demonstrated by its spectrum, constructed by Fourier transforming $\langle \Psi^5(0) | \Psi^5(t) \rangle$ and, as seen in fig. 27, it perfectly fits the eigenvalues calculated in section 3 using matrix diagonalization.

The comparison for the C_{jk} between the semiclassical theory (perturbative regime) and the quantum calculation is summarized in table 6. Let us first recall what we expect to predict on semiclassical grounds. The value of the time averages C_{54}, C_{55}, and C_{56}, corresponding to scarring-free wave packets located in the same or adjacent regions, should be reliably predicted by the theory described [eq. (6.22)]. In contrast, because the packet $\Psi^{6'}$ is heavily affected by scarring, $C_{56'}$ should not be correctly predicted by eq. (6.22). For C_{53}, C_{52}, etc., namely for time averages concerning wave packets not belonging to adjacent regions, or, a fortiori, when one packet is in a regular island, one expects that the time averages will be small (in fact zero from the first order perturbation theory described). By inspecting table 6, one sees indeed that all these features are present in the exact quantum results and that the hierarchy in the barriers is respected. As a comparison, would the classical phase space considered be structureless, the expected result for the C_{jk}, eq. (6.23), would be a constant (about 4.3×10^{-3}), except for small variations due to the shape of the Gaussians (in particular for Ψ^4).*) The predicted values for C_{54}, C_{55}, and C_{56} agree to within 30%–50%, which we consider as very satisfactory for a theory having no adjustable parameter and dealing with such intricate dynamics. In addition to what is due to modeling the classical motion by a Markovian process (scarring), the departures between exact and predicted values may be due to several other mechanisms. First, although not clearly out, we are rather at the border of validity

*) C_{55}, which derives from an autocorrelation function, would also have to be multiplied by a factor three.

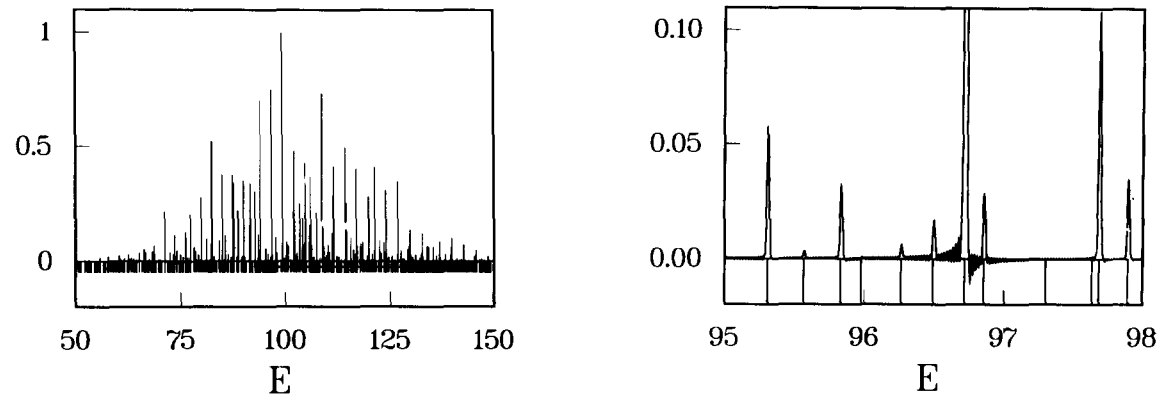

Fig. 27. Spectrum of the wave packet Ψ^5 (see table 5), intensity in arbitrary units, obtained by Fourier transforming the autocorrelation function $\langle\Psi^5(0)|\Psi^5(t)\rangle$. $\Psi^5(t)$ is propagated quantum mechanically for the quartic oscillators with $(\lambda, b) = (-0.35, \pi/4)$, during a time $t_f \simeq 300$. Left: total spectrum; right: blow up of the energy range $95 < E < 98$. The location of the eigenvalues calculated in section 3 are indicated bellow the abscissa axis. The perfect correspondence between the two sets of data insures that the quantum propagation of $\Psi^5(t)$ has been properly done.

of the perturbative regime. For instance, the departure from 1 of Δ_5^5 at $E = 100$ [see eq. (6.10)] is 30%, which is not that small. Also, even in the general framework of the statistical model, one may expect fluctuations in the values of the C_{jk}, due to the particular choice of the wave packet, fluctuations which have not been evaluated. Finally, even if there exist strong indications that semiclassical propagation is accurate at the energies considered here [5], there exist non-classical effects, like, for instance, the value of C_{5a}, which are beyond the scope of the present approach.

Table 6

Comparison, for the wave packets corresponding to table 5, between the perturbative semiclassical prediction eq. (6.22) and the quantum values of the time average of the correlation functions, C_{jk} [see eq. (6.18)]. The moving packet Ψ^5 is propagated for the quartic oscillators system with $(\lambda, b) = (-0.35, \pi/4)$. C_{55} derives from the autocorrelation function $\langle\Psi^5(0)|\Psi^5(t)\rangle$ and therefore a factor of three has to be included (see footnote on page 122). When more than one barrier has to be crossed by the moving packet the first order perturbation result is insufficient to approximate the ensemble prediction since it gives a zero value. This is indicated by a dash in the right hand column.

	quantum result	semiclassical prediction
C_{51}	0.21×10^{-3}	–
C_{52}	0.44×10^{-3}	–
C_{53}	0.72×10^{-3}	–
C_{54}	2.43×10^{-3}	3.64×10^{-3}
C_{55}	$3 \times 6.40 \times 10^{-3}$	$3 \times 9.50 \times 10^{-3}$
C_{56}	4.62×10^{-3}	4.37×10^{-3}
$C_{56'}$	1.72×10^{-3}	4.25×10^{-3}
C_{57}	1.50×10^{-3}	–
C_{5a}	0.15×10^{-3}	–

As a final comment, let us mention some of the interesting problems remaining. In a very simple situation, such as the perturbative regime treated above for crossing a single barrier, the generalized ensembles are quickly manipulated to give an answer about how the wave functions are localized. One may imagine however more complicated situations, as may occur where there are many barriers, each one being too "open" to imply localization by itself, but when acting collectively producing strong localization effects. Such conditions may be realized in the hydrogen atom in the presence of a microwave field for certain ranges of the experimental parameters. In this case, the ensemble is easily constructed, but its theoretical predictions would still require Monte-Carlo calculations. There are also interesting possibilities which violate some of the assumptions behind the statistical modeling. Two examples would be when there exists a dense set of partial barriers or poor mixing inside the regions before they begin communicating amongst themselves. There are still purely classical questions remaining to be resolved in these cases as well. We leave these things for future work.

6.2. Semiclassical versus quantum localization

In the previous subsection the term localization has been used to express that there is a known region in the phase space where the Wigner transform (or Husimi representation) of a state is largely concentrated. This, moreover, takes place in a bounded system within a compact energy surface. This is not the conventional terminology and is different from the usage, found predominantly in condensed matter physics, where one is interested in the long range behavior of wave functions in an infinite momentum or configuration space [93]. For instance, the electronic conduction in periodic metallic lattices (assuming zero temperature) is related to the electron's wave function being a Bloch state delocalized throughout the entire solid. The crucial question is not where the wave function is maximum, but whether it is sensitive to what is occurring on the distant boundary of the system. It has been shown by Anderson [94] however that, if one introduces a sufficient amount of disorder by replacing at random some atoms of the lattice by others with a different chemical nature, for example, the electronic wave functions localize. They then have a noticeable probability of presence only in the neighborhood of some site of the lattice and well beyond they decay exponentially. This therefore has drastic consequences on the conduction properties. Many of the studies of localization properties have been done using the deceptively simple model of Anderson to describe the electrons' motion. It consists of a tight-binding Hamiltonian in which the electrons are moving on a regular lattice with a site energy, or diagonal term, E_m (m is the site index), chosen as a random distribution of width W, and a term connecting neighboring sites of magnitude $V_{jk} = V$ if j and k are nearest neighbors, 0 elsewhere. For one-dimensional systems, the eigenstates are localized no matter how weak the measure of the disorder W. For higher dimensionality, the wave functions are localized if W is large compared to V and delocalized in the opposite case near the center of the band. The states corresponding to the border of the band remain localized however, since a site with an energy in the tail of the E_m distribution is usually surrounded by sites with very different energies.

Anderson's quantum interpretation of disorder and exponential localization sidesteps any questions as to the classical electron's behavior. Despite the difference of this point of view from that of section 6.1, we suspect that semiclassical and quantum localization are not of a fundamentally distinct nature. It seems plausible that the differences are more due to the fact that the simple systems we have focused on have little directly in common with a macroscopic solid. In particular, working in bounded phase spaces instead of open ones does not as simply lend itself to defining "long distance" wave function behavior. However, our approach is, in principle, applicable to a larger

class of systems. The example treated in section 6.1 is such that each partial barrier largely blocks a wave function from exiting the region. This is convenient for our work because the modeling matrix ensemble is in a perturbative regime for which leading order analytic results can be derived. One could just as easily have found a problem with more intricate classical mechanics characterized by a large number of barriers, each being too insignificant to affect the wave functions appreciably, but which acting together would presumably lead to an exponential decay. Such a situation goes beyond the kind of "perturbative localization" of an isolated barrier we have treated explicitly (and would probably involve a diffusion constant from the collective effect of the barriers), but it begins to blur the distinction noted above.

In fact, it appears reasonable to us, and was suggested by Laughlin [95], that the whole point of introducing random potentials or disorder to begin with is to induce classically chaotic motion of the electrons. An interesting direction, which at the present time is still speculative, would consist in applying the same logic as we have done for closed systems to ones which are usually treated by an Anderson (or Anderson-like) model. To outline the idea, let us concentrate as above on the motion of an electron in a disordered solid. Although the Anderson model might not possess any clear classical analog, the original physical problem does. Namely, it could be classically associated to a diffusion process (brownian motion) described by some master equation. As the classical diffusion of brownian motion or even as chaos in a deterministic system, the classical "analog" perfectly suits the image we have been using to describe the classical transport (cf. section 2.4) whereby the microscopic evolution is seen locally as a Markovian process. Therefore, the construction of a generalized matrix ensemble, which depends on this Markovian image, is presumably possible for these systems also.

Without entering into the details, one would thus end up with some matrix ensemble which would have to be dealt with. In some cases, existing results (techniques) from random matrix matrix theory would apply such as those already existing for banded random matrices [96, 97]. In other cases, it might happen that one faces problems of a similar nature as those encountered in the treatment of the Anderson model, where techniques could be borrowed from localization theory, or perhaps Monte-Carlo calculation or numerical work is required. Nevertheless, a few points should be kept in mind. The ensembles will most likely give predictions for the localization in its usual sense, i.e. for the long distance behavior of the wave function. Therefore, semiclassical localization will recover the conventional meaning when applied to large or open disordered systems. What is more interesting though is that the classical mechanics would fix the localization properties which are generally viewed as purely quantum effects. If one considers a system for which our modeling applies, but treats it with the Anderson approach, this link between the classical mechanics and the localization properties will still exist, but will remain hidden.

A place where such a link between localization and classical mechanics obviously exists but is not fully understood is the quantum version of the Chirikov kicked rotor. The study of its quantum versus classical behavior was originated by Casati et al. [33]. This system describes the motion of a free particle on a circle, kicked periodically in time by a position dependent force. It is governed by the Hamiltonian

$$H = p_\theta^2/2I + \hat{k}V(\theta)\delta_T(t)\,, \tag{6.24}$$

where $\delta_T(t) = \Sigma_{n=-\infty}^{+\infty}\delta(t-nT)$, θ is the angle variable, p_θ its conjugate momentum and $V(\theta) = V(\theta + 2\pi)$. Classically speaking [98], the dynamics is determined by a single parameter $K = \hat{k}T$. For small K, the movement resembles the one of the free rotor for which the momentum is a constant of the motion. A set of trajectories with the same initial momentum $\tilde{p}_\theta$ will continue to

possess about the same momentum even for infinite times. However, above some critical value K_{cr} of K the motion is no longer confined in momentum space, and a diffusive process take place. It is characterized by the diffusion law

$$\langle (p_\theta - \tilde{p}_\theta)^2 \rangle_{cl} = Dt , \tag{6.25}$$

where $\langle\ \rangle_{cl}$ stands for an averaging over the initial conditions and D is the diffusion constant.

The quantum evolution of equivalent quantities has also been studied. Namely, starting from an initial state $\Psi_{\tilde{n}} = e^{i\tilde{n}\theta}$, the eigenstate with momentum $\hbar n$ of the free Hamiltonian $H_0 = p_\theta^2/2I$, one can look at the time evolution of the quantum analog of $\langle (p_\theta - \tilde{p}_\theta)^2 \rangle_{cl}$, i.e.,

$$\hbar^2 \langle (n - \tilde{n})^2 \rangle_{qm} = \hbar^2 \langle \Psi_{\tilde{n}}(t) | (n - \tilde{n})^2 | \Psi_{\tilde{n}}(t) \rangle . \tag{6.26}$$

In the classically diffusive regime, it has been observed numerically that, depending on the time, two drastically different types of behavior occur (in the generic situation, that is excluding the resonant cases [99]). For short enough times [33], the diffusion in momentum space follows the classical behavior

$$\hbar^2 \langle (n - \tilde{n})^2 \rangle_{qm} = Dt , \tag{6.27}$$

with the same value of D as in the classical case. However, as time increases, the diffusion stops and the quantum momentum (or the energy) remains bounded [34, 35], in complete opposition with the classical behavior. This reflects the localization, in the $\Psi_n = \exp(in\theta)$ basis, of the kicked rotor eigenstates, which also has been observed numerically by Fishman et al. [36].

In addition, these authors [36] have been able to map the kicked rotor eigenstate equations onto those of a one-dimensional tight binding problem with pseudorandom diagonal elements. Except for the difference between randomness and pseudorandomness, their work allows techniques now well understood in solid state physics to be applied. In that sense one may consider that the most important questions are answered since the localization of the eigenfunctions and the discreteness of the quasi-energy spectrum are demonstrated by this means. On the other hand, a full understanding of the problem is still missing since it is known that the localization length l simply behaves as [34]

$$l \simeq \alpha D \tag{6.28}$$

from heuristic general arguments and numerical verification, but α is some (still unknown) constant. Such a relation remains to be actually understood, which obviously supposes some way of semiclassically treating the localization problem. A mechanism like the one we described seems well adapted for this task, and should presumably give the value of α.

7. Summary and conclusions

We have investigated the quantum mechanics of simple systems whose classical analogs have varying mixtures of regular and chaotic motion. A significant part of this study consisted of illustrating the various phenomena involved by taking the example of two coupled quartic oscillators. This system is well suited because dynamics from an integrable to an essentially chaotic nature can be selected and because of its scaling properties.

Two technical considerations are worth mentioning. The first is that for differentiable Hamiltonians a simple method exists to expand $\overline{N}(E)$, the smoothed part of the cumulative density of states, in powers of $\hbar^2$ to as high an order as one wishes. Some symmetry decompositions may be included and they typically introduce terms of odd powers in $\hbar$. This is unlike billiards, for which odd terms appear, such as the perimeter term, without considering symmetry decompositions. The second technical aspect is that, guided by semiclassical logic, a proper choice can be made of the, in principle, arbitrary basis in which a Hamiltonian matrix $\widehat{H}$ is being computed. As a result, better accuracy can be achieved, and one insures exponential convergence of the results as the dimensions of the basis set is increased.

With the help of the discrete symmetries, it has been possible to study Percival's semiclassical classification scheme, which asserts that once $\hbar$ is small enough it should be possible to separate individual eigenstates into a regular or an irregular class. This works quite well for the majority of states indicating that tunneling effects between the regular and irregular classes can be initially ignored and their separate study is warranted. There are exceptional states of intermediate nature though, which are mostly associated with the region of phase space near the KAM island–chaos interface. By assigning quantum numbers and inferring actions of tori via the EBK relations, eq. (4.10), we have compared quantally derived actions for the tori to the actual classical values; the agreement is quite precise when both are defined. We find that the quantum system interpolates gaps due to resonances in a seemingly analytic way. Furthermore the quantum derived actions extend beyond the edge of the island in some cases and they do not reach the edge in others. This appears to be related to the dynamics just outside the island's boundaries. We also discuss how resonances get resolved as $\hbar$ shrinks and one case where the resonance should be resolved by the top of our spectra is treated in detail.

The irregular class of states (and levels) are analyzed from a statistical and ensemble point of view. The naive expectation that their spectral fluctuations should correspond to those of a classical random matrix ensemble (the GOE), as assumed in the Berry–Robnik surmise, is not borne out. The mechanism for the departure is found to lie in the introduction of long time scales due to partial barriers deep within the chaotic sea.

In a treatment which applies quite generally to systems with isolated sets of partial barriers, we derive how the nearly separate volumes of phase space, their barriers and the fluxes that cross them, can be related semiclassically to values of certain mean square matrix element admixings when viewed from relevant bases. This in turn leads to the introduction of generalized random matrix ensembles which recover the Berry–Robnik surmise and, for fully chaotic systems, the Bohigas–Giannoni–Schmit conjecture as limiting cases. For one case of coupling $(-0.35, \pi/4)$ the classical dynamics is thoroughly investigated thus fixing the generalized ensemble and it is found that its fluctuation properties match those of the quartic oscillators.

An interesting consequence of the modeling in terms of generalized random matrix ensembles concerns the localization of eigenfunctions. With the help of a degenerate perturbation theory we have derived for some parameter ranges the extent of localization and how it translates into "quantum suppression of classical chaos". This prediction is quantitatively confirmed in the quantum dynamics. An experimental realization of this with the kind of recent and beautiful experiments on absorption by microwave cavities seems possible [100].

Throughout our investigation we have been struck by the richness of the quantum asymptotics of such simple a system as two coupled quartic oscillators. From a semiclassical vantage point this is not surprising in view of the fact that simple classical systems themselves, and, in particular, the quartic oscillators, exhibit an immense variety of dynamical features. Nevertheless, identifying

how this variety of dynamics is manifest in quantum mechanics is still a subject in its infancy and this paper represents a step forward toward this goal. This is not a purely theoretical or aesthetic endeavor even if here we have not attempted to make connection to a particular physical system. The results of our investigation should concern those small systems caught between the quantum and classical worlds such as the highly excited diamagnetic hydrogen atom, some simple molecules, Rydberg molecules, mesoscopic systems, collective nuclear motion in transition regions, etc.

In fact, local mode excitations in molecules with discrete symmetries are related to the dynamical quasidegeneracies which we have found to be so useful both in confirming Percival's classification scheme and as a probe into the working of semiclassical quantization (EBK) of certain states of mixed phase space systems. Note that the quasidegeneracies' investigative potential by no means has been exhausted in our study. They can serve as promising tools for tackling interesting physical problems. Among them are cantorus quantization, an issue which needs to be further explored. The observed poor working of torus quantization near the regular–chaos interface of small islands may also be of interest even though the evidence at present is restricted to small quantum numbers. Both points, which may be interrelated, are presently just empirical observations and call for a theoretical understanding. For instance, the standard route "à la Maslov" to EBK requires the existence of a genuine invariant torus but does not take into account the neighboring classical dynamics. Whereas it has been seen, by others as well as us, that a torus is not always mandatory, it also appears that the local dynamics is not necessarily innocuous. The comparison with actual data, supplied by the quasidegeneracies, may be crucial in the search of a semiclassical theory interpreting why and when such quantization does or does not take place.

Of direct bearing on this subject is the study of tunneling between regular and chaotic states. Another consequence of this is found beyond the quasi-integrable regime, where the tunneling between quasidegenerate doublets located on twin tori of KAM islands becomes sensitive to the presence of the chaotic sea. A dramatic enhancement of the tunneling rate follows, giving rise to a new mechanism called chaos assisted tunneling by Tomsovic and Ullmo [43]. This dynamical tunneling between symmetric regular states strongly depends on an external parameter and should be detectable experimentally in semiconductors, microwave cavities or perhaps the hydrogen atom in a strong magnetic field.

Perhaps the most important outcome of the present work concerns the chaotic states, a theory of which is a challenging problem. First of all we have qualified the assumption, implicit in both the Bohigas–Giannoni–Schmit conjecture and the Berry–Robnik surmise, that for the purpose of the quantum system the chaos is a featureless entity which translates into universal fluctuation properties, at least at small scale, and little else. Classically speaking it is known though that there is structure of various kinds in the chaotic regions of phase space, which can be rather complex; up to now, none of these structures has been related to the quantum asymptotics. We have shown that some of these structures induce noticeable departures from the universality prediction, and the picture which emerges is richer and more complex than suggested by the above mentioned conjecture and surmise.

We have moreover gone a long way in section 5 toward putting the standard treatment of quantum fluctuations, by which we mean their modeling by random matrix ensembles, on a physical footing. The decorrelation and repartition of matrix elements in relevant bases finds an interpretation in the Maslov image in terms of evolution of the non-invariant tori defining the basis, and their mixing. The notion of relevant bases has been introduced more or less intuitively, and effort towards putting it on a more formal footing would be well deserved. Generalized ensembles come naturally by studying the Hamiltonian matrix in these bases, in which classical transport properties can be semiclassically expressed. The transition parameter–flux relation expressing constraints on the

quantum system implied by partial classical transport barriers allows then quantitative predictions, such as has been done for the quartic oscillators' spectral fluctuations. Coming back to the Bohigas–Giannoni–Schmit conjecture and the Berry–Robnik surmise, they should be, at best, considered to apply when no identifiable small A_{jk} exist, which means that the rate of exploration of the entire energy surface is structureless. If structures are present, depending on the energy scale considered, departures, which may be more or less difficult to exhibit in practice, are expected. It may be interesting to find systems which may be considered, from the present discussion, as the most featureless, and eventually to find out if there are some for which no structure at all is present. For most mixed systems we expect that the chaotic region of the phase space will be far from being featureless, therefore showing significant departures from the GOE regime.

Similarly, as discussed in section 6, the partial barriers in the chaotic sea which have fingerprints in the quantum spectral fluctuations, strongly affect the wave functions and wave packet propagation. Times scales characterizing the rate of exploration of phase space give rise to localization phenomena. The generalized random matrix ensembles, introduced to describe spectral fluctuations, whose parameters are fixed by the classical dynamics, can be used to predict structures in the wave packet propagation in the chaotic sea. Strong departure from the classical evolution of a Liouville density, as predicted by the generalized random matrix model, are found when studying the evolution of a wave packet in the quartic oscillators. They give rise to partial transport semiclassical localization and provide another example of quantum dynamical suppression of chaos.

Some extensions of these problems remain to be addressed. The quantum translation of partial barriers requires that they be isolated in order for the derivation to be valid. Furthermore, there is an assumption of uncorrelated matrix elements so that special coherent behaviors are not expected to be described with these generalized ensembles. One may imagine many interesting problems such as how to treat barriers which are dense or fractal in nature. Moreover, due to the complexities possible even for simple classical systems, the prescription for building generalized ensembles can lead to quite varied ensembles; there will be many interesting consequences, which, of course, have not all been foreseen.

Let us finally mention that some of the problems discussed here have some significance in the physics of disordered media. Indeed, as discussed, for instance, in ref. [95], the physics of quantum electronic transport, instead of being considered as due to the motion of electrons in dirty metals (random potentials), can be re-examined as a problem of electronic motion in a chaotic system. And quantum mechanical coherence of electron wave functions in materials with imperfections has led to new developments in the description of conductivity and to novel quantum interference effects in electrical resistance measured in submicron devices [101]. It seems quite clear that in the future the two areas, namely dynamical chaos and the physics of disordered media, will be more and more closely related.

Acknowledgements

We gratefully acknowledge discussions with A. Comtet, M.J. Giannoni, E. Heller, C. Jacquemin and C. Schmit. Computing was performed at STIC, Institut de Physique Nucléaire, Orsay, and at Centre de Calcul Vectoriel pour la Recherche, Ecole Polytechnique. One of us (S.T.) was supported by the Joliot-Curie Foundation, the Centre National de la Recherche Scientifique and the National Science Foundation (Grant number CHE-9014555). One of us (D.U.) was supported in part by DRET (contrat 88/1425).

Appendix A

For the GOE [16–18], the $Y_2(r)$ cluster function [see eq. (5.30)], $I(r)$ [see eq. (5.35)] and $\Sigma^2(r)$ [see eq. (5.32)] are given as

$$Y_2(r) = \left(\frac{\sin \pi r}{\pi r}\right)^2 - \left(\frac{\cos \pi r}{r} - \frac{\sin \pi r}{\pi r^2}\right)\left(\frac{\mathrm{Si}(\pi r)}{\pi} - \frac{\epsilon(r)}{2}\right), \tag{A.1}$$

$$I(r) = \epsilon(r)\frac{\sin \pi r}{\pi r} - 1 - 4r\left(\frac{\sin \pi r}{\pi r}\right)^2 + \frac{1}{\pi}\left(4\,\mathrm{Si}(2\pi r) - 2\,\mathrm{Si}(\pi r)\frac{\sin \pi r}{\pi r}\right), \tag{A.2}$$

$$\Sigma^2(r) = \frac{2}{\pi^2}[\ln(2\pi r) + \gamma + 1 - \cos(2\pi r) - \mathrm{Ci}(2\pi r)] + 2r\left(1 - \frac{2}{\pi}\mathrm{Si}(2\pi r)\right) + \frac{\mathrm{Si}^2(\pi r)}{\pi^2} - \frac{\mathrm{Si}(\pi r)}{\pi}, \tag{A.3}$$

with

$$\epsilon(r) = 0 \quad \text{if } r = 0, \qquad \epsilon(r) = 1 \quad \text{if } r > 0, \qquad \epsilon(r) = -1 \quad \text{if } r < 0, \tag{A.4}$$

$$\mathrm{Si}(x) = \int_0^x \mathrm{d}y\, \frac{\sin y}{y}, \qquad \mathrm{Ci}(x) = \gamma + \ln(x) + \int_0^x \mathrm{d}y\, \frac{\cos y - 1}{y}, \tag{A.5}$$

and where $\gamma = 0.5772...$ is Euler's constant. The small r behavior of $I(r)$ [see eq. (5.35)] and $\hat{R}_2(r)$ [see eq. (5.33)] is

$$I(r) = 2r - \tfrac{1}{6}\pi^2 r^2 + \tfrac{1}{120}\pi^4 r^4 + \mathrm{O}(r^5), \qquad \hat{R}_2(r) = \tfrac{1}{18}\pi^2 r^3 - \tfrac{1}{600}\pi^4 r^5 + \mathrm{O}(r^6). \tag{A.6}$$

For a Poisson spectrum

$$Y_2(r) = I(r) = 0, \qquad \Sigma^2(r) = r, \qquad \hat{R}_2(r) = r^2. \tag{A.7}$$

References

[1] A.M. Ozorio de Almeida, Hamiltonian Systems: Chaos and Quantization (Cambrige University Press, 1988).
[2] M. Tabor, Chaos and Integrability in Nonlinear Dynamics. An Introduction (Wiley, New York, 1989).
[3] M.C. Gutzwiller, Chaos in Classical and Quantum Mechanics (Springer, New York, 1990).
[4] M.J. Giannoni, A. Voros and J. Zinn-Justin, eds., Chaos et Physique Quantique / Chaos and Quantum Physics, Proc. Les Houches Summer School, Session LII (1989) (North-Holland, Amsterdam, 1991).
[5] S. Tomsovic and E.J. Heller, Phys. Rev. Lett. 67 (1991) 664.
[6] H. Friedrich and D. Wintgen, Phys. Rep. 183 (1989) 37;
D. Delande, Thèse, Université Paris (1988); and in: Chaos et Physique Quantique / Chaos and Quantum Physics, Proc. Les Houches Summer School, Session LII (1989), eds. M.J. Giannoni, A. Voros and J. Zinn-Justin (North-Holland, Amsterdam, 1991).
[7] A. Holle, J. Main, G. Wiebusch, H. Rottke and K.H. Welge, Phys. Rev. Lett. 61 (1988) 161, and references therein;
C.-h. Iu, G.R. Welch, M.M. Kash, D. Kleppner, D. Delande and J.C. Gay, Phys. Rev. Lett. 66 (1991) 145.
[8] M.J. Davis, J. Phys. Chem. 92 (1988) 3124, and references therein.
[9] Y. Imry, in: Directions in Condensed Matter Physics, eds. G. Grinstein and G. Mazenko (World Scientific, Singapore, 1986);
H.U. Baranger, D.P. DiVincenzo, R.A. Jalabert and A.D. Stone, IBM preprint (1991).

[10] M.C. Gutzwiller, J. Math. Phys. 12 (1971) 343; see also: Chaos in Classical and Quantum Mechanics (Springer, New York, 1990), ch. 17.
[11] R. Aurich and F. Steiner, Physica D 32 (1988) 451;
R. Artuso, E. Aurell and P. Cvitanović, Nonlinearity 3 (1990) 325, 361;
M.V. Berry and J.P. Keating J. Phys. A 23 (1990) 4839;
E.B. Bogomolny, Nonlinearity 5 (1992) 805;
C. Schmit, in: Chaos et Physique Quantique / Chaos and Quantum Physics, Proc. Les Houches Summer School, Session LII (1989), eds. M.J. Giannoni, A. Voros and J. Zinn-Justin (North-Holland, Amsterdam, 1991);
G. Tanner, P. Scherer, E.B. Bogomolny, B. Eckhardt and D. Wintgen, Phys. Rev. Lett. 67 (1991) 2410;
P. Cvitanović, I.C. Percival and A. Wirzba, eds., Proc. NATO Advanced Research Workshop on Quantum Chaos—Theory and Experiment (Copenhagen, 1991), (Kluwer, Dordrecht, 1992).
[12] F. Haake, Quantum Signature of Chaos (Springer, Berlin, 1991).
[13] L.E. Reichl, The Transition to Chaos in Conservative Classical Systems: Quantum Manifestations (Springer, Berlin, 1992).
[14] O. Bohigas, M.-J. Giannoni and C. Schmit, Phys. Rev. Lett. 52 (1984) 1; J. Physique Lett. 45 (1984) L-1015.
[15] O. Bohigas and M.-J. Giannoni, in: Mathematical and Computational Methods in Nuclear Physics, eds. J.S. Dehesa, J.M.G. Gomez and A. Polls, Proc. 6th Granada Workshop (Spain, 1983), Lecture Notes in Physics 209 (Springer, Berlin, 1984), p. 1;
O. Bohigas, in: Chaos et Physique Quantique / Chaos and Quantum Physics, Proc. Les Houches Summer School, Session LII (1989), eds. M.J. Giannoni, A. Voros and J. Zinn-Justin (North-Holland, Amsterdam, 1991).
[16] C.E. Porter, Statistical Theories of Spectra: Fluctuations (Academic Press, New York, 1965).
[17] M.L. Mehta, Random Matrices and the Statistical Theory of Energy Levels (Academic Press, New York, 1967), new revised and enlarged edition (1990).
[18] T.A. Brody, J. Flores, J.B. French, P.A. Mello, A. Pandey and S.S.M. Wong, Rev. Mod. Phys. 53 (1981) 385.
[19] M.V. Berry and M. Robnik, J. Phys. A 19 (1986) 649;
E. Caurier and B. Grammaticos, Phys. Lett. A 136 (1989) 387.
[20] F.M. Izraelev, Phys. Rev. Lett. 56 (1986) 541;
J.V. José and R. Cordery, Phys. Rev. Lett. 56 (1986) 280;
R. Scharf, B. Dietz, M. Kus, F. Haake and M.V. Berry, Europhys. Lett 5 (1988) 383;
R. Blümel and U. Smilansky, Physica D 36 (1989) 111;
see also the contributions of U. Smilansky and B.V. Chirikov, in: Chaos et Physique Quantique / Chaos and Quantum Physics, Proc. Les Houches Summer School, Session LII (1989), eds. M.J. Giannoni, A. Voros and J. Zinn-Justin (North-Holland, Amsterdam, 1991).
[21] M.V. Berry, Proc. R. Soc. London A 400 (1985) 229.
[22] J.H. Hannay and A.M. Ozorio de Almeida, J. Phys A 17 (1984) 3429.
[23] M.V. Berry and M. Tabor, Proc. R. Soc. London A 356 (1977) 375.
[24] B. Eckhardt, Phys. Rep. 163 (1988) 205.
[25] T.H. Seligman, J.J.M. Verbaarschot and M.R. Zirnbauer, J. Phys. A 18 (1985) 2751; Phys. Rev. Lett. 53 (1984) 215.
[26] M.V. Berry and M. Robnik, J. Phys. A 17 (1984) 2413.
[27] Th. Zimmermann, H.-D. Meyer, H. Köppel and L.S. Cederbaum, Phys. Rev. A 33 (1986) 4334.
[28] M.V. Berry, Philos. Trans. R. Soc. London A 287 (1977) 237;
A. Voros, in: Stochastic Behaviour in Classical and Quantum Hamiltonian Systems, eds. G. Casati and G. Ford, Lecture Notes in Physics 93 (Springer, Berlin, 1979), p. 326.
[29] M.V. Berry, J. Phys. A 10 (1977) 2083.
[30] S.W. Mc Donald and A.N. Kaufman, Phys. Rev. Lett. 42 (1979) 1189;
S.W. Mc Donald, Ph. D. Thesis, UC Berkeley LBL14837 (1983);
S.W. Mc Donald and A.N. Kaufman, Phys. Rev. A 37 (1988) 3076.
[31] E.J. Heller, Phys. Rev. Lett. 53 (1984) 1515.
[32] E.J. Heller, Wavepacket dynamics and quantum chaology, in: Chaos et Physique Quantique / Chaos and Quantum Physics, Proc. Les Houches Summer School, Session LII (1989), eds. M.J. Giannoni, A. Voros and J. Zinn-Justin (North-Holland, Amsterdam, 1991).
[33] G. Casati, B.V. Chirikov, J. Ford and F.M. Izrailev, in: Stochastic Behavior in Classical and Quantum Hamiltonian Systems, eds. G. Casati and J. Ford, Lecture Notes in Physics 93 (Springer, Berlin, 1979), p. 334.
[34] B.V. Chirikov, F.M. Izrailev and D.L. Shepelyansky, Sov. Sci. Rev. 2C (1981) 209.
[35] T. Hogg and B.A. Huberman, Phys. Rev. Lett. 48 (1982) 711.
[36] S. Fishman, D.R. Grampel and R.E. Prange, Phys. Rev. Lett. 49 (1982) 509; Phys. Rev. A 29 (1984) 1639.

[37] A. Carnegie and I.C. Percival, J. Phys. A 17 (1984) 801;
R.L. Waterland, J.M. Yuan, C.C. Martens, R.E. Gillilan and W.P. Reinhardt, Phys. Rev. Lett. 61 (1988) 2733;
E. Caurier and B. Grammaticos, Europhys. Lett. 2 (1986) 417.
[38] A. Einstein, Verh. Deutsch. Phys. Ges. Berlin 19 (1917) 82; English translation by C. Jaffé, JILA report No. 116;
L. Brillouin, J. Phys. Radium 7 (1926) 353;
J.B. Keller, Ann. Phys. (NY) 4 (1958) 180.
[39] I.C. Percival, Adv. Chem. Phys. 36 (1977) 1.
[40] I.C. Percival, J. Phys. B 6 (1973) L229.
[41] P. Leboeuf, J. Kurchan, M. Feingold and D.P. Arovas, Phys. Rev. Lett. 65 (1990) 3076.
[42] M.J. Davis and E.J. Heller, J. Chem. Phys. 75 (1981) 246.
[43] S. Tomsovic and D. Ullmo, in preparation.
[44] T. Uzer, D.W. Noid and R.A. Marcus, J. Chem. Phys. 79 (1983) 4412.
[45] O. Bohigas, S. Tomsovic and D. Ullmo, Phys. Rev. Lett. 64 (1990) 1474; 65 (1990) 5.
[46] P. Dahlqvist and G. Russberg, Phys. Rev. Lett. 65 (1990) 2837.
[47] V.I. Arnold, Mathematical Methods of Classical Mechanics (Springer, Berlin, 1978).
[48] B. Dorizzi, B. Grammaticos and A. Ramani, J. Math. Phys. 24 (1983) 2282.
[49] B. Simon, Ann. Phys. (NY) 146 (1983) 209; J. Funct. Anal. 53 (1983) 84.
[50] R.S. MacKay, J.D. Meiss and I.C. Percival, Physica D 13 (1984) 55; Phys. Rev. Lett. 52 (1984) 697.
[51] R.S. MacKay, J.D. Meiss and I.C. Percival, Physica D 27 (1987) 1.
[52] S.R. Channon and J.L. Lebowitz, Proc. NY Acad. Sci. 357 (1980) 108.
[53] D. Bensimon and L.P. Kadanoff, Physica D 13 (1984) 82.
[54] N.L. Balazs and B.K. Jennings, Phys. Rep. 104 (1984) 6.
[55] J.E. Moyal, Proc. Camb. Philos. Soc. 45 (1949) 99.
[56] E.P. Wigner, Phys. Rev. 40 (1932) 749.
[57] H. Weyl, Z. Phys. 46 (1927) 1.
[58] R. Balian and C. Bloch, Ann. Phys. (NY) 63 (1971) 592; reprinted in: Claude Bloch: Oeuvre Scientifique, eds. R. Balian, C. de Dominicis, V. Gillet and A. Messiah (North-Holland, Amsterdam, 1975), tome 2, p. 1476.
[59] S. Tomsovic, J. Phys. A 24 (1991) L733.
[60] F.T. Hioe, E.W. Montroll and M. Yamawaki, in: Perspectives in Statistical Physics, ed. H.J. Raveché (North-Holland, Amsterdam, 1981), ch. 16.
[61] K. Banerjee, S.P. Bhatnagar, V. Choudry and S. Kanwal, Proc. R. Soc. London A 360 (1978) 575.
[62] A.M. Ozorio de Almeida, in: Quantum Chaos and Statistical Nuclear Physics, eds. T.H. Seligman and H. Nishioka, Lecture Notes in Physics 263 (Springer, Berlin, 1986).
[63] D.W. Noid and R.A. Marcus, J. Chem. Phys. 67 (1977) 559;
D.W. Noid, M.L. Kosykowski and R.A. Marcus, J. Chem. Phys. 71 (1979) 2864;
R.T. Swimm and J.B. Delos, J. Chem. Phys. 71 (1979) 1706;
C. Jaffé and W.P. Reinhardt J. Chem. Phys. 71 (1979) 1862.
[64] J.G. Leopold, I.C. Percival and D. Richards, J. Phys A 15 (1982) 805.
[65] B. Lauritzen, Phys. Rev. A 43 (1991) 603.
[66] R.B. Shirts and W.P. Reinhardt, J. Chem. Phys. 77 (1982) 5204.
[67] B. Eckhardt, G. Hose and E. Pollak, Phys. Rev. A 39 (1989) 3776.
[68] A.M. Ozorio de Almeida, J. Phys. Chem 88 (1984) 6139.
[69] V.P. Maslov and M.V. Fedoriuk, Semiclassical Approximation in Quantum Mechanics (Reidel, Dordrecht, 1981) (original Russian edition 1965).
[70] M. Wilkinson, Physica D 21 (1986) 341.
[71] M. Wilkinson, J. Phys. A 20 (1987) 635.
[72] W.A. Lin and L.E. Ballentine, Phys. Rev. Lett. 65 (1990) 2927.
[73] R.T. Lawton and M.S. Child, Mol. Phys. 37 (1979) 1799.
[74] For a review on superlattices and quantum wells, see L. Esaki, IEEE J. Quantum Electron. 22 (1986) 1611;
and F. Capasso, K. Mohamed and A. Y. Cho, IEEE J. Quantum Electron. 22 (1986) 1853.
[75] G. Livescu, A.M. Fox, D.A.B. Miller, T. Sizer and W.H. Knox, Phys. Rev. Lett. 63 (1989) 436;
K. Leo, J. Shah, E.O. Göbel and Th.C. Damen, Phys. Rev. Lett. 66 (1991) 201.
[76] M.V. Berry, Proc. R. Soc. London 423 (1989) 219.
[77] D. Ullmo, thèse de doctorat de l'université Paris 7 (1992).
[78] M.V. Berry, in: Comportement Chaotique des Systèmes Déterministes / Chaotic Behaviour of Deterministic Systems, eds. R.H.G. Helleman and G. Joos, Proc. Les Houches Summer School, Session XXXVI (1981) (North-Holland, Amsterdam, 1983), p. 171.

[79] J.B. French, V.K.B. Kota, A. Pandey and S. Tomsovic, Ann. Phys. (NY) 181 (1988) 198.
[80] A. Pandey, Ann. Phys. (NY) 119 (1979) 170.
[81] O. Bohigas, R.U. Haq and A. Pandey, Phys. Rev. Lett. 54 (1985) 1675.
[82] A. Pandey and M.L. Mehta, Commun. Math. Phys. 87 (1983) 449.
[83] T. Guhr and H.A. Weidenmüller, Ann. Phys. (NY) 193 (1989) 472; 199 (1990) 412.
[84] T.H. Seligman and F. Leyvraz, J. Phys. A 23 (1990) 1555.
[85] S. Tomsovic, Ph. D. thesis, Univ. of Rochester Report No. 974 (1987) (unpublished).
[86] G. Casati, B.V. Chirikov and I. Guarneri, Phys. Rev. Lett. 54 (1985) 1350.
[87] S. Tomsovic, in preparation.
[88] P.W. O'Connor, J.N. Gehlen and E.J. Heller, Phys. Rev. Lett. 58 (1987) 1296.
[89] E.B. Bogomolny, Physica D 31 (1988) 169.
[90] G. Radons and R.E. Prange, Phys. Rev. Lett. 61 (1988) 1691;
T. Geisel and G. Radons, Phys. Scr. 40 (1989) 340.
[91] E.J. Heller, J. Chem. Phys. 75 (1981) 2923.
[92] J.P. Draayer, J.B. French and S.S.M. Wang, Ann, Phys. 106 (1977) 472.
[93] For a review on localization, see, for instance, D.J. Thouless, in: La Matière Mal Condensée / Ill-Condensed Matter, eds. R. Balian, R. Maynard and G. Toulouse, Proc. Les Houches Summer School, Session XXXI (1978) (North-Holland, Amsterdam, 1979);
R.E. Prange, in: Adriatico Summer Programme on Quantum Problems: Miniworkshop on Quantum Chaos (World Scientific, Singapore, 1991).
[94] P.W. Anderson, Phys. Rev. 109 (1958) 1492; Rev. Mod. Phys. 50 (1978) 191.
[95] R.B. Laughlin, Nucl. Phys. B (Proc. Suppl.) 2 (1987) 213.
[96] Y.V. Fyodorov and A.D. Mirlin, preprint.
[97] F.M. Izrailev, Phys. Rep. 196 (1990) 299.
[98] B.V. Chirikov, Phys. Rep. 52 (1979) 263.
[99] F.M. Izrailev and D.L. Shepelyansky, Dokl. Akad. Nauk SSSR 249 (1979) 1103 [Sov. Phys. – Dokl. 249 (1979) 996].
[100] H.-J. Stöckmann and J. Stein, Phys. Rev. Lett. 64 (1990) 2215, and private communication.
[101] G. Grinstein and G. Mazenko, eds., Directions in Condensed Matter Physics (World Scientific, Singapore, 1986).